Studies on Radio-over-Fiber OFDM Transmission by Envelope Pulse-Width Modulation

Xiaoxue Yu

Department of Communication Engineering and Informatics
The University of Electro-Communications

A Dissertation Submitted in Partial Fulfillment
of the Requirements for the Degree of
Doctor of Philosophy

June 2014

Studies on Radio-over-Fiber OFDM Transmission by Envelope Pulse-Width Modulation

APPROVED BY SUPERVISORY COMMITTEE:

Professor Yasushi Yamao

Professor Kazuhiko Honjo

Professor Yoshio Karasawa

Professor Naoto Kishi

Associate Professor Motoharu Matsuura

概要

スマートホンの爆発的普及に伴うデータ通信およびインターネットアクセスへの需要の急激な増加とともに、無線通信はさらなるブロードバンド化と大容量化をめざして発展している。ブロードバンド化された無線通信では伝送速度の高速化に伴って、より高い受信信号入力レベルが必要となる。しかし使用周波数の高周波化と相まって、屋内外において十分な受信電力が得られない場所が多数発生する。このため基地局の大幅な追加が必要であり、そのためになるべく簡易な構成でかつ柔軟な展開が可能な基地局ネットワーク構成が望ましい。

光ファイバ無線 (Radio over Fiber ; RoF) 技術は上記問題の対処方法として利用が期待されている。光ファイバ無線では、RF 信号処理を基地局で行う。基地局から RF 信号は光ファイバによってユーザにより近接して設置されるリモート・アンテナ・ユニット(Remote Antenna Unit ; RAU) に低損失で伝送される。このように、RAU が光/電気 (O/E) 変換と増幅の機能のみ実行するため, RAU の構成を簡易化することができる。さらに、RF 信号処理は基地局にて集中されているため、設備共有および動的資源配分ができる。したがって、システム運用とメンテナンスが効率化できる。

しかし、ブロードバンド無線システムに使用される直交周波数分割多重 (Orthogonal Frequency Division Multiplex; OFDM) 信号は、RoF チャネルにて送信される場合、電気/光(E/O) 変換の非線形性の影響を受け，伝送特性が劣化し易いことが知られている。さらに光ファイバ通信では、光の多重反射が存在する。光の多重反射はファイバ端の間に屈折率の不連続性があるために生じ、その遅延時間はファイバ長で決定され、数百ｍのファイバ長に相当する長いエコーが発生する。RoF チャンネルのエコーがシステム性

能を劣化させる可能性があるため、エコーの RF 信号伝送に対する影響を評価する必要がある。

本論文ではこのような問題を解決するため、E/O 変換の非線形性とエコーの影響を原理的に受けない送信法として、Envelope Pulse-Width Modulation (EPWM) 法を用いた RoF 伝送システムを提案した。EPWM 送信機では、OFDM 信号の振幅は Pulse-Width-Modulated (PWM) フォーマットに変換され、包絡線が 0 または一定値になる。そのため、EPWM 信号は非線形性の影響を受けない。本論文では、代表的な E/O 変換器として、Mach-Zehnder (MZ) 変調器および Distributed Feedback (DFB)レーザーダイオードの非線形性を取り上げ、解析している。これらの非線形性は実験によって測定され、数学モデルで表わされて解析を可能にしている。特に DFB レーザーダイオードをモデル化するために、新たに修正された Rapp モデルを提案し、実際の特性によくフィッティングできることが示されている。これら提案されたモデルの有効性は実験によって確認されている。次にこれらの非線形性の OFDM-RF 信号に対する影響をまずシミュレーションによって解析している。シミュレーション結果の妥当性を確認するため、MZ 変調器と DFB レーザーダイオードを E/O 変換器として、シングルモードファイバを用いた OFDM 信号の EPWM 送信方による RoF 伝送実験を行った。シミュレーションと実験の両者の結果から、OFDM 信号の EPWM-RoF 送信法は非線形歪に対して劣化が少なく、従来の RoF 伝送に比べ良好な変調誤差特性を得ることが確認できた。

次に RoF チャネルでのエコーの影響を確認するため２回反射までのエコーの影響をモデル化した RoF-echo モデルを検討した。このモデルを用いてエコーの影響を数学的に分析した。さらにエコーによって発生する EPWM 信号の振幅変動を除いてエコーによる劣化を軽減するため、光検波器（PD）から出力された EPWM 信号を class-C 動作の電力増幅器（PA)を用いて非線形増幅する方法を提案した。PA のバイアス電圧を調整することによって、出力 EPWM 信号の振幅変動を解消することができる。OFDM 信号および

EPWM 送信による OFDM 信号に対するエコーの影響をシミュレーションによってまず分析され、実験によって RoF-echo モデルの有効性とエコーの影響が分析・確認された。以上の結果から OFDM 信号の光ファイバ無線伝送に EPWM 送信法を適用することにて、信号の劣化を抑えられることを結論づけている。

Abstract

Wireless communications is developing towards higher data rate and higher capacity to satisfy the increasing demands for data communication and Internet access. At the same time, area coverage of wireless communication services is required to be ubiquitous, which aims at “communication anytime, anywhere, and with anything”. In general, higher data rate wireless transmission requires higher input signal power for receivers because the thermal noise power is proportional to bandwidth. Thus, above requirements cannot be consistent each other unless the cell size of base stations (BSs) are shrank. However, reducing the cell size of all BSs needs large amount of investment and will be difficult in a short period. Then introducing higher data rate systems in current BS layout results in many dead spots of wireless coverage both in outdoor and indoor environments. Another way to solve this issue is to add small BSs or remote Antenna Units (RAU) among current BSs so that they cover such dead spots. Since they are smaller, it is easier to install them than normal BSs.

Radio over Fiber (RoF) is a promising technology to enhance the coverage of broadband wireless communication systems with reduced deployment cost. In the RoF system, RF signal processing such as modulation/demodulation with advanced encoding/decoding schemes is centralized in the BS, then RF signals are delivered and collected through the optical fibers to / from Remote Antenna Units (RAU) that are installed closer to the users. In this way, the RAUs are significantly simplified and their cost is reduced because the RAUs are only equipped with optical to electrical conversion and amplification functions. In addition, it enables RF processing circuit sharing in the BS and dynamic resource allocation among RAUs.

Thus the system operation and maintenance cost can be reduced. However, when a wireless signal is transmitted via a RoF channel, nonlinearities of the channel become a big concern for multicarrier signals such as Orthogonal Frequency Division Multiplexing (OFDM). Moreover, in most of the optical transmission systems, multiple light reflections are inevitable because of discontinuities of refractive-index between fiber ends, Electrical/Optical (E/O) and Optical/Electrical (O/E) converters. This echo effect should be evaluated because it can degrade the system performance.

In this thesis, an Envelop Pulse-Width Modulation-RoF (EPWM-RoF) transmission scheme is proposed to solve the RoF nonlinearity and echo effect issues. The EPWM transmitter can remove the continuous amplitude variation of OFDM signals by converting the amplitude to Pulse-Width-Modulated (PWM) format that has binary amplitude of either a non-zero constant value or zero. Then, the EPWM signal does not suffer from nonlinearity of the channel. In RoF channels, nonlinearity is commonly caused by the E/O converters. Two different types of E/O converters: Mach-Zehnder (MZ) modulator and Distributed Feedback Laser Diode (DFB LD) are investigated. Their nonlinearity are measured by experiment and mathematically modelled. In order to model the DFB LD, a modified Rapp model is proposed to obtain more flexibility and applicability. The nonlinear distortions caused by the E/O converters are analyzed and simulated by using the models. Some experiments are conducted to confirm the simulation results and validity of the model. The simulation and experiment results indicate that the EPWM-RoF transmission scheme has good performance in dealing with the E/O nonlinearity.

To analyze the effect of echo on the RF signal, a RoF-echo model is proposed considering a maximum of two reflections. By employing the model, composite effect of MZ modulator nonlinearity and echoes on RF signal transmission is mathematically analyzed. To eliminate the amplitude fluctuations of output EPWM

signal caused by the echo effect, a class-C operated PA is added after the transmission of RoF channel. By choosing a proper DC bias voltage, the amplitude fluctuations can be suppressed. Simulations of the echo effect on the original OFDM and EPWM formatted OFDM signals are conducted to confirm the theoretical analysis and to compare two schemes. The validity of the RoF-echo model and the theoretical analysis are also confirmed by experimental results.

Through the theoretical analysis, simulation and experimental results, it can be concluded that EPWM-RoF transmission is effective in dealing with E/O nonlinearity and echo effect in RoF channel.

Acknowledgements

I would like to express my deepest thanks and appreciation to Prof. Yasushi Yamao who has been a great mentor. I am very honored that I can join his laboratory. Prof. Yasushi Yamao has given me so much help and consideration not only for my research works, but also for my life in Japan. He is always tireless and willing to spend time to discuss with me and give me valuable advises when I ask for his help. He cleared all the possible obstacles that could affect me to let me concentrate on my research. Without Prof. Yasushi Yamao, my life in Japan will not be so wonderful, substantial and memorable.

I would like to express my gratitude to other members of this dissertation committee: Professor Kazuhiko Honjo, Yoshio Karasawa, Professor Naoto Kishi and Associate Professor Motoharu Matsuura. I would like to thank them for their valuable comments and suggestions to improve my dissertation. Associate Professor Motoharu Matsuura has given me so much valuable guidance on the optical experiments. He has always been ardent and patient when helping me.

I would like to thank the members of Yamao-Fujii Lab for being supportive and friendly.

Finally, I want to thank my wonderful husband who has given me so much supports and considerations. He has always encouraged and taken care of me kindly. I also want to thank my newborn son. He brings me so much happiness and power to keep strong.

Contents

List of Figures

List of Tables

Acronyms

2G	2nd Generation
3G	3rd Generation
4G	4th Generation
ADSL	Asymmetrical Digital Subscriber Loop
AM-AM	Amplitude-to-Amplitude
AM-PM	Amplitude-to-Phase
ANC-EPWM	Amplitude Noise Compensation-EPWM
BPF	Bandpass Filter
BRAN	Broadband Radio Access Networks
BS	Base Station
CCDF	Complementary Cumulative Distribution Function
CP	Cyclic Prefix
CW	Continuous Wave
DFB LD	Distributed Feedback LD
DMT	Discrete MultiTone

DR	Dynamic Range
E/O	Electrical/Optical
EPWM	Envelop Pulse-Width Modulation
ETSI	European Telecommunication Standards Institute
EVM	Error Vector Magnitude
FFT	Fast Fourier Transform
FWA	Fixed Wireless Access
GSM	Global System for Mobile Communications
ICI	Inter Carrier Interference
IFFT	Inverse Fast Fourier Transform
IM	Intermodulation
IM-DD	Intensity Modulation with Direct Detection
ISI	Intersymbol Interference
LD	Laser Diode
LPF	Low Pass Filter
LTE	Long Term Evolution
MMAC	Metropolitan Milwaukee Association of Commerce
MMF	Multi-Mode Fiber

MZ	Mach-Zehnder
NF	Nosie Figure
O/E	Optical /Electrical
OFDM	Orthogonal Frequency Division Multiplexing
OSR	Oversampling Ratio
PA	Power Amplifier
PAPR	Peak to Average Power Ratio
PC	Polarization Controller
PD	Photo Detector
PM	Phase Modulated
PSD	Power Spectral Density
PWM	Pulse Width Modulated
RAP	Radio Access Point
RAU	Remote Antenna Unit
RF	Radio Frequency
RIN	Relative Intensity Noise
RoF	Radio over Fiber
SCM	Sub-Carrier Multiplexing

SFDR	Spurious-Free Dynamic Range
SMF	Single Mode Fiber
UTMS	Universal Mobile Telecommunication System
WDM	Wavelength Division Multiplex
WiMAX	Worldwide Interoperability for Microwave Access
WLAN	Wireless Local Area Network

Symbols

$a(t)$	Amplitude component
$a_{in}(t)$	Input amplitude signal of the Rapp model or modified Rapp model
$a_{out}(t)$	Output amplitude signal of the Rapp model or modified Rapp model
$a_{RF}(t)$	Amplitude of RF signal
$a_{\omega c\text{-}EPWM}$	Amplitude of output EPWM-OFDM signal from the RoF channel using MZ modulator
$a'_{\omega c\text{-}EPWM}$	amplitude of output EPWM-OFDM signal from the RoF cThermal noise in PD
A_{opt}	Amplitude of light source
$\beta(t)$	Amplitude compensation coefficient
c	Velocity of light in vacuum
C	Burst off EPWM-OFDM signal from the RoF channel using MZ modulator
C'	Burst off EPWM-OFDM signal from from the RoF channel using DFB LD
C_{mz}	Burst off $v_{EPWM\text{-}MZ}(t)$ signal
d_i	Coded data symbols
D	Dispersion parameter Shot noise in PD

Δ	Step-size of Δ-Σ modulator
Δf	Effective noise bandwidth of PD
$e_a(t)$	Pulse Width Modulated amplitude signal
$e_{ANC\text{-}EPWM}(t)$	ANC-EPWM signal
$e_B(t)$	Complex baseband signal
$e_{EPWM}(t)$	EPWM signal
$e_{out}(t)$	Output signal from the BPF
$e_{rf}(t)$	Ideal RF signal
$e_\phi(t)$	Phase modulated signal
$E_{\max}$	Limiting output amplitude of the Rapp model
f_c	RF carrier frequency
f_s	Oversampling frequency
F_n	Factor that enhances thermal noise by various resistors used in pre- and main amplifiers
G_{fiber}	optical fiber attention
G_p	Pass signal gain
G_{p1}	Power gain of the signals that pass though B2 for the first time
G_{p2}	Power gain of the signals that pass though B2 for the second time

G_r	Reflected signal gain
G_{r1}	Power gain of the reflected signal at B1
G_{r2}	Power gain of the reflected signal at B2
$h_{BPF}(t)$	Impulse response of BPF
$h_{LPF}(t)$	Impulse response of LPF
$H(f)$	Transfer function of the single mode fiber
i_{PD}	Output electrical current of PD
$i_{\omega c}$	Output RF signal from RoF channel at ω_c
$i_{\omega c\text{-}EPWM}$	Output EPWM-OFDM signal from the RoF channel using MZ modulator
I_d	Dark current in PD
I_p	Average current of the PD
k_B	Boltzmann constant
K	Small signal gain of the Rapp model
λ_0	Operating wavelength of optical fiber
L	Length of fiber
μ	Introduced parameter in the modified Rapp model
n_f	Refractive index of the optical fiber
N	Number of subcarriers in OFDM symbol

p	Knee factor of the Rapp model
P_{opt}	Input optical power of PD
q	Charge of an electron
$q_e(t)$	Quantization noise output from the Δ-Σ modulator
$q'_e(t)$	EPWM transmitter output noise
$q''_e(t)$	Suppressed quantization noise in ANC-EPWM transmitter
$q_L(t)$	Output signal of LPF
R	Conversion gain of PD
$R(\eta)$	Autocorrelation function of input RF signal
R_L	Load resister
σ	Normalized amplitude corresponding to the average power of the OFDM signal
σ_S^2	Shot noise in PD
σ_T^2	Thermal noise in PD
$s(t)$	Baseband OFDM signal
$S(\omega)$	PSD of input RF signal
$S_{RoF}(\omega)$	PSD of output signal from the RoF channel
$S_{S1}(\omega)$	PSD of $v_{s1}(t)$
$S_{S2}(\omega)$	PSD of $v_{s2}(t)$

$S_{S3}(\omega)$	PSD of $v_{s3}(t)$
τ	Traveling time of light in the optical fiber
T	Absolute temperature
T_s	Period of the OFDM symbol
$\phi(t)$	Phase component
$\Phi(t)$	$\omega_c t+\phi(t)$
$v_{EPWM\text{-}Echo}(t)$	Output optical EPWM-Echo signal from the RoF-echo model
$v_{EPWM\text{-}MZ}(t)$	Output EPWM signal from MZ modulator
$v_{EPWM\text{-}RF}(t)$	EPWM RF signal
$v_{EPWM\text{-}RoF\text{-}Echo}(t)$	Output EPWM signal from the RoF channel with echo effect
$v_{in}(t)$	Input light signal of the RoF-echo model
$v_{mz}(t)$	Burst on $v_{EPWM\text{-}MZ}(t)$ signal
$v_{out}(t)$	Output of the RoF-echo model
$v_{p1}(t)$	Pass signal for the first time reflection
$v_{p2}(t)$	Pass signal for the second time reflection
$v_{r1}(t)$	Once reflected light signal
$v_{r2}(t)$	Twice reflected light signal
$v_{RF}(t)$	Input RF signal

$v_{RoF}(t)$	Output signal from the RoF channel
$v_{RoF\text{-}echo}(t)$	Output of the RoF channel with echo effect
$v_{s1}(t)$	RF signal component in $v_{RoF\text{-}echo}(t)$
$v_{s2}(t)$	2nd order harmonic wave component in $v_{RoF\text{-}echo}(t)$
$v_{s3}(t)$	3rd order harmonic wave component in $v_{RoF\text{-}echo}(t)$
V_{bias}	Input DC bias voltage
V_{in}	light source signal
V_{π}	Extinction voltage
ω_c	Carrier angular frequency of RF signal
ω_{opt}	Angular frequency of light source

Chapter 1. Introduction

1.1 Background and Motivations

Wireless communications is developing towards higher data rate and higher capacity to satisfy the increasing demands for data communication and Internet access. At the same time, area coverage of wireless communication services is required to be ubiquitous, which aims at “communication anytime, anywhere, and with anything”. Therefore wireless communications have developed in both coverage area and transmission capacity.

In general, a trade-off exists between capacity and coverage area. Table 1-1 shows the service data rate and coverage of several communication systems [1, 2].

Table 1-1 Wireless communication systems

Communication Systems	*Downlink Data rate (Mbps)*	*Service range*
2G/GSM	0.022-0.115	Wide area
3G/UTMS	0.384-2.048	Wide area
4G/LTE	100-326	Wide area
WiMAX (802.16)	74.8-134.4	Wide area
WLAN (802.11a/b/g/n)	11-300	Short range
Bluetooth	0.72-42	Short range

High mobility needs wide coverage. For example, Global System for Mobile Communications (GSM) and the third-generation (3G) cellular systems can provide services both indoor and outdoor, however, their data rates are limited to a few of Mbps [2]. WLAN can provide transmission rates up to several hundreds of Mbps, but it can only be utilized in short-range communication. Therefore, mobile communication systems seek for high capacity, while wireless data communication systems are eager for extending coverage area. A case that aims both high capacity and wide coverage is the IEEE802.16, which provides high bit rate mobile and Fixed Wireless Access (FWA) services [3-4]. LTE also can provide transmission rates up to a hundreds of Mbps in wide area [5].

For broadband wireless communications, one way to increase capacity is to deploy smaller cells. However, to satisfy ubiquitous communications, smaller cell size requires larger number of Base Stations (BS) and Radio Access Points (RAP), which means expensive costs are needed for the BSs and RAPs. Another way to increase capacity is to increase the number of RF carriers, which results in the increasing of costs of the BSs. Therefore, unless the costs of the BSs or RAPs can be drastically reduced, increasing capacity of such systems is difficult.

A promising method to reduce the costs of BSs and RAPs is Radio over Fiber (RoF) technology. RoF has been proposed as an effect way to deal with the demands for small radio cell networks [6]. As shown in Fig. 1.1, the RF signal processing is centralized in the BS, and then the RF signals are delivered through the optical fibers to the Remote Antenna Units (RAU). In this way, the RAUs are significantly simplified since they only need to realize optical to electrical conversion and amplification functions. In addition, equipment sharing and dynamic resource allocation is achievable by the centralization of RF signal processing in the BS, thus the system operation and maintenance is simplified.

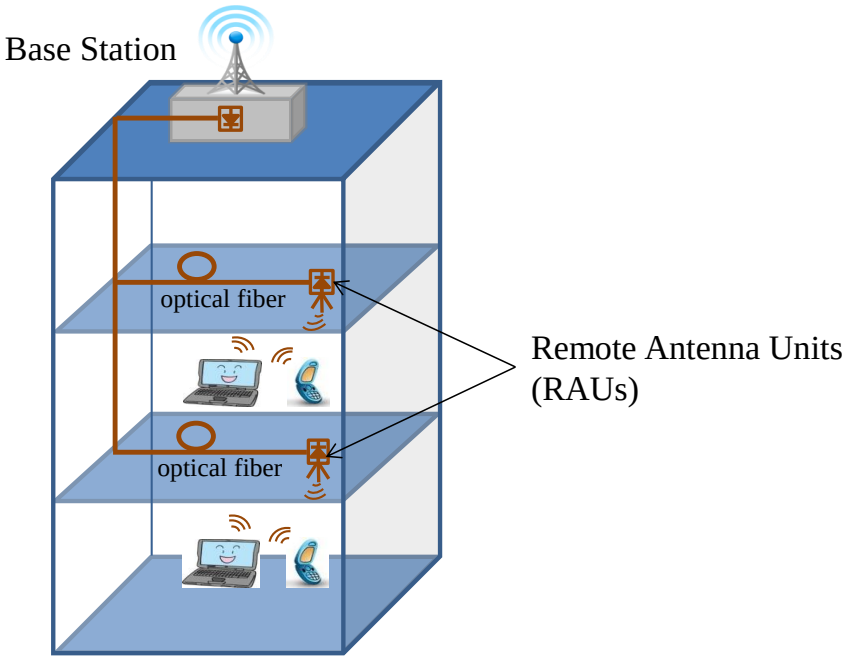

Fig. 1.1 Radio over Fiber Concept

Several major merits of RoF technology are given as follows.

- *Low attenuation loss*: Commercially available Single Mode Fiber (SMF) has attenuation losses below 0.2dB/km in 1310nm window and 0.5dB/km in 1550 nm window, respectively [7]. Since RoF technology offers low loss, it can be used to achieve both low-loss distribution of any RF signals, and simplification of RAUs at the same time.
- *Immunity to electromagnetic interference*: Electrical distribution of high-frequency microwave signals either in free space or through transmission lines is problematic and costly [8]. Since signals in RoF channel is transmitted in the form of light, they are immunity to radio frequency interference [9].
- *Large bandwidth*: For SMF, the combined bandwidth of the three optical windows, which are 850nm, 1310nm and 1550nm wavelengths, is in excess of 50THz [10]. Besides the high capacity for transmitting microwave signals, the enormous bandwidth offered by optical fiber has

other benefits. The high optical bandwidth enables high speed signal processing which could be more difficult or impossible to achieve in electronic systems. In other words, some of the demands of microwave functions such as filtering, mixing, up- and down-conversion, can be implemented in the optical domain [11].

- *Dynamic resource allocation*: Since the RF signal processing is centralized in the BS, according to different demands for different communication systems, capacity allocation can be performed dynamically [12].
- *Easy installation and maintenance*: As we have explained, centralization of RF signal processing and extreme simplification of the RAUs result in simple system installation, maintenance and reduced costs [10] [12].

Although RoF has so many benefits, several limitations of RoF still should be noticed. Signal quality degradation caused by noise and distortions in RoF channel are not ignorable. These impairments tend to limit the Nosie Figure (NF) and Dynamic Range (DR) of RoF systems [8]. Noise sources in RoF channel include chromatic dispersion in optical fiber, Relative Intensity Noise (RIN), shot noise and dark current noise in photodiodes, and so on. In SMF based RoF system, transmission length may be limited due to the chromatic dispersion.

Distortions are caused by the nonlinearity in RoF channel. Major factor that causes nonlinearity in RoF channel comes from the Electrical/Optical (E/O) converter. Different types of E/O converters may cause different nonlinear distortions. Therefore, elimination of nonlinear distortion in the transmitted signals is very important. In addition, in most of the optical transmission systems, multiple light reflections are inevitable because discontinuities of refractive-index exist between fiber ends, E/O and Optical /Electrical (O/E) converters [13]. This phenomenon can also be called echo effect. Echo effect should be evaluated because even relatively small echoes in RoF channel can degrade the signal quality.

The delay of the echoes is relatively longer than the permissible delay spread in radio propagation.

1.2 Scope and Methodology

This dissertation focuses on dealing with the E/O nonlinearity and echo effect in RoF channel. Since multi-carrier signals such as Orthogonal Frequency Division Multiplexing (OFDM), which is widely employed in broadband wireless communication systems, have high Peak to Average Power Ratio (PAPR), they are vulnerable against nonlinear distortions while transmitted through the RoF channel. Echo effect exists in most of the RoF systems. Although the feedback light can be eliminated by an optical isolator, the echo still causes non-ignorable distortions to the signals. Therefore, study on the echo effect is also important. Some mathematical analysis on the spectrum of the interferometric noise have been presented [14][15]. Since the nonlinearity and echo exist simultaneously in RoF channels, their composite effect should be discussed. However, no studies have been covered this issue.

Many studies have been performed on the nonlinearity of E/O converters [16-20]. The most commonly used and studied E/O converters are Mach-Zehnder modulator (MZ) and direct modulation Laser Diode (LD). Although the two types of E/O converters have totally different nonlinearities, methods in dealing with that are almost same, and can be concluded as follows.

- *Postcompensation*: The nonlinearity information of the employed E/O converter should be studied at first. As shown in Fig. 1.2, the compensation method is developed mathematically or digitally, and it is performed after the nonlinear component [20][21][22].
- *Predistortion:* Contrary to the postcompensation, the compensation for the nonlinearity is performed right before the nonlinear component, as shown in Fig. 1.3. [23-25].

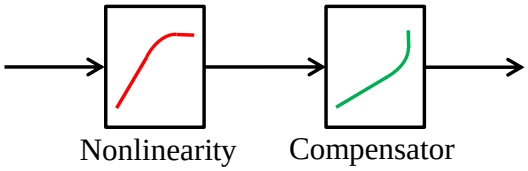

Fig. 1.2 Postcompensation concept

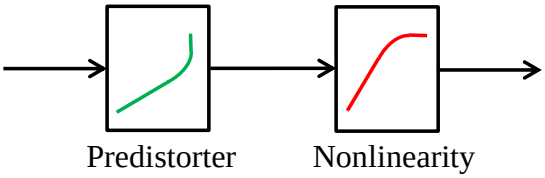

Fig. 1.3 Predistortion concept

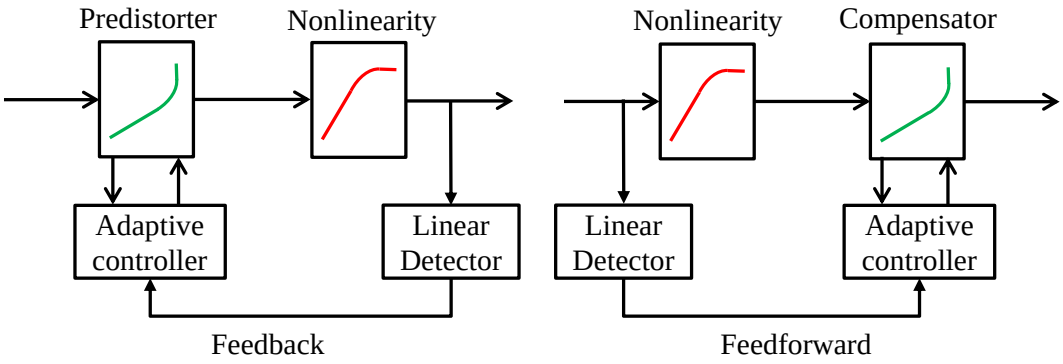

Fig. 1.4 Adaptive linearization

- *Adaptive linearization method*: Adaptive linearization can be employed in form of either feedback or feedforward, as shown in Fig.1.4. It can be employed with postcompensation or predistortion to improve compensation accuracy. No matter which form it takes, a feedback or feedforward link and an adaptive controller are needed. Adaptive linearization can provide more accurate compensation than the other methods [26-28]. However, extra circuits increase the complexity of the system.

Envelop Pulse-Width Modulation (EPWM) transmitter has been proposed for achieving high power efficiency and linear amplification of OFDM signals and its performance has been evaluated for nonlinear RF power amplifiers (PAs) [29-32]. By converting the envelope of input signal to a Pulse-Width Modulation (PWM) format, the EPWM transmitter removes the envelop variation of the input RF signal so that it can protect the input signal against nonlinear distortion.

In this dissertation, a new RoF transmission scheme employing EPWM transmitter has been proposed to efficiently suppress the impact of RoF nonlinearity and echo effect on OFDM signals. Nonlinearities of two typical E/O converters, which are MZ modulator and Distributed Feedback LD (DFB LD), are studied through experiments. The measured nonlinearity characteristics are modelled mathematically. A RoF-echo model is proposed for the analysis of echo effect in RoF channel. The feasibility of the model is confirmed by experiments. The nonlinear distortion and echo effects on OFDM signals are analyzed and the performance of the proposed scheme is evaluated by simulations.

1.3 Main Contributions of the Dissertation

Main contributions of this dissertation are as follows.

- A new transmission scheme (EPWM-RoF) is proposed to eliminate nonlinear distortions caused by the nonlinearity of RoF channel. Different from the exiting postcompensation and predistortion methods, the proposed scheme can remove nonlinear distortions without requiring for any nonlinearity information. Since the nonlinearity in RoF channel may change with operation environment, the postcompensation and predistortion methods cannot track the change without adaptive methods. Although the adaptive linearization method can compensate the RoF nonlinearity dynamically, extra circuit is necessary to obtain the

nonlinearity information. Therefore, this method increases the complexity and cost of the RoF system. The proposed scheme can deal with the changing nonlinearity without any extra circuits because the nonlinearity information is not necessary. This research work has been accepted for publication in the *IEICE Transactions on Communications, February 2014,* and has been presented at the *IEEE 75th Vehicular Technology Conference (VTC2012-Spring), Yokohama, Japan on May 2012.*

- A modified Rapp model is proposed for the modelling of DFB LD. Although the original Rapp model has already been widely accepted for the modelling of PA nonlinearity, it cannot present nonlinearity of the DFB LDs. The modified Rapp model extends the flexibility of the original Rapp model to cover the nonlinear characteristics of DFB LDs. It does not only inherit the Rapp model's applicability, but also enlarges the scope of the application.
- Echo effect in RoF channel is studied and a RoF-echo model is proposed for the analysis of echo effect. The proposed model is confirmed by experiments. By using the RoF-echo model, the echo effect can be analyzed more comprehensive. The performance of the proposed EPWM-RoF transmission scheme in dealing with the echo effect is also evaluated by simulations and experiments. This research work has been presented at the *IEEE 2013 16th International Symposium on Wireless Personal Multimedia Communications (WPMC), Atlantic City, New Jersey, USA, June 2013.*
- An echo effect suppression scheme is proposed for mitigating the echo influence on the EPWM signal. By employing a designed class-C PA at the output of the RoF channel with echo effect and optimizing the operating parameters for the PA, the performance of EPWM-RoF transmission against RoF-echo can be improved.

1.4 Outline of the Dissertation

The structure of this dissertation is shown in Fig. 1.5. The dissertation consists of five chapters and is outlined below.

Chapter1 Introduce the background, motivations and scope of the research. Explain the existing methodologies in the research area, and the methods used in this dissertation. List the main contributions of the dissertation.

Chapter2 Explain the technical background of the research. First, introduce the RoF technology. Second, state the issues may exist in each element in the RoF system. Third, introduce the principle of OFDM, which is employed as an example of broadband wireless signals in all the simulations and experiments in this dissertation.

Chapter3 The principles and architectures of EPWM transmitter and its improved version Amplitude Noise Compensation-EPWM (ANC-EPWM) are

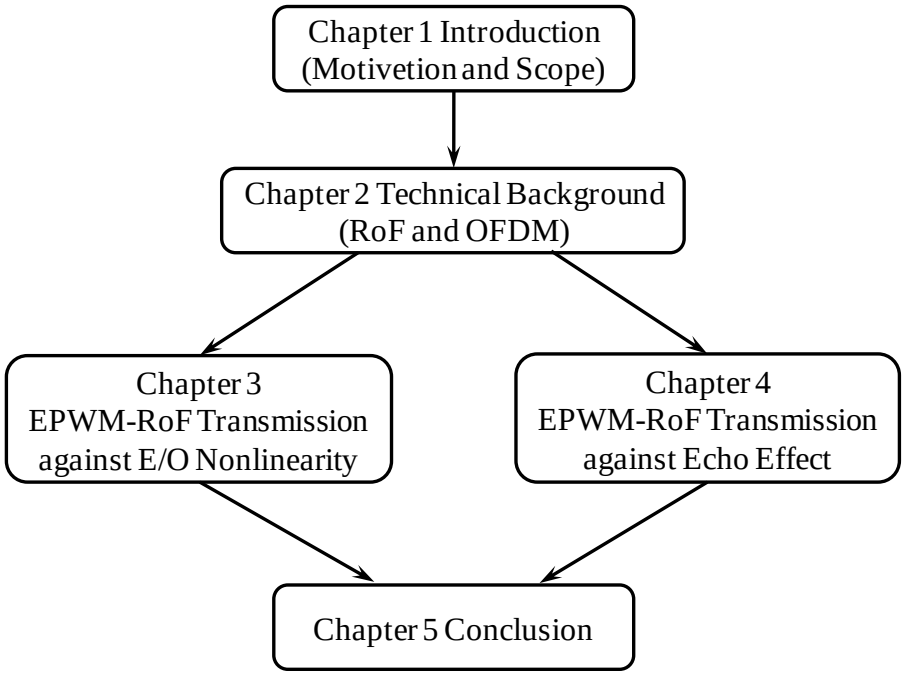

Fig. 1.5 Dissertation structure

described. EPWM-RoF transmission scheme proposed for OFDM signal transmission in RoF channel is presented. MZ modulator and DFB LD which are two commonly used E/O converters in optical fiber communications are studied. Their nonlinearity characteristics are measured by experiments and modelled mathematically. A modified Rapp model is proposed for DFB LD. Based on the researches on the E/O converters, the performance of EPWM-RoF transmission against E/O nonlinearity is evaluated by simulations and experiments.

Chapter4 A RoF-echo model is proposed for echo effect in RoF channel. Theoretical analysis of echo effect on the OFDM and EPWM signals is presented. The validity of the proposed model and the theoretical analysis are confirmed through experiments. By using the RoF-echo model, the performance of EPWM-RoF transmission against echo effect is evaluated by simulations. An echo effect suppression scheme is proposed for mitigating the echo influence on the EPWM signal. The performance of the proposed scheme is evaluated by simulations.

Chapter5 The research results on E/O nonlinearity and echo effect in RoF channel are summarized. Related future works are presented.

Chapter 2. Technical Background

This chapter explains the technical background of the researches in this dissertation. Principle of RoF technology is presented. Issues that exist in each element in the RoF channel is described. Principle of OFDM which is employed as an example of broadband wireless signal transmission in RoF channel is introduced.

2.1 Radio over Fiber (RoF) Technology

RoF is a technology that RF signals are transmitted through optical fibers. It is a promising technology that satisfies the demands for extending the coverage of wireless communication services. It employs optical fiber links that penetrate closer to users to deliver RF signals from central BS to RAUs with low cost.

Figure 2.1 shows a typical RoF system. In the downlink, the modulated RF signal is converted to optical signal by an E/O converter in a BS. The optical signal is then transmitted through the optical fiber to the RAUs. In the uplink, the received RF signals from users are converted to optical signals in RAUs, delivered by the optical fiber and reconverted to RF signals by an O/E converter in the BS. This system is a simplest form of RoF channel, and it is called Intensity Modulation with Direct Detection (IM-DD).

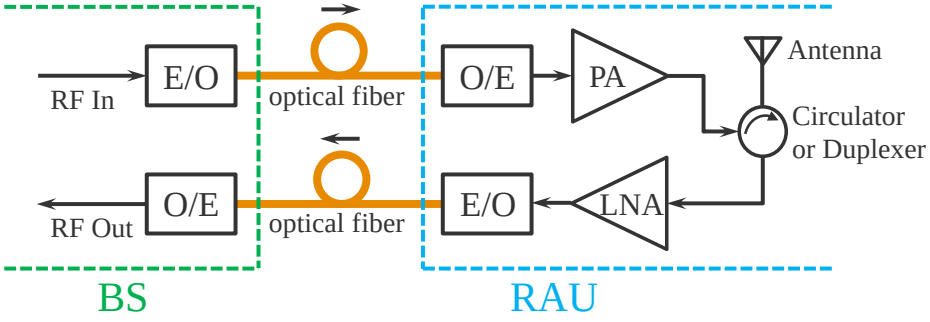

Fig. 2.1 RoF system

The advantage of IM-DD is that it is simple. The system could become linear if a low dispersion fiber is employed together with a linearized external modulator. As a result, the RoF channel acts as an amplifier or attenuator and it is thus transparent to the modulation format of RF signals [33]. RoF system does not need any upgrade whatever RF signal format changes. Sub-Carrier Multiplexing (SCM), which transmits many different communication signals along a single optical fiber, can also be used in such systems. Moreover, when mm wave signals are employed as RF signals, the system communication bandwidth can approach 100 GHz [11].

2.1.1 E/O Converter

There are two ways of modulating the light source. One way is to let the RF signal directly modulate the bias current of laser diode. The other way is to operate the laser in continuous wave (CW) mode and then use an external modulator such as the MZ modulator, to modulate the intensity of the light. Both options are shown in Fig. 2.2. In the two modulating forms, the modulating signal is the actual RF signal to be transmitted. The RF signal must be appropriately modulated with data before transmission. Nonlinearity of direct intensity modulation LD can vary with

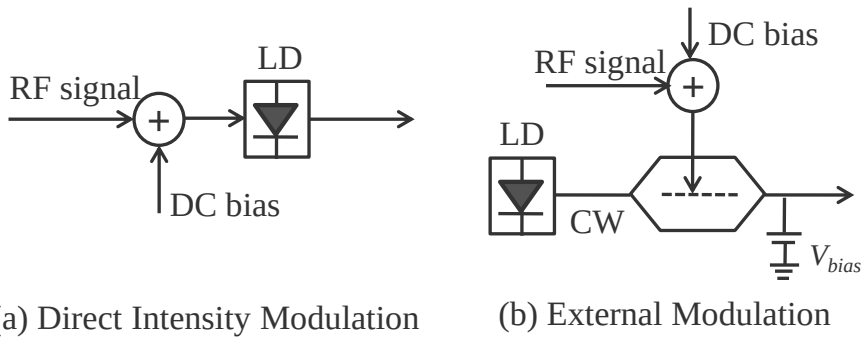

(a) Direct Intensity Modulation (b) External Modulation

Fig. 2.2 Two forms of modulating light source

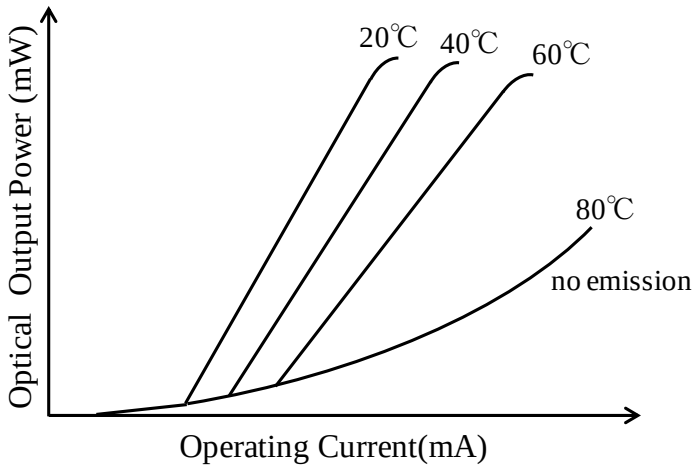

Fig. 2.3 LD transfer characteristic with temperature variation

temperature variations, changing of internal parameters and improper modulation. LD is highly sensitive to temperature variations. An increase in temperature will increase the threshold current and brings a drop in output power, as shown in Fig. 2.3. The laser cavity becomes very unstable when the LD operating temperature changes [34]. In addition, leakage current and axial hole burning can also vary the LD nonlinearity. The leakage current increases with injected current and temperature rise. The axial hole burning is caused by nonuniform optical power density along the length of the LD cavity [35].

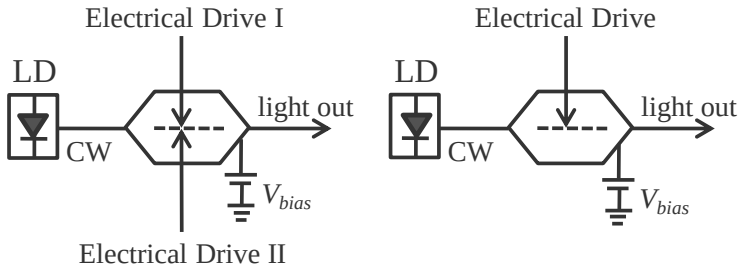

(a) Dual electrode (b) Single electrode

Fig. 2.4 Configurations of MZ modulator

There are few types of external modulators described in the literature: loss modulator, directional coupler modulator, total internal reflection modulator and MZ modulator [36, 37]. The MZ modulator is the most common external modulator and it is based on electro-optic effect, which provides a change in the optical waveguide refractive index proportional to the applied electric field. As a result, a phase change occurs for the incident optical field polarized in the direction of the electric field [36, 37]. Figure 2.4 (a) shows the configuration of a dual electrode MZ modulator. Although this type of modulator can achieve zero frequency chirp at very high frequencies, it is very difficult to match the impedance of the electrode to the RF source for a broadband frequency range [37]. High frequency modulators are mostly implemented with only one electrode, as shown in Fig. 2.4 (b). This electrode is matched to the characteristic impedance of the signal source, so that no standing waves are formed along the interaction region [38]. In this way, a broadband device can be built.

2.1.2 Optical Fiber

There are two types of optical fiber: Single Mode Fiber (SMF) and Multi-Mode Fiber (MMF). The major problem in optical fiber is dispersion, which includes

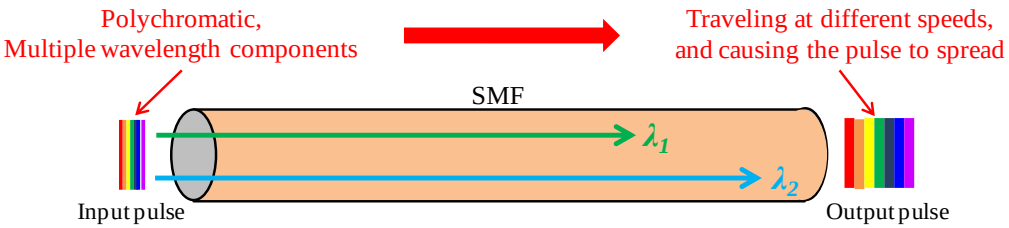

Fig. 2.5 Chromatic dispersion in SMF

mode and chromatic dispersion. Since the SMF can fully avoid mode dispersion, it is suitable for high capacity and long distance optical communications. Although mode dispersion exists in the MMF, it is easier than the SMF for manufacture, coupling and connection. In this dissertation, we mainly discuss the SMF. Attenuation and chromatic dispersion are two major factors of concern for SMF. Attenuation of SMF at operating wavelength of 1.55μm achieves minimum value that is about 0.2dB/km. Chromatic dispersion is an important characteristic in optical fiber. The speed of light in fiber is determined by the refractive index of the fiber. In an ideal situation, the refractive index would not depend on the wavelength of the light. However, different wavelengths travel at different speeds within an optical fiber, as shown in Fig. 2.5. The incident light is polychromatic and consists of multiple wavelength components. When the light travels through the SMF, different wavelength components have different propagation speeds, which result in a pulse spread in the output light signal. The chromatic dispersion of a fiber is expressed in ps/(nm*km), representing the differential delay, or time spreading (in ps), for a source with a wavelength of 1 nm traveling on 1 km of the fiber. It depends on the fiber type, and it limits the bit rate or the transmission distance for a good quality of service.

The transfer function of the single mode fiber can be modeled as below [39, 40]

$$H(f) = e^{-j\left[\pi D \frac{\lambda_0^2}{c} L f^2\right]}, \tag{2.1}$$

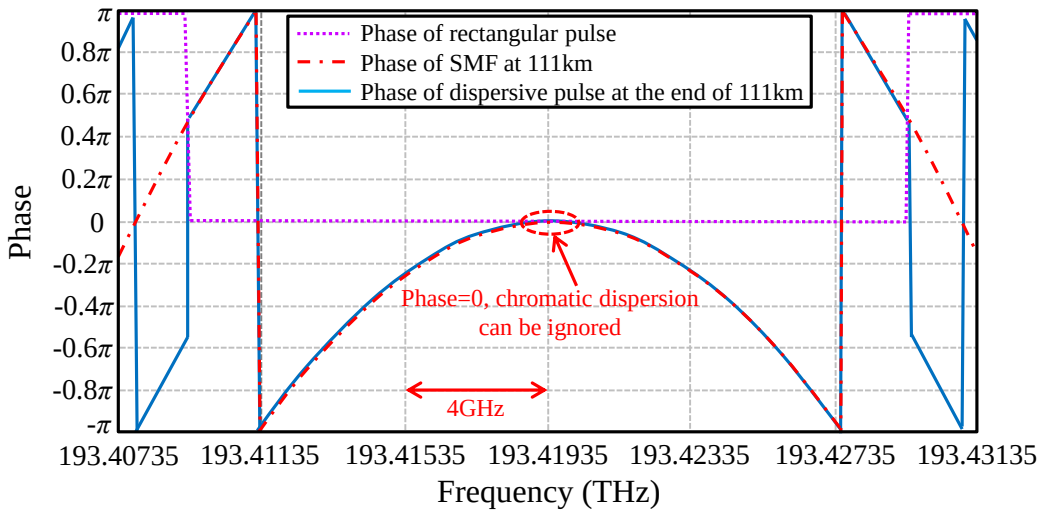

Fig. 2.6 Phase of $H(f)$ for an SMF operating at λ_0=1.55μm (193.41935 THz) over a length L=111 km. [40]

where D is the dispersion parameter. In the wavelength region near 1.55μm, D is about 17ps/nm*km. λ_0 is the operating wavelength, c is the velocity of light in vacuum, L is the length of fiber, and $f = f_{opt} - f_{carrier}$. f_{opt} is the optical frequency and $f_{carrier}$ is the optical carrier frequency. Figure 2.6 presents the phase change for a SMF operating at 1.55μm over a length of 111 km [40]. As shown in the figure, when the optical frequency is very close to the optical central frequency (193.41935 THz), the phase characteristic is flat and almost unchanged for the bandwidth of 1GHz or less. It means that the chromatic dispersion can be ignored in such situation. Therefore, if the bandwidth of input RF signal is smaller than a gigahertz, the chromatic dispersion can be neglected.

2.1.3 O/E Converter

Photo Detector (PD) which is also called O/E converter is an electronic device which converts optical power to electrical currents. For an ideal PD, its output

electrical current is proportional to the input light power. However, several noises are generated due to the photon to electron conversion, which include thermal noise, shot noise and dark current noise.

Thermal noise is a kind of current fluctuation phenomenon that caused by the random motion of electron in the load resister of the PD. Thermal noise is given by [13]

$$\sigma_T^2 = (4k_B T / R_L) F_n \Delta f \ , \tag{2.2}$$

where k_B is the Boltzmann constant, T is the absolute temperature, R_L is the load resister and Δf is the effective noise bandwidth. F_n represents the factor by which thermal noise is enhanced by various resistors used in pre- and main amplifiers.

Shot noise is a manifestation of the fact that an electric current consists of a stream of electrons that are generated at random times. Shot noise is expressed by [13]

$$\sigma_S^2 = 2q\left(I_p + I_d\right)\Delta f \ , \tag{2.3}$$

where q is the charge of an electron, I_p is the average current of the PD and I_d is the dark current which also generates shot noise.

Since the noises in PD do not affect the nonlinearity of RoF channel, these noises are neglected in this dissertation that focuses on the RoF nonlinearity.

2.2 Orthogonal Frequency Division Multiplexing (OFDM) Technique

OFDM technology is widely employed in broadcast services and broadband telecommunications including WLAN, 4G, WiMAX, television and radio broadcasting. In Digital Subscriber Loop (ADSL) applications, OFDM is also

called Discrete MultiTone (DMT) that provides 8Mbit/s data rate in 1MHz bandwidth [41]. OFDM scheme is employed as the physical access for the WLAN by the IEEE802.11standards. This is the first time OFDM is employed in packet service communications. Since then, OFDM is also employed as the physical standard in European Telecommunication Standards Institute (ETSI), Broadband Radio Access Networks (BRAN) and Metropolitan Milwaukee Association of Commerce (MMAC) [42].

2.2.1 OFDM System Description

OFDM improves the efficiency of utilizing the spectrum by transmitting parallel data streams onto different overlapping subcarriers [41, 42]. The subcarrier spacing is designed orthogonal to each other, which allows overlapping of the subcarriers, as show in Fig. 2.7.

OFDM system employs orthogonal subcarriers to transmit multiple data symbols simultaneously. As depicts in Fig. 2.8, the coded data symbols d_i are grouped into N parallel data streams and then they are modulated with the orthogonal subcarriers, which is expressed by $\exp(j2\pi f_i t)$. As shown in Fig. 2.8, this step can be simply implemented by Inverse Fast Fourier Transform (IFFT). Then the

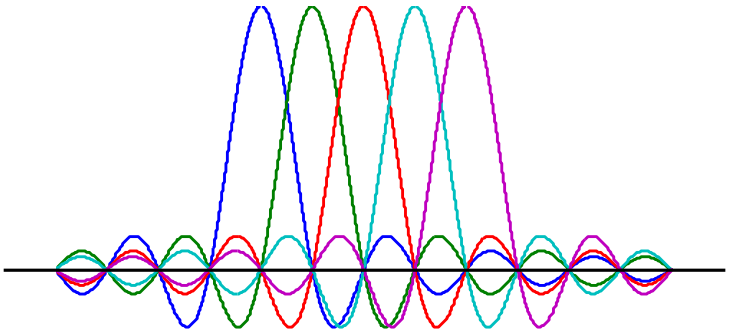

Fig. 2.7 Spectra of OFDM subcarriers

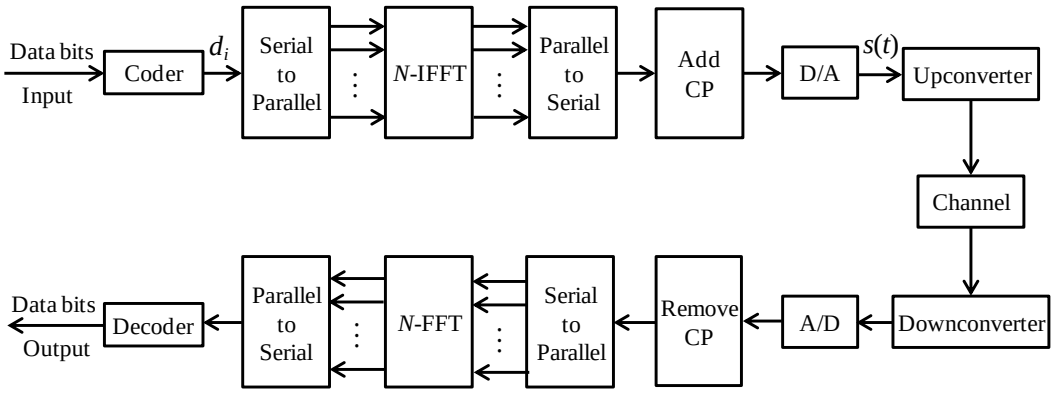

Fig. 2.8 Basic OFDM system block diagram

modulated symbols are rearranged to a serial stream and a Cyclic Prefix (CP), which is a copy of the last part of an OFDM symbol, is added to the beginning of the symbol. As long as the channel impulse response is shorter than the length of the CP, the received signal is just the cyclic convolution of the transmitted OFDM symbol and the channel impulse response. Thus, the orthogonality of the subcarriers is protected by the CP.

A baseband OFDM signal is expressed as

$$s(t) = \sum_{i=0}^{N-1} d_i \exp(j2\pi f_i t), \quad 0 \le t \le T_s, \tag{2.4}$$

where T_s is the period of the OFDM symbol. To ensure the orthogonality of the subcarriers, the correlation between the subcarriers should satisfy

$$\int_0^{T_s} \exp(j2\pi f_i t)\exp(j2\pi f_k t)dt = \begin{cases} 0, & (i \ne k) \\ T_s, & (i = k) \end{cases}. \tag{2.5}$$

Therefore, the subcarrier spacing of OFDM signal is a multiple of 1/ T_s. Demodulation of the OFDM signal is the opposite of the previous process as show in Fig. 2.8.

2.2.2 Advantages and Disadvantages of OFDM

Some advantages of the OFDM are described as follows.

- Robust against intersymbol interference (ISI) and fading caused by multipath propagation.
- High spectral efficiency.
- Efficient implementation using IFFT and FFT.
- Can realize different transmitting data rates for downlink and uplink by using different number of subcarriers for them.
- Dynamically allocate subchannels and data bits for users.
- Low sensitivity to time synchronization errors.
- Robust against narrow-band interference.

Since OFDM is a multi-carrier system, comparing with the single carrier system, it has several drawbacks as below.

- Sensitive to frequency errors: frequency offset can ruin the orthogonality of the subcarriers, thus causes Inter Carrier Interference (ICI) to the system.
- High Peak to Average Power Ratio (PAPR): An OFDM signal is formed by adding a number of data modulated independent subcarriers. This can produce a large PAPR when all subcarriers added up coherently [43]. When N signals are added with the same phase, they produce a peak power that is N times the average power [44]. PAPR is the ratio of the maximum power and the average power of a transmitted OFDM symbol, and it is defined as

$$PAPR = 10\log_{10}\frac{\max\{|s(t)|^2\}}{E\{|s(t)|^2\}}, \tag{2.6}$$

where E{・} denotes the expectation operation.

A Complementary Cumulative Distribution Function (CCDF) curve is shown in Fig. 2.9. It shows the amplitude distribution of OFDM signal. Due to the high PAPR, for amplification of OFDM signal, RF power amplifiers should be operated in a linear region. Otherwise, the signal peaks get into nonlinear or saturated region of the power amplifier causing signal distortion. The signal distortion introduces intermodulation among the subcarriers and out of band radiation. To avoid the nonlinear distortion, the power amplifiers should be operated with large power back-offs, which leads to very inefficient amplification and expensive transmitters. Thus, it is highly desirable to reduce the PAPR. To reduce the PAPR, several techniques have been proposed such as clipping, peak windowing [41, 43, 45, 46], coding [47-50], peak cancellation [41, 43, 47, 51, 52] and symbol scrambling [47, 53-55]. But, most of these methods are unable to achieve simultaneously a large reduction in PAPR with low complexity, with low coding overhead, without performance degradation and without transmitter /receiver symbol handshake [44].

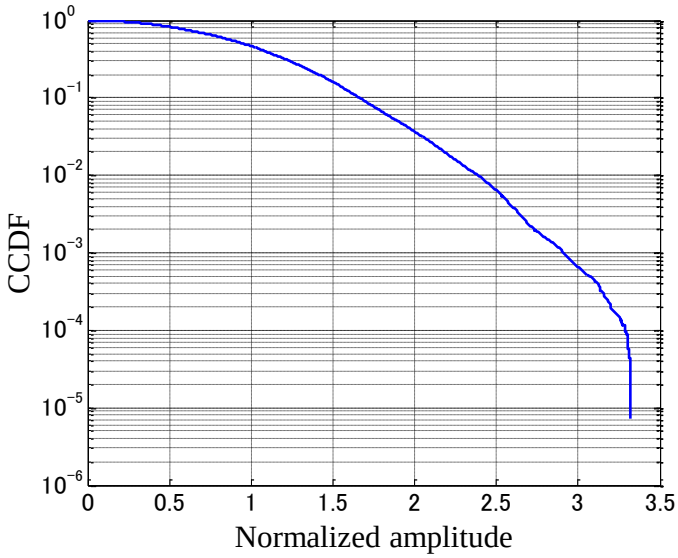

Fig. 2.9 CCDF of OFDM signal

 错误!使用“开始”选项卡将 見出し 1,Chapter 应用于要在此处显示的文字。

Chapter 3. EPWM-RoF Transmission against E/O Nonlinearity

Wireless communications is tending towards higher data rate and higher capacity to satisfy the increasing demands for data communication and Internet access. Since broadband transmission requires higher input level for receivers, dead spots of wireless coverage both in outdoor and indoor environments have become a serious issue. Radio over Fiber (RoF) is a promising technology to extend the coverage in such areas. However, when a wireless signal is transmitted via a RoF channel, nonlinearities in the channel become a concern for multicarrier signals such as Orthogonal Frequency Division Multiplexing (OFDM).

The nonlinearities in RoF channel mostly come from the Electrical/Optical (E/O) converters. In recent years, many studies on the nonlinear effects of E/O converters have been performed. Nonlinear effects of Mach-Zehnder (MZ) modulator on the OFDM signal have been studied and analyzed in [56-59]. In [57, 58], the nonlinear distortion caused by MZ modulator is compensated through predistortion method. The nonlinearity of direct modulation Laser Diode (LD) has been investigated in [35] [60-63]. Polynomial model is frequently employed to study the nonlinearity of LD [60-62]. However, the characteristic of LD is generally device dependent and changes with the operating environment. Therefore the coefficients of the

polynomial model must be updated by measuring the mutative characteristic of the LD. Adaptive linearization method for RoF channel has been proposed in [35, 63]. Although these methods can capture the changing characteristic of the LD, calculation of the coefficients of the polynomial model needs much computing and feedback circuit is also necessary to track the characteristic variation, which makes the RoF system more complicated and expensive.

In this chapter, we present a new RoF transmission scheme that is suitable for downlink OFDM signal transmission via nonlinear RoF channel. It is based on the concept of EPWM transmitter and ANC-EPWM transmitter [30-32]. The EPWM and ANC-EPWM transmitters are originally proposed for achieving linear power amplification of OFDM signals with high power efficiency. To deal with the E/O nonlinearity, EPWM transmitters are employed for OFDM signal propagation in RoF channel and the EPWM-RoF transmission system is presented. The proposed scheme can inherit full benefit of the EPWM/ANC-EPWM that protects the OFDM transmission from nonlinearity. It is not a compensation scheme but the scheme in which the OFDM signal is converted to a burst RF signal with constant amplitude and not affected by any nonlinearity.

In the RoF channel, two types of E/O converters, which are external modulation MZ modulator and direct modulation Distributed Feedback LD (DFB LD), are employed. The nonlinearities of the E/O converters are studied and extracted though experiment measurement. Based on the measured nonlinearity of the MZ modulator, a classic mathematical model is used in simulations to study the nonlinear distortion effect on OFDM and EPWM signals due to the MZ modulator nonlinearity. For the DFB LD, a modified Rapp model is given to fit the measured characteristic. The capability of the modified Rapp model is presented by simulations and experiments. Using this model, the nonlinearity effect of DFB LD on the OFDM and EPWM signals are also investigated. The EPWM-RoF transmission system is evaluated by Power Spectral Density (PSD) and Error

Vector Magnitude (EVM) performance through MATLAB simulations and experiments.

The rest of this chapter is arranged as follows. Section 3.1 and 3.2 introduce the EPWM and ANC-EPWM transmitters. EPWM-RoF system is described in Sec. 3.3. MZ modulator, DFB LD and corresponding analysis, simulation results are given in Sec. 3.4 and Sec. 3.5. Section 3.6 present the simulation and experiment results, respectively. The chapter is simply concluded in Sec. 3.7.

3.1 Envelope Pulse-Width Modulation (EPWM) Transmitter

The architecture of EPWM transmitter is shown in Fig. 3.1 [31]. From a complex baseband signal $e_B(t)$, the amplitude component $a(t)$ and phase component $\phi(t)$ are extracted by a complex envelop generator. The relationship between the baseband signal $e_B(t)$ and the modulating components is expressed as

$$e_B(t) = a(t)e^{j\phi(t)}. \tag{3.1}$$

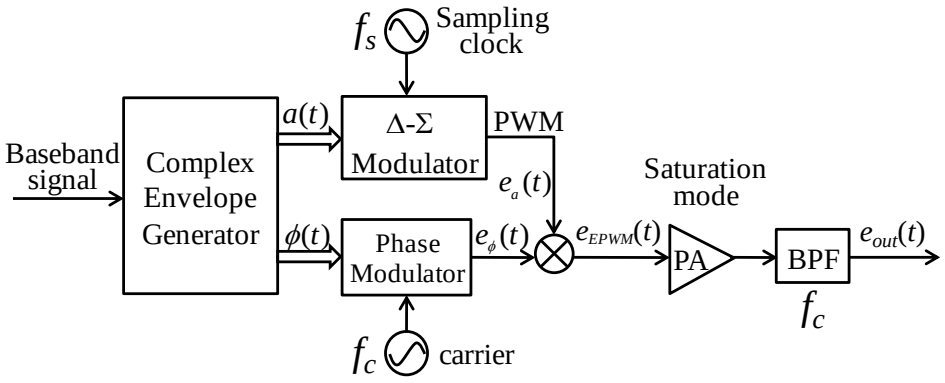

Fig. 3.1 EPWM transmitter [31]

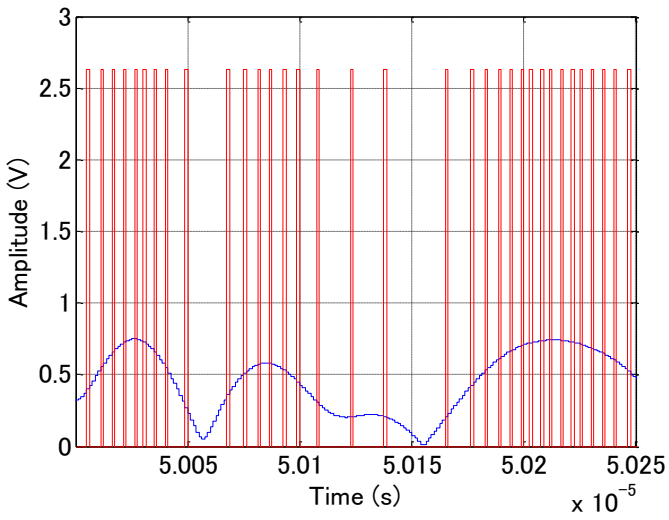

Fig. 3.2 Time domain PWM signal

Then the amplitude component $a(t)$ is converted to a Pulse Width Modulated (PWM) amplitude signal $e_a(t)$ by a Δ-Σ modulator using an oversampling frequency f_s. The PWM signal is shown in Fig. 3.2. It has only two statuses which are zero and constant value. The binary property of the PWM signal makes the EPWM signal immune to nonlinearity. However, quantization noise is generated by the Δ-Σ modulator. The quantization noise can be modelled as an additive noise [64]. Therefore, the PWM signal can be expressed as

$$e_a(t) = a(t) + q_e(t), \tag{3.2}$$

where $q_e(t)$ is the quantization noise output from the Δ-Σ modulator that has a shaped noise spectrum of reduced noise density in low frequency range.

The phase component $\phi(t)$ modulates an RF carrier with a carrier frequency of f_c. The phase modulated (PM) signal is written as

$$e_\phi(t) = \mathrm{Re}\left[e^{j\{2\pi f_c t + \phi(t)\}}\right]. \tag{3.3}$$

The resultant EPWM signal is the product of the PWM signal $e_a(t)$ and the PM signal $e_\phi(t)$, which is given by

$$\begin{aligned} e_{EPWM}(t) &= e_a(t)e_\phi(t) \\ &= \mathrm{Re}\left[a(t)e^{j\{2\pi f_c t+\phi(t)\}}\right]+q'_e(t) \end{aligned}, \tag{3.4}$$

where $q'_e(t)$ is the EPWM transmitter output noise given by [31]

$$q'_e(t) = q_e(t)e_\phi(t)\,. \tag{3.5}$$

The noise $q'_e(t)$ also has a noise-shaped spectrum similar to the $q_e(t)$ and most of the noise power appears in the outband of the input signal, as shown in Fig. 3.3 (a). Since the ideal RF signal $e_{rf}(t)$ at f_c can be expressed by

$$e_{rf}(t) = \mathrm{Re}\left[a(t)e^{j\{2\pi f_c t+\phi(t)\}}\right], \tag{3.6}$$

then the EPWM signal is

$$e_{EPWM}(t) = e_{rf}(t)+q'_e(t)\,. \tag{3.7}$$

A narrow bandpass filter (BPF) with central frequency f_c and a bandwidth more than 1.5 times of the bandwidth of the original signal is employed to remove the quantization noise $q'_e(t)$ that radiates outside the signal spectrum [31]. The output signal from the BPF is then given by

$$\begin{aligned} e_{out}(t) &= e_{EPWM}(t) * h_{BPF}(t) \\ &= e_{rf}(t)+q'_e(t) * h_{BPF}(t)\,. \\ &\approx e_{rf}(t) \end{aligned} \tag{3.8}$$

where $h_{BPF}(t)$ is the impulse response of the BPF and * denotes the convolution operation. The suppressed quantization noise $q'_e * h_{BPF}$ by the BPF is shown in Fig. 3.3 (b), where f_b denotes the single side bandwidth of the BPF.

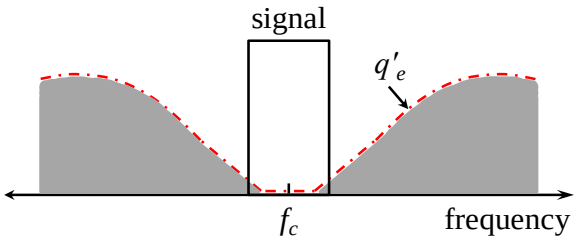

(a) Noise-shaped spectrum without BPF

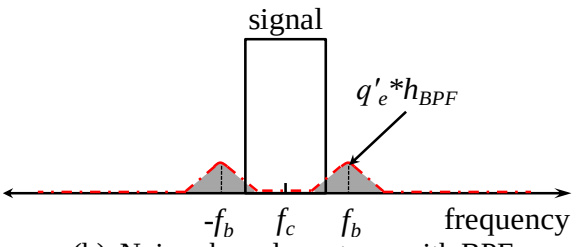

(b) Noise-shaped spectrum with BPF

Fig. 3.3 Noise-shaped spectrum in EPWM

In Fig. 3.1, the PA has nonlinearity that causes Amplitude-to-Amplitude (AM-AM) and Amplitude-to-Phase (AM-PM) conversions. If an input signal has a constant envelope like an FM signal, it does not suffer from nonlinearity. The other example of signal that is robust against nonlinearity is a burst RF signal having fixed amplitude. Any kind of frequency or phase modulation can be applied to the burst signal without suffering from nonlinear distortion. For EPWM signal, amplitude variation in the original input signal is removed by the Δ-Σ modulator and the resultant amplitude $e_a(t)$ appears as the PWM format that is either zero or constant. Thus, the input signal to the PA is a burst RF signal with fixed amplitude and does not suffer from nonlinearity.

Suppose a transmission system with AM-AM nonlinearity that is expressed by

$$y = y(x), \tag{3.9}$$

and the input of the transmission system is OFDM signal, where x and y are the

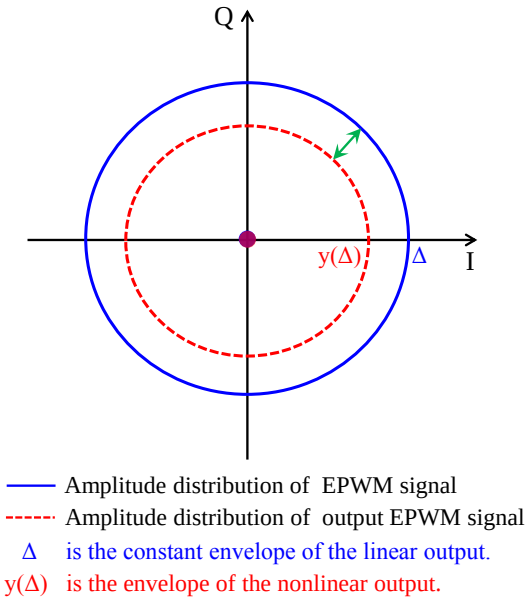

Fig. 3.4 Signal space diagram of input and output EPWM signals suffering from nonlinear transmission

input and output amplitude of the system. Due to the AM-AM nonlinearity, the original amplitude distribution of the OFDM signal is damaged and nonlinear distortion is caused. For EPWM signal, its amplitude distribution is shown in Fig. 3.4. The amplitude distribution of the output EPWM from the transmission system with the AM-AM nonlinearity is also shown in the figure. The output signal is similar to the input signal. We can see that binary property of the amplitude of the EPWM signal cannot be destroyed by the nonlinearity. Therefore, the EPWM signal has immunity to the nonlinear distortion.

3.2 Amplitude Noise Compensated EPWM (ANC-EPWM) Transmitter

To relax the narrow bandwidth requirement for the BPF, ANC-EPWM transmitter has been proposed [32]. Principle of the ANC-EPWM transmitter is shown in Fig. 3.5. The quantization noise $q_e(t)$ generated by the Δ-Σ modulator is extracted and filtered by a Low Pass Filter (LPF). The output of the LPF then undergoes an amplitude control function. An amplitude compensation coefficient $\beta(t)$ is generated by the function and controls the amplitude of the PM signal. Thus the quantization noise close to the signal spectrum can be suppressed. The amplitude compensation coefficient $\beta(t)$ is set as [32]

$$\begin{aligned}\beta(t) &= \frac{a(t)}{a(t)+q_L(t)} \\ &= \frac{a(t)}{a(t)+h_{LPF}(t)*q_e(t)} \\ &= 1-\frac{h_{LPF}(t)*q_e(t)}{a(t)+h_{LPF}(t)*q_e(t)}\end{aligned}, \tag{3.10}$$

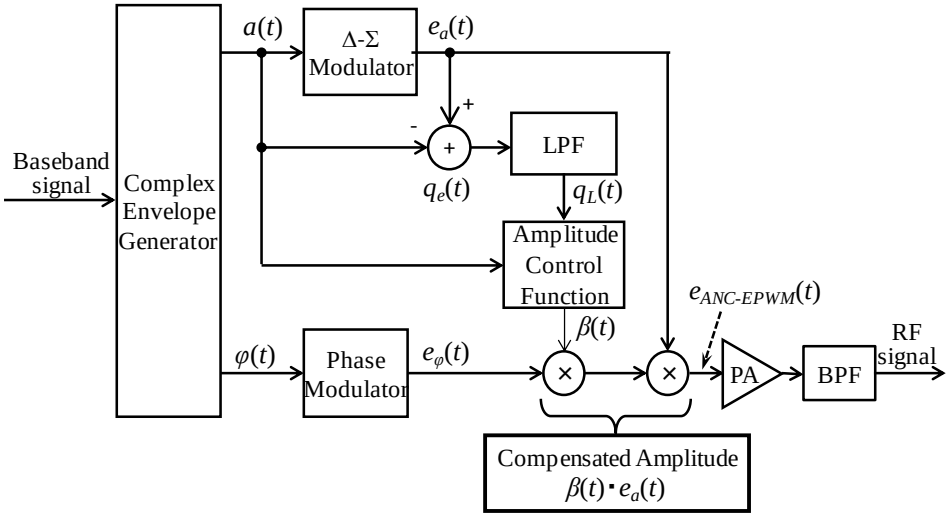

Fig. 3.5 ANC-EPWM transmitter [32]

where $h_{LPF}(t)$ is the impulse response of the LPF, $q_L(t)$ is the output signal of the LPF. Then the ANC-EPWM signal is given by

$$e_{ANC-EPWM}(t) = \beta(t)e_a(t)e_\phi(t). \tag{3.11}$$

The quantization noise suppression capability of ANC-EPWM transmitter is discussed in [32]. The amplitude of the ANC-EPWM signal $\beta(t)e_a(t)$ can be calculated as

$$\begin{aligned}\beta(t)e_a(t) &= \frac{a(t)}{a(t)+h_{LPF}(t)*q_e(t)}\left[a(t)+q_e(t)\right] \\ &= a(t)+\frac{a(t)\left[q_e(t)-h_{LPF}(t)*q_e(t)\right]}{a(t)+h_{LPF}(t)*q_e(t)}\end{aligned}. \tag{3.12}$$

The first term in Eq. 3.12 is the original amplitude of the input RF signal, and the second term is the suppressed quantization noise. Since the power of the quantization noise close to the signal spectrum is already suppressed by the noise-shaping property of the Δ-Σ modulator and the bandwidth of the LPF is several folds narrower than the overall bandwidth of the quantization noise, the output of the LPF $q_e(t)*\ h_{LPF}(t)$ is much smaller than $a(t)$. Thus, Eq. 3.12 can be approximated by

$$\begin{aligned}\beta(t)e_a(t) &= a(t)+\frac{a(t)\left[q_e(t)-h_{LPF}(t)*q_e(t)\right]}{a(t)+h_{LPF}(t)*q_e(t)} \\ &\approx a(t)+\left[q_e(t)-h_{LPF}(t)*q_e(t)\right]\end{aligned}, \tag{3.13}$$

Then Eq. 3.11 can be approximated by

$$e_{ANC-EPWM}(t) \approx e_{rf}(t)+q''_e(t), \tag{3.14}$$

where $q''_e(t)= [q_e(t)- h_{LPF}(t)*q_e(t)]e_\phi(t)$ is the suppressed quantization noise. Since the quantization noise close to the signal spectrum is suppressed, ANC-EPWM

scheme can relax the narrow bandwidth requirement for the BPF. On the other hand, ANC-EPWM adds an amplitude perturbation to the EPWM signal. The amplitude perturbation is given by the second term of Eq. 3.10.

To avoid the input signal overloading the Δ-Σ modulator, clipping level control is necessary for OFDM signals with high PAPR. The clipping level control is performed by using a clipping ratio Δ/σ [31], where Δ is the step-size of Δ-Σ modulator output and σ is the normalized amplitude corresponding to the average power of the OFDM signal.

3.3 EPWM-RoF Transmission System

The proposed EPWM-RoF transmission system is shown in Fig. 3.6. An EPWM formatted OFDM signal with RF carrier frequency f_c is generated in a central BS and then it is fed to the E/O convertor and converted to optical signal. After transmitted through the optical fiber, the optical signal is reconverted to electrical signal by an O/E convertor in a RAU. The RF signal is then amplified by a power amplifier which is operated in saturation mode and recovered as its original OFDM signal by a BPF, as shown in Eq. 3.8.

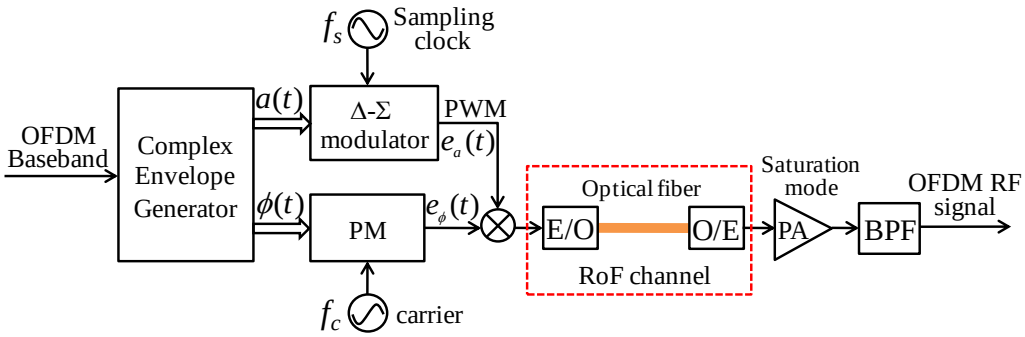

Fig. 3.6 EPWM-RoF transmission system

Although the proposed transmission scheme can employ any E/O convertors with different nonlinearity characteristics, we pick up two typical E/O converters to analyze the effects of E/O nonlinearity. They are MZ modulator and DFB LD which are commonly used in RoF systems.

3.4 Mach-Zehnder (MZ) Modulator

3.4.1 Theoretical Analysis

Figure 3.7 shows the structure of a single electrode MZ modulator. Suppose that the light source signal is given as $V_{in}=A_{opt}\cos(\omega_{opt}t)$, then the output optical signal from the modulator is given by [56-59]

$$v_{MZ}(t)=A_{opt}\cos\left[\frac{\pi}{2V_{\pi}}\left(v_{RF}(t)+V_{bias}\right)\right]\cos(\omega_{opt}t), \tag{3.15}$$

where A_{opt} and ω_{opt} are the amplitude and angular frequency of input light source, respectively. $v_{RF}(t)$ is an input RF signal and V_{bias} is the input DC bias voltage. V_{π} is called extinction voltage that is determined by the material of the modulator.

Figure 3.8 depicts the input/output characteristic of an MZ modulator that is measured from an actual device. Parameter V_{π} equals to the half cycle voltage. The input RF signal can be expressed as follows

$$\begin{aligned} v_{RF}(t) &= a_{RF}(t)\cos\left(\omega_c t+\phi(t)\right) \\ &= a_{RF}(t)\cos\left(\Phi(t)\right) \end{aligned}, \tag{3.16}$$

where $\Phi(t)=\omega_c t+\phi(t)$ and $\omega_c=2\pi f_c t$ is the carrier angular frequency of the RF signal. $a_{RF}(t)$ is the amplitude of the RF signal. If the maximum output power of the E/O converter is far less than the input saturation power of the PD, the PD can be

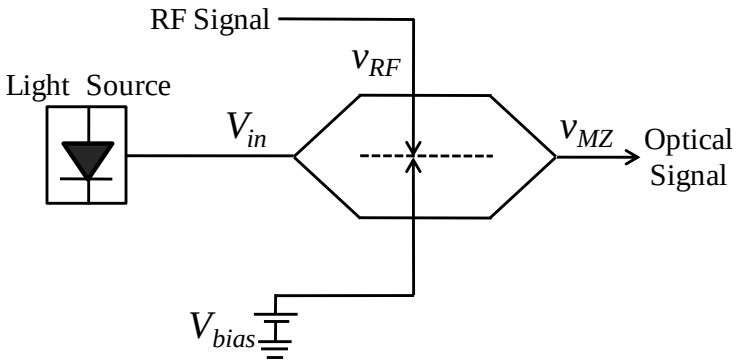

Fig. 3.7 Mach-Zehnder Modulator

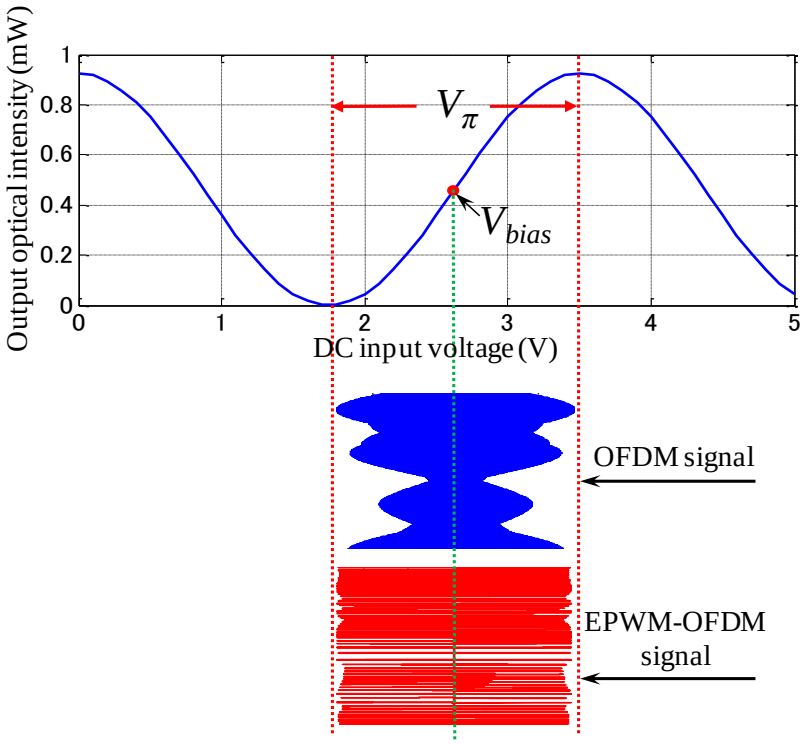

Fig. 3.8 Measured input/output characteristic of MZ modulator

assumed to be linear in the RoF transmission system. Then the output electrical current of PD is

$$i_{PD} = RP_{opt}, \tag{3.17}$$

where R is the conversion gain of the PD, and P_{opt} is the input optical power. Substitute Eq. 3.15 to Eq. 3.17, then

$$\begin{aligned} i_{PD} &= RP_{opt} \\ &= R\left|K_f v_{MZ}(t)\right|^2 \\ &= RK_f^2 A_{opt}^2 \cos^2\left[\frac{\pi}{2V_\pi}\left(v_{RF}(t)+V_{bias}\right)\right] \end{aligned} . \tag{3.18}$$

where K_f=$10^{(-G_{fiber}/20)}$, G_{fiber} (dB) is the optical fiber attention. Optimization of V_{bias} for the MZ modulator has been investigated in [65]. It concludes that when the DC bias is set at quadrature point (V_{bias}=KV_π/2), the maximum Spurious-Free Dynamic Range (SFDR), modulation efficiency and output/input gain of RF power can be achieved. Therefore, the value of V_{bias} is set to $3V_\pi$/2 as shown in Fig. 3.8. Substitute V_{bias} to Eq. 3.18, then

$$i_{PD} = \frac{RK_f^2 A_{opt}^2}{2}\left[1+\sin\left(\frac{\pi}{V_\pi}v_{RF}(t)\right)\right]. \tag{3.19}$$

Perform Taylor expansion to Eq. 3.19, then

$$i_{PD} = \frac{RA_{opt}^2}{2}\left[1+\frac{\pi}{V_\pi}v_{RF}(t)-\frac{\pi^3}{6V_\pi^3}v_{RF}^3(t)+\cdots\right]. \tag{3.20}$$

The first term in Eq. 3.20 is DC component and it can be removed at the output of PD by AC coupling. The second term is the recovered RF signal. The third term is the third order nonlinear distortion caused by the MZ modulator.

If we ignore the nonlinear components with orders higher than the third order in Eq. 3.20, substitute Eq. 3.16 to Eq. 3.20 and perform trigonometric formula will give the desired RF signal at ω_c, which is expressed as

$$i_{\omega_c} = \frac{RK_f^2 A_{opt}^2}{2}\left[\frac{\pi}{V_\pi} a_{RF}(t) - \frac{\pi^3}{8V_\pi^3} a_{RF}^3(t)\right]\cos\left(\omega_c t + \phi(t)\right). \tag{3.21}$$

Since the amplitude of EPWM-OFDM signal is converted to PWM format and it is either zero or constant, it can be written as

$$e_a(t) = \begin{cases} 0 \\ \Delta \end{cases}, \tag{3.22}$$

where Δ is the step-size of the Δ-Σ modulator output. Substitute Eq. 3.22 to Eq. 3.21, then the output EPWM-OFDM signal from PD at ω_c can be expressed as

$$i_{\omega_c - EPWM} = \begin{cases} 0, & e_a(t) = 0 \\ C\cos\left(\omega_c t + \phi(t)\right), & e_a(t) = \Delta \end{cases}, \tag{3.23}$$

where

$$C = \frac{RK_f^2 A_{opt}^2}{2}\left[\frac{\pi}{V_\pi}\Delta - \frac{\pi^3}{8V_\pi^3}\Delta^3\right], \tag{3.24}$$

Then the amplitude of $i_{\omega_c\text{-}EPWM}$ can be written as

$$a_{\omega_c - EPWM} = \begin{cases} 0, & e_a(t) = 0 \\ \mathrm{C}, & e_a(t) = \Delta \end{cases}, \tag{3.25}$$

Eq. 3.25 shows that the amplitude of the EPWM-OFDM signal at the PD output keeps zero or constant. Therefore, EPWM-OFDM signal does not suffer from the nonlinear distortion.

3.4.2 Simulation Results

Based on the model of the MZ modulator several simulations were performed to investigate the MZ modulator nonlinear effects on the OFDM and EPWM/ANC-EPWM- OFDM signals in detail. Simulation diagram is shown in Fig. 3.9. OFDM-RF signal is obtained by up converting the baseband signal to the RF frequency f_c. Meanwhile, EPWM-OFDM or ANC-EPWM-OFDM signal is generated with the same RF frequency. The RF signals are then converted to optical signals by an E/O converter which in this section is an MZ modulator. After transmitted through the optical fiber, a PD that is supposed to be linear is employed to recover the RF signals. The DC component in the PD output signals is then removed and the PSD and EVM are measured. Attenuation and chromatic dispersion are two major factors that should be considered for SMF. Typical attenuation of the SMF at operating wavelength of 1.55μm is 0.2dB/km. When the frequency of input RF signal is less than a few GHz and the fiber length is shorter than a few tens of kilometers, the chromatic dispersion is small enough to be ignored [69]. Therefore, the SMF can be modelled as an all pass filter with attenuation.

Simulation conditions are listed in Table. 3-1. The baseband OFDM signal was generated according to the IEEE 802.11a standard, and its major parameters are listed in Table. 3-1. The PAPR of the baseband OFDM signal is 11.5dB with

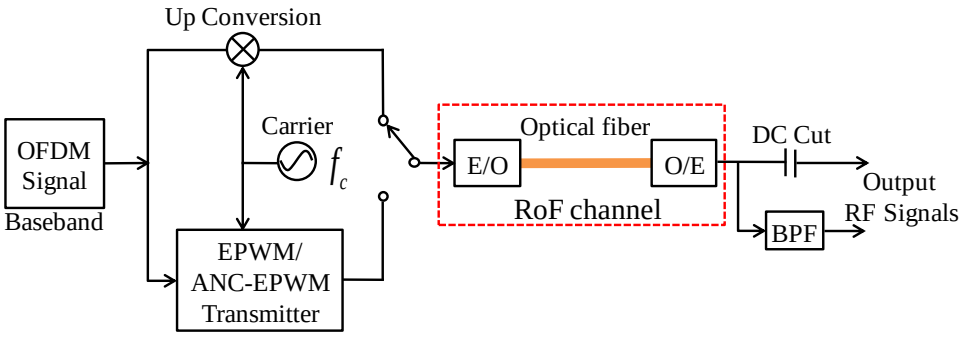

Fig. 3.9 Simulation diagram

Table 3-1 Simulation conditions

Baseband OFDM Signal	modulation	64QAM
	subcarriers	52
	symbol duration	4μs
	guard interval	0.8μs
	bandwidth	16.6MHz
	IFFT time domain window	trapezoidal window
	PAPR (CCDF of 10^{-4})	11.5dB
EPWM Transmitter	1st-order Δ-Σ modulator, OSR=32,	
ANC-EPWM Transmitter	2nd-order Δ-Σ modulator, OSR=32, f_0=f_L=30 MHz, PAPR=3dB for burst on	
RF Frequency	f_c=1.28 GHz	
MZ Modulator	V_π=1.75 V, V_{bias}=2.625 V, λ_0=1.55μm	
DFB LD	I_{bias}=38 mA, λ_0=1.55μm	
Optical Fiber	Single mode, 5km	
PD	R=0.6 A/W, 3dB bandwidth is 12GHz	
BPF	2-pole Butterworth filter with 3dB bandwidth of 33.2MHz	

CCDF of 10^{-4}. The RF frequency defined by the IEEE 802.11a standard is in 5 GHz band. In our simulation, it was changed to 1.28GHz, for the consistency with the experimental condition. First-order and 2nd-order Δ-Σ modulators were employed for EPWM and ANC-EPWM transmitters, respectively. For both of the transmitters, their oversampling ratio (OSR) and clipping probability were 32 and 0.1%, respectively. The null response frequency f_0 and the cut-off frequency f_L of the LPF for the ANC-EPWM transmitter were set to 30MHz. The PAPR of the generated ANC-EPWM-OFDM signal for burst-on status is 3dB. Figure 3.10 shows the PSD of the generated OFDM signals.

The characteristics of the MZ modulator is same as described in Fig. 3.8. The peak amplitudes of input RF signals were set equally so that the input signals undergo the same level of nonlinear distortion at the MZ modulator. At the output of the RoF channel, a 2- pole Butterworth BPF with 3dB bandwidth of 33.2MHz was employed to remove the outband radiation of intermodulation (IM) distortion and quantization noise.

Figure 3.11 depicts the PSDs of output RF signals from the RoF channel employing MZ modulator. The peak amplitudes of input signals were set 1.3V. In Fig. 3.11, we can see for the three transmission schemes that the 3rd order harmonic waves are generated due to the nonlinearity of MZ modulator, as analyzed in Eq. 3.20. The PSDs for output RF signals after filtered by the BPF are shown in Fig. 3.12. The quantization noise and the harmonic waves in EPWM-OFDM and ANC-EPWM-OFDM signals in Fig. 3.11 are almost removed by the BPF.

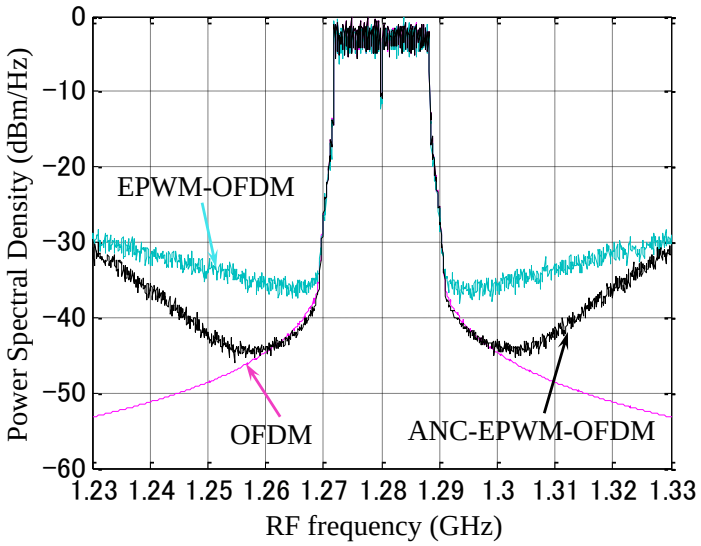

Fig. 3.10 PSD of input RF signal

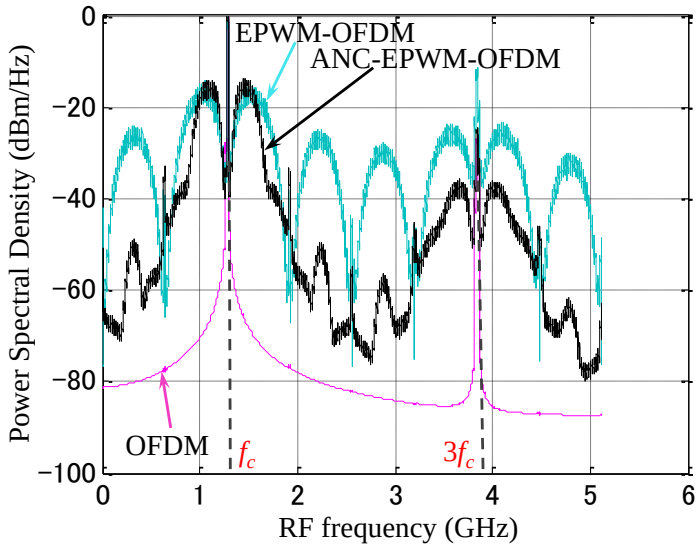

Fig. 3.11 PSD of PD output for MZ modulator RoF without BPF

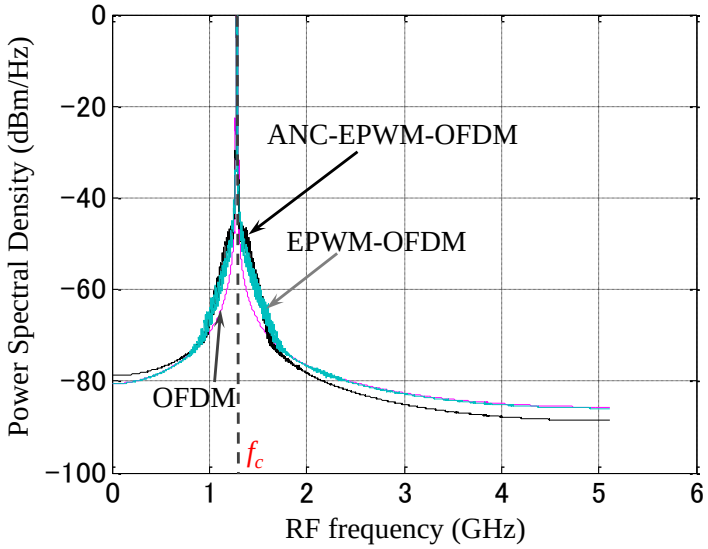

Fig. 3.12 PSD of PD output for MZ modulator RoF with BPF

Fig. 3.13 (a) and (b) closes up the PSDs for output RF signals. Nonlinear distortion spectrum around the signal band can be observed for OFDM and ANC-EPWM-OFDM signals with and without BPF. It is obvious that the nonlinear effect of MZ modulator on the ANC-EPWM-OFDM signal is smaller than on the original OFDM signal. The EPWM-OFDM signal is not affected by the nonlinearity. The SFDR of ANC-EPWM-OFDM signal is about 6dB larger than that of the OFDM signal. As shown in Fig. 3.13 (b), after filtered by the BPF, the quantization noise in EPWM-OFDM and ANC-EPWM-OFDM signals are suppressed. However, the nonlinear distortion in the OFDM signal band cannot be removed by the BPF. For reference, the spectrum mask specified in IEEE 802.11a is added in the figure. The EVMs for OFDM, EPWM-OFDM and ANC-EPWM-OFDM signals in Fig. 3.13 (b) are 9.88%, 1.67% and 4.85% respectively.

EVM is a measure of the difference between the reference symbols and the measured symbols. Figure 3.14 shows the error vector. Suppose $\hat{v}$ is the ideal symbol and $\hat{w}$ is the received symbol. Then $\hat{e}$ is the error vector. EVM is calculated by

$$EVM = \sqrt{\frac{\sum_{n=1}^{N} |\hat{v}_n - \hat{w}_n|^2}{\sum_{n=1}^{N} |\hat{v}_n|^2}} \tag{3.26}$$

where N is the number of the symbols. The EVM measurement diagram is shown in Fig. 3.15.

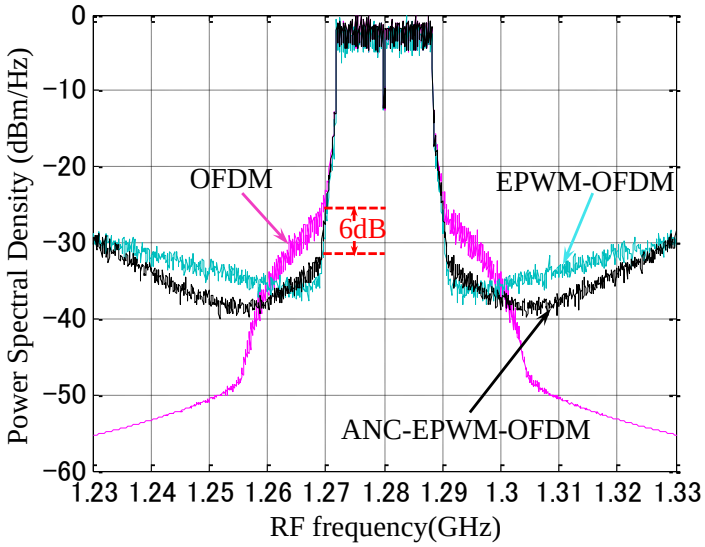

(a) Without BPF

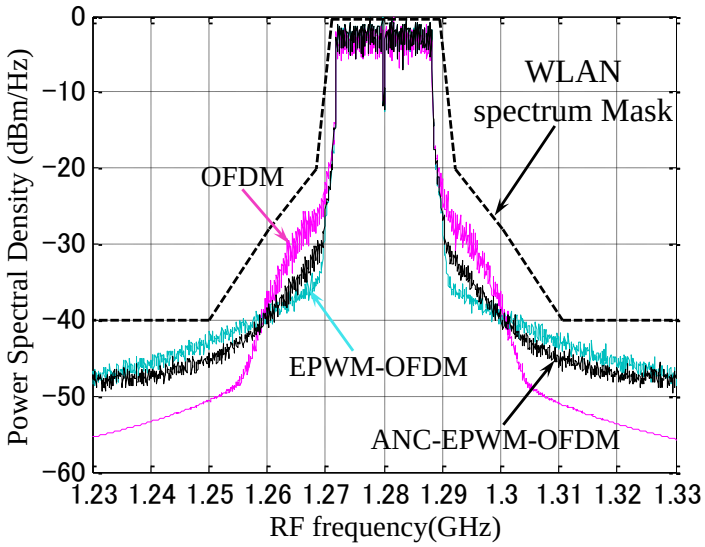

(b) With BPF

Fig. 3.13 PSD of output signals from RoF channel employing MZ modulator

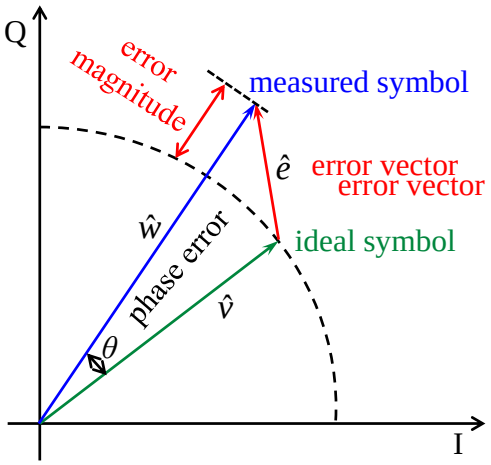

Fig. 3.14 Error vector diagram

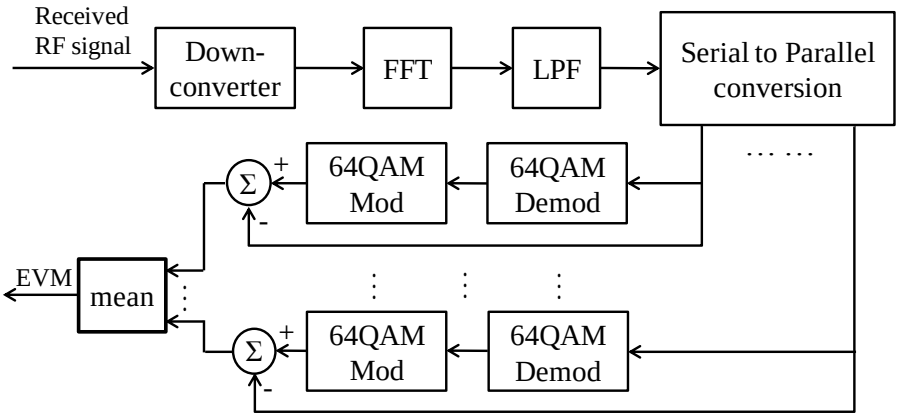

Fig. 3.15 EVM measurement

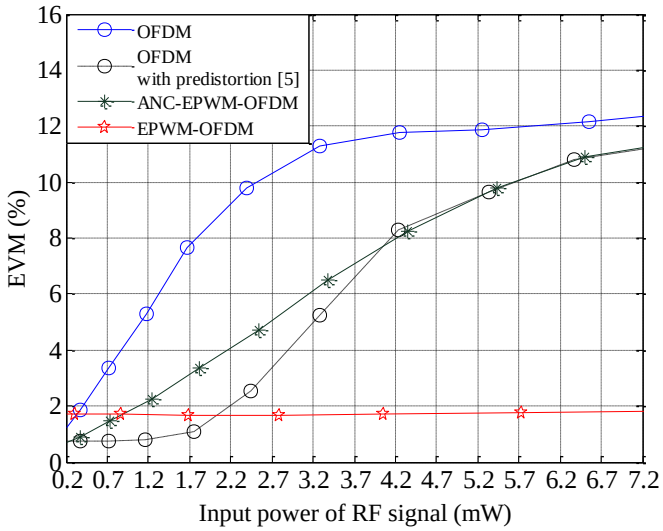

Fig. 3.16 EVM performance for MZ modulator RoF

Figure 3.16 compares the EVM performance of the proposed RoF schemes with that of the predistortion method employed in [57]. EPWM-OFDM signal keeps low EVM performance comparing with the other signals. Its EVM is almost constant benefiting from its binary amplitude property, as analyzed in Eq. 3.25. On the other hand, OFDM with or without predistorter and ANC-EPWM-OFDM signals are contaminated by the nonlinear distortion caused by the MZ modulator and their EVMs increase as the input signal power increases. Nevertheless, the EVM of ANC-EPWM-OFDM signal is better than that of the original OFDM signal, because its amplitude fluctuation is smaller. Although the EVM for the original OFDM signal is improved by the predistortion, it is still larger than that of the EPWM-OFDM signal and similar to that of the ANC-EPWM-OFDM signal when the input signal power is large.

3.5 Distributed Feedback Laser Diode (DFB LD)

3.5.1 Modified Rapp Model and Theoretical Analysis

Direct modulation LD is another commonly used E/O converter. In general, nonlinearity is classified into static nonlinearity without memory effect, and dynamic nonlinearity that has memory effect. When the RF frequency of input signal is lower than at least one fifth of the resonance frequency of LD, the LD nonlinearity can be assumed to be memoryless [66]. The resonance frequency of LD employed in this paper is 15 GHz, which is more than 10 times higher than the RF frequency (1.28GHz) we used in the experiments. Therefore, the LD nonlinearity is assumed to be memoryless. Since the nonlinearity of LD mainly appears as an AM/AM characteristic [67], we only consider the AM/AM characteristic of LD in this paper.

Figure 3.17 depicts the measured AM/AM characteristic of a DFB LD with a bias current (I_{bias}) of 38mA. Carrier frequency of the input RF signal is 1.28GHz.

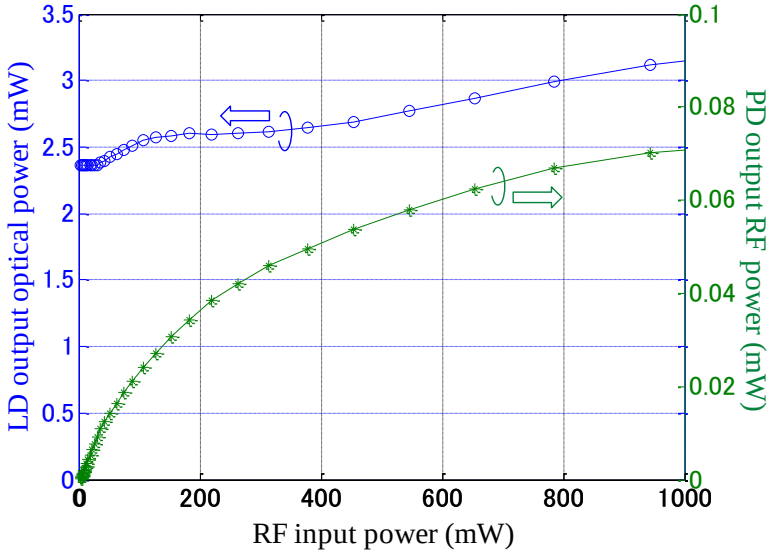

Fig. 3.17 Measured LD characteristics

The upper curve and the left vertical axis show the relationship between the LD output optical power and the input RF signal power. The curve exhibits a class AB operation: when the input RF power is small, the output optical power is constant; as the RF power increases, the output optical power increases gradually. The lower curve and the right vertical axis show the characteristic of output RF power from PD versus the input RF power.

To model the measured AM-AM modulation characteristic of the DFB LD, a modified Rapp model is introduced in this section. The original Rapp model is given by [68]

$$a_{out}(t) = \frac{Ka_{in}(t)}{\left[1+\left(\frac{Ka_{in}(t)}{E_{\max}}\right)^{2p}\right]^{\frac{1}{2p}}}, \tag{3.27}$$

where $a_{in}(t)$ and $a_{out}(t)$ are the input and output amplitude signal of the model, respectively. K is the small signal gain, E_{max} is the limiting output amplitude. p is called “knee factor” that controls the smoothness of the transition from the linear region to the saturation region of the nonlinearity characteristic. The nonlinear AM-AM characteristics generated by the Rapp model with different value of p are shown in Fig. 3.18. With p increases, the “knee” becomes more salient.

Generally, nonlinearity is expressed by the Taylorseries to study the nonlinear components it caused. Perform Taylor expansion to Eq. 3.27, then

$$a_{out}(t) = Ka_{in}(t) - \frac{K^{2p+1}}{2pE_{\max}^{2p}}a_{in}^{2p+1}(t) + \frac{(2p+1)K^{4p+1}}{8p^2E_{\max}^{4p}}a_{in}^{4p+1}(t) + \cdots. \tag{3.28}$$

The second term and the terms behind it are the nonlinear components, and they are the input signal $a_{in}(t)$ to the power n, where n is a positive integer larger than one. Therefore, to apply the Rapp model for the mathematical analysis of nonlinearity

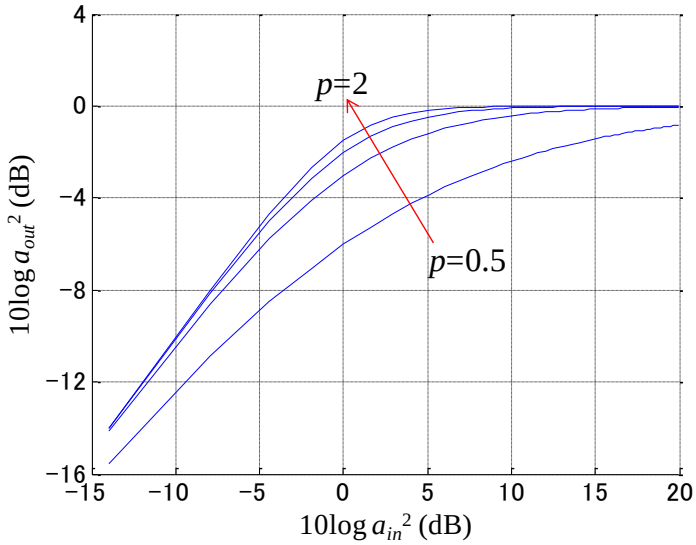

K=1, E_{max}=1, p=0.5~2 (step size = 0.5)

Fig. 3.18 AM-AM characteristics generated by the original Rapp model

effects, p has to be integer times of 0.5, which result in a discontinuity of the “knee”. This imperfection makes the Rapp model inflexible and limits its scope of application.

We propose a modified Rapp by which the flexibility and the application extent of the original Rapp model can be extended. The modified Rapp is given by

$$a_{out}(t) = \frac{Ka_{in}(t)}{\left[1+\left(\frac{Ka_{in}(t)}{E_{\max}}\right)^{2p}\right]^{\frac{\mu}{2p}}}. \tag{3.29}$$

Comparing with the original Rapp model, a parameter μ is introduced. Perform Taylor expansion to Eq. 3.29, then

$$a_{out}(t) = Ka_{in}(t) - \frac{\mu K^{2p+1}}{2pE_{\max}^{2p}} a_{in}^{2p+1}(t) + \frac{\mu(\mu+2p)K^{4p+1}}{8p^2E_{\max}^{4p}} a_{in}^{4p+1}(t) + \cdots. \tag{3.30}$$

Although p still has to be integer times of 0.5, the “knee” can be controlled

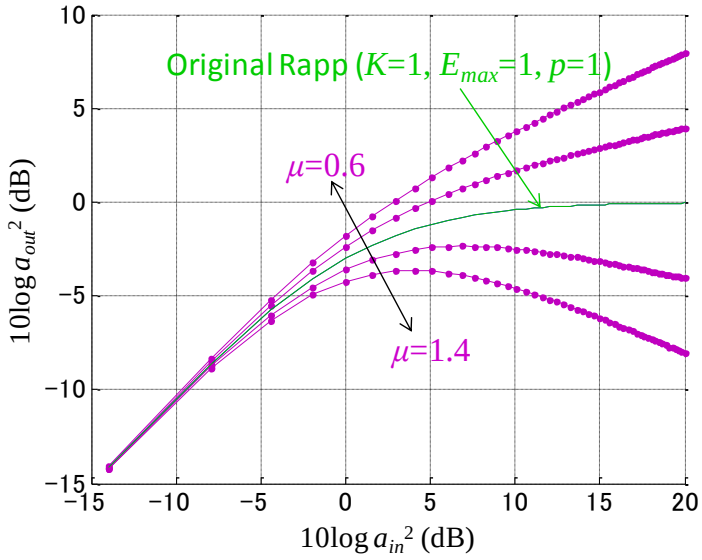

K=1, E_{max}=1, p=1, μ=0.6~1.4 (step size = 0.2)

Fig. 3.19 AM-AM characteristics generated by the modified Rapp model

continuously by continue values of μ. The effect of introducing μ is shown in Fig. 3.19. The figure shows that even if p is fixed, different “knee” can be achieved by controlling μ. Moreover, the characteristics after saturation are represented by μ. If μ is larger than p, the output power decreases after saturation. Otherwise, the output power increases. Comparing Fig. 3.18 and Fig. 3.19, it can be observed that the flexibility of the Rapp model is extended by the proposal. To illustrate the validity of the modified Rapp model, we measured two different characteristics of DFB LD with different bias currents. The measured and simulated DFB LD characteristics are shown in Fig. 3.20. The optimized parameters of the model to fit the measured DFB LD characteristics are listed in Table. 3-2. As shown in Fig. 3.20, the simulated AM-AM characteristics by the modified Rapp model fit the actually measured characteristics very well, even if the characteristic changes with the operating bias current.

Table 3-2 Parameters for the modified Rapp model

I_{bias}	K	E_{max}	p	μ
38mA	0.0031	0.0533	0.5	2.1
70mA	0.00248	0.00625	1	7.1

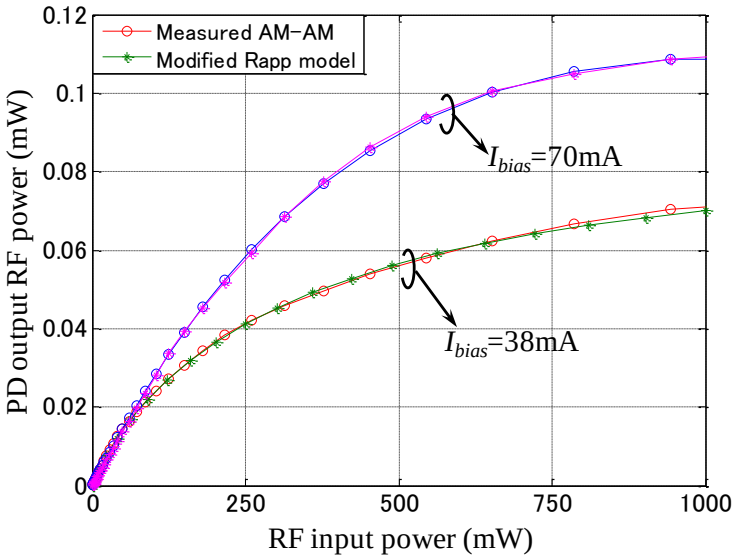

Fig. 3.20 Modified Rapp model fitting for a LD with different bias.

For the characteristic of LD with bias current of 38mA, substitute p=0.5 to Eq. 3.30, we can get

$$a_{out}(t) = m_1 a_{in}(t) - m_2 a_{in}^2(t) + m_3 a_{in}^3(t) + \cdots, \tag{3.31}$$

where m_1=K, m_2=$\mu K^2/E_{\max}$ and $m_3 = \mu(\mu-1)K^3/2E_{\max}^2$. The first term in Eq. 3.31 is the amplitude of output RF signal. The second and the third terms are the nonlinear distortions caused by the DFB LD. Unlike MZ modular, the nonlinearity of LD biased at 38mA is composed of both even and odd order nonlinearities. The final PD output RF signal at ω_c is then given by

$$v_{PD}(t) = a_{out}(t)\cos\left(\omega_c t + \phi(t)\right). \tag{3.32}$$

It should be noticed that only the signal at fundamental RF frequency ω_c is focused for the DFB LD and no harmonic components are shown in Eq.3.32. For EPWM-OFDM signal, the input amplitude of the Modified Rapp model $a_{in}(t)$ corresponds to $e_a(t)$. Then, by substituting Eq. 3.22 to Eq. 3.31, the amplitude of output EPWM-OFDM signal from the RoF channel using DFB LD can be derived to

$$a'_{\omega_c - EPWM} = \begin{cases} 0, & e_a(t) = 0 \\ C', & e_a(t) = \Delta \end{cases}, \tag{3.33}$$

where

$$C' = m_1 \Delta - m_2 \Delta^2 + m_3 \Delta^3. \tag{3.34}$$

Equation 3.33 shows that the binary amplitude property of the EPWM-OFDM signal keeps unchanged. Therefore, EPWM-OFDM signal does not suffer from the nonlinear distortion caused by the DFB LD.

3.5.2 Simulation Results

The simulation diagram and conditions are same as shown in Fig. 3.9 and Table 3-1. Figure 3.10 and Fig. 3.17 show the PSD of input RF signals and the characteristic of the DFB LD employed in the simulation. The PSDs of output RF signals from the RoF channel employing DFB LD is shown in Fig. 3.21. The peak amplitudes of input signals were set 5.5V. It can be observed in Fig. 3.21 (a) that ANC-EPWM-OFDM signal is much less affected by the nonlinearity of DFB LD. The SFDR of ANC-EPWM-OFDM signal is about 8dB larger than OFDM signal. As shown in Fig. 3.21 (b), the quantization noise and IM distortion in outband are removed by the BPF. However the nonlinear distortion in the signal band is not

suppressed. The EVMs for OFDM, EPWM-OFDM and ANC-EPWM-OFDM signals in Fig. 3.21 (b) are 8.24%, 1.59% and 2.69%, respectively.

Figure 3.22 compares the EVM performance of the output RF signals. The EVM for EPWM-OFDM signal is still not affected by the nonlinearity of DFB LD. Comparing the nonlinear distortion effects caused by the two E/O converters on the OFDM and ANC-EPWM-OFDM signals, EVMs in Fig. 3.16 and Fig. 3.22 exhibit different trends with input RF power increases. Since the nonlinearity of the DFB LD generates both odd and even order nonlinear components, EVMs for DFB LD increase rapidly, whereas the increase of EVMs for MZ modulator is moderate.

For the two E/O converters with different nonlinearities, the proposed schemes have good SFDR and EVM performance, which indicates the robustness of EPWM/ANC-EPWM transmission against the E/O nonlinearity.

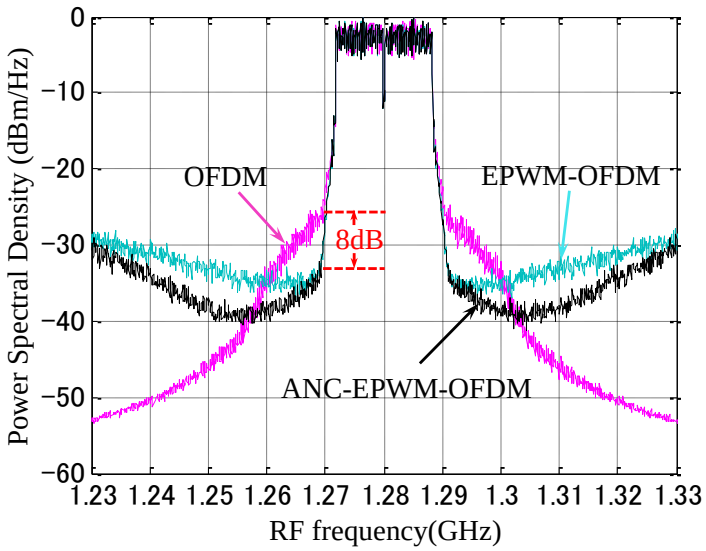

(a) Without BPF

Fig. 3.21 PSD of output signals from RoF channel employing DFB LD

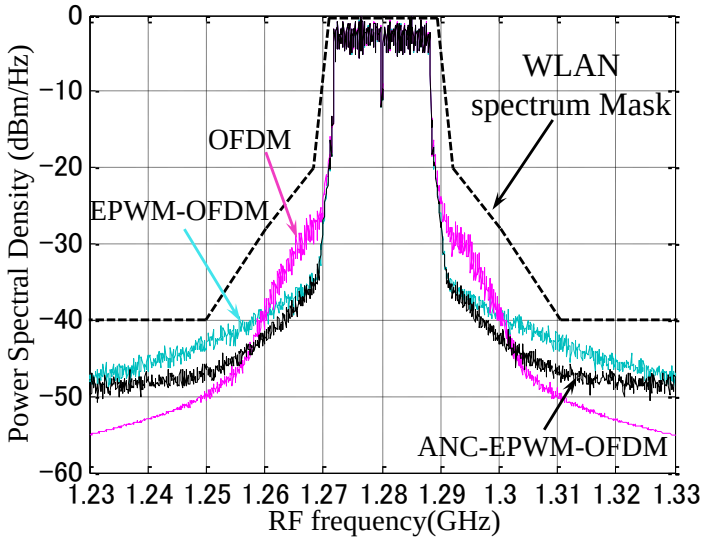

(b) With BPF

Fig. 3.22 PSD of output signals from RoF channel employing DFB LD

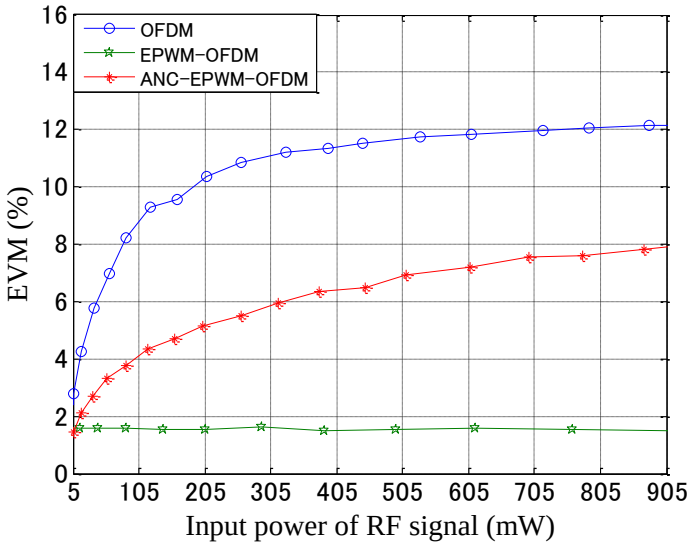

Fig. 3.23 EVM performance for DFB LD RoF

3.6 Experiment Results

To confirm the simulation results shown in Sec. 3.4.2 and Sec. 3.5.2, several experiments were conducted. The experiment setup is shown in Fig. 3.23. The input RF signals were generated by Agilent M8190A waveform generator. The signal parameters were the same as those listed in Table 3-1. T· MZH1.5-10PD-ADC-S-Y-Z MZ modulator made by SUMITOMO OSAKA CEMENT CO.,LTD. and NLK5C5EBKA DFB laser diode made by NEL with the characteristics shown in Fig. 3.8 and Fig. 3.17 were employed as E/O converters. A DSC50S type PD made by Discovery Semiconductors, Inc. with the characteristic shown in Fig. 3.24 was employed as the O/E converter. The horizontal axis denotes the input optical power of PD and the vertical axis denotes the PD output current. The measured characteristic is linear in the working region for the use of the RoF system. The

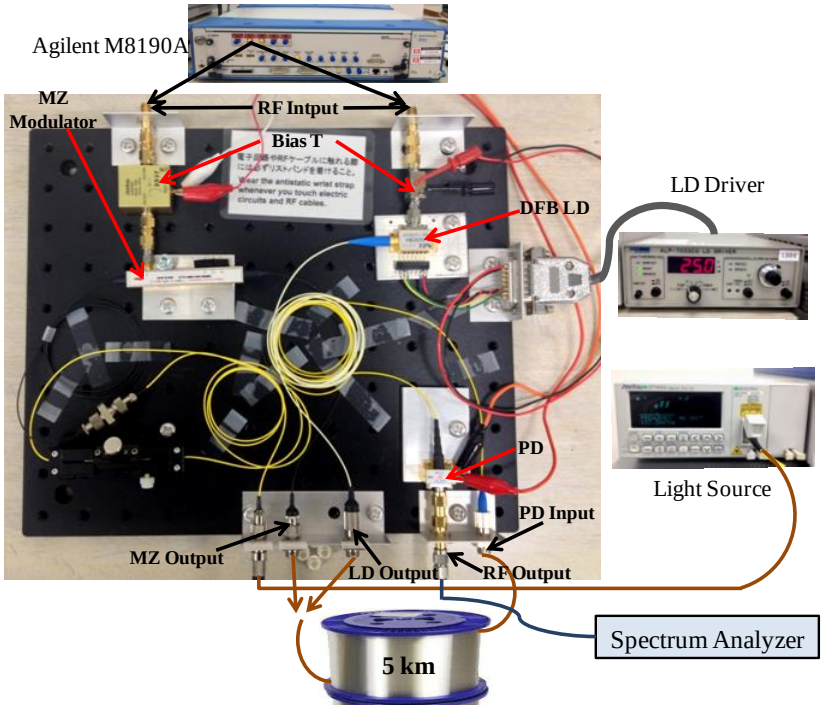

Fig. 3.24 Experiment setup

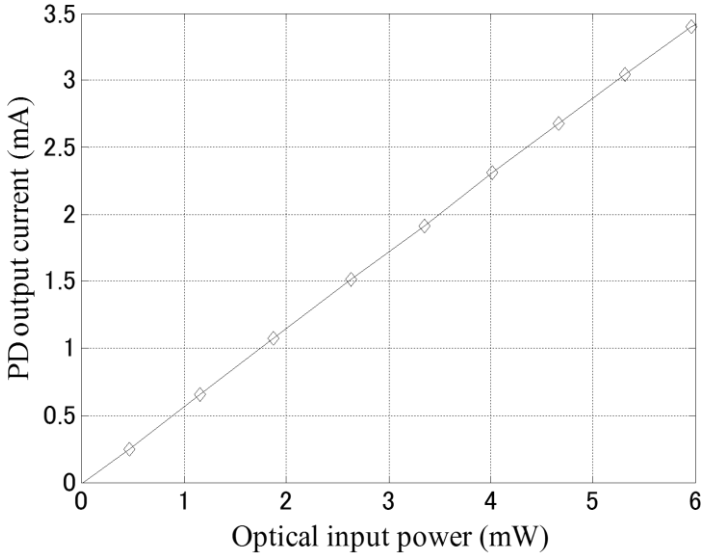

Fig. 3.25 Measured PD input/output characteristic

3dB bandwidth of the PD is 12GHz, which is wide enough for the input RF signal. A single mode optical fiber of five kilometers was used for the RoF transmission. An external light source was added when the MZ modulator was employed. An LD driver was employed to provide DC bias current and maintain the operating temperature at 25°C for the DFB LD. The optical wavelength for both of the E/O converters is 1.55μm.

Fig. 3.25 (a) and (b) show the experimental spectra of the output OFDM and ANC-EPWM-OFDM signals from the RoF channel employing MZ modulator, respectively. The peak amplitudes of input signals were set same as in the simulation. From figure (a), it can be clearly observed that the experimental output spectrum of OFDM signal is same as the simulation result shown in Fig. 3.13 (a). Comparing Fig. 3.25 (a) and (b), 5dB improvement of SFDR is obtained by the ANC-EPWM-OFDM transmission, which is close to the simulation result.

Fig. 3.26 (a) and (b) present the experimental spectra of OFDM and ANC-EPWM-OFDM signals output from the RoF channel when the DFB LD is

employed. The peak amplitudes of input signals were set same as in the simulation. The spectrum in Fig. 3.26 (a) presents the same nonlinear distortion as that shown in Fig. 3.21 (a). The SFDR of ANC-EPWM-OFDM signal is about 7dB larger than the OFDM signal. These results show conformity with the simulation results. Therefore, the modified Rapp model well fits the actual device and it is valid for analysis of the DFB LD.

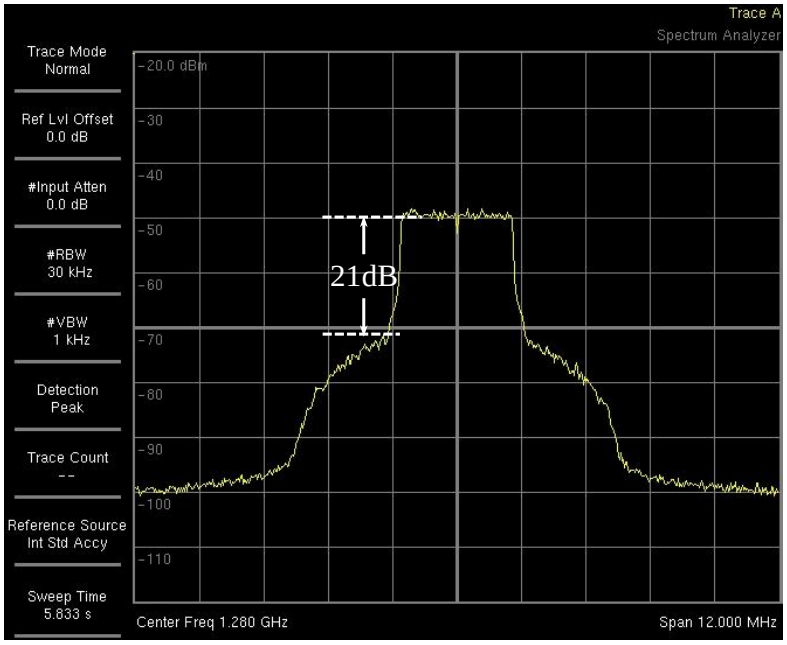

(a) OFDM signal output

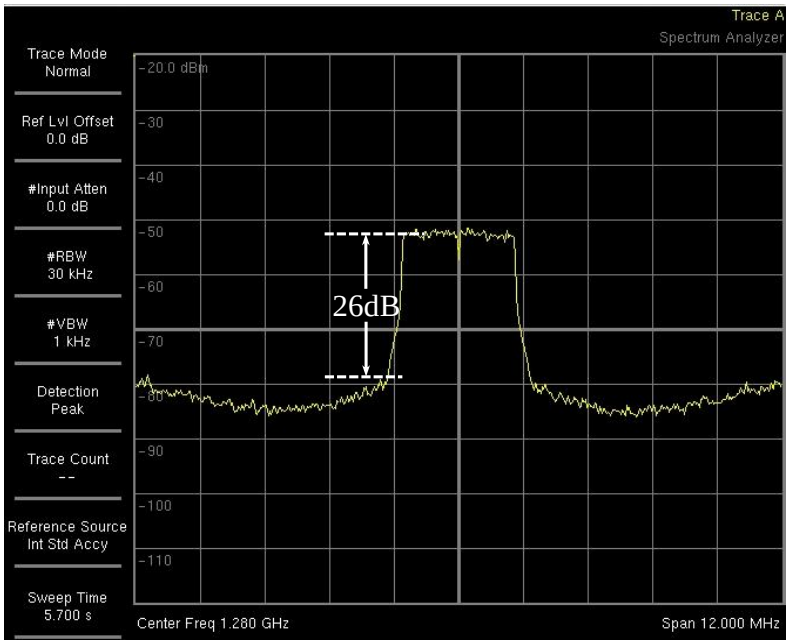

(b) ANC-EPWM-OFDM signal Output

Fig. 3.26 Experimental output signals of RoF channel employing MZ modulator

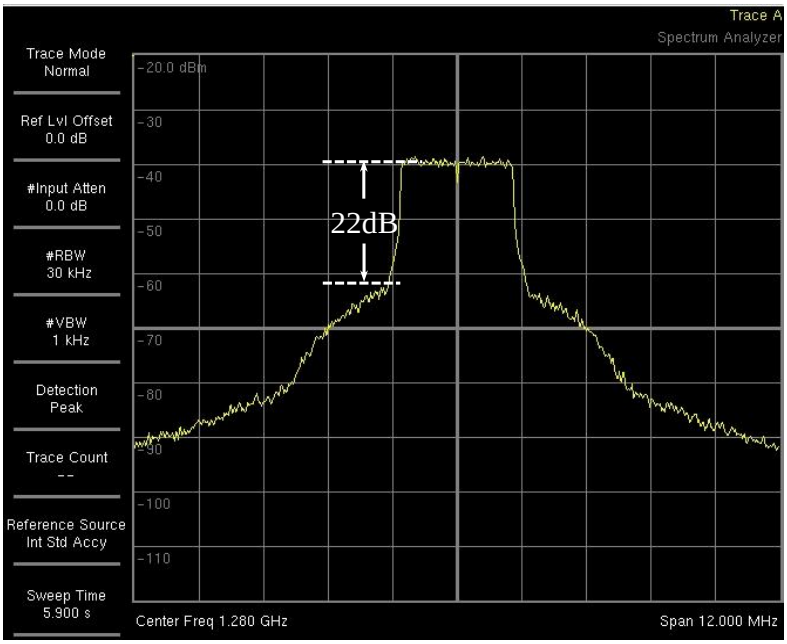

(a) OFDM signal Output

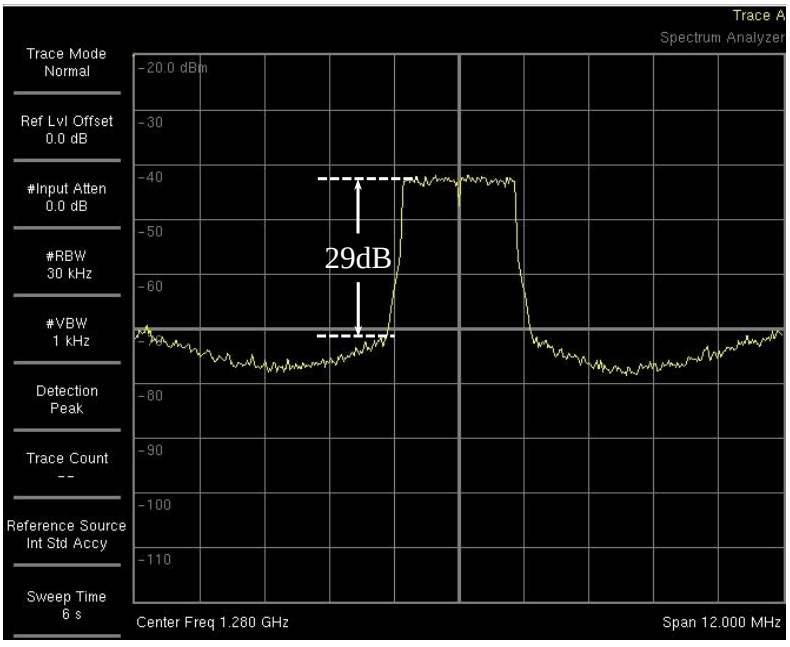

(b) ANC-EPWM-OFDM signal Output

Fig. 3.27 Experimental output signals of RoF channel employing DFB LD

3.7 Chapter Summary

In this chapter we presented the EPWM-RoF schemes for OFDM signal transmission in nonlinear RoF channel. Two different nonlinear E/O converters of MZ modulator and direct modulation DFB LD were measured, modelled and analyzed in this chapter. For both types of the E/O converters, EPWM and ANC-EPWM transmission schemes improve the SFDR of OFDM signal spectrum by several decibels and reduce the EVM to less than half that of the normal OFDM transmission. Among the two schemes, EPWM offers perfect nonlinearity suppression. However it has higher outband noise radiation level that should be suppressed by a narrowband BPF. ANC-EPWM-OFDM transmission has lower outband noise level and thus relaxes the bandwidth requirement for the BPF. Based on the simulation and experiment results, it is concluded that the proposals are efficient for OFDM signal transmission in nonlinear RoF channels without any complicated nonlinear compensation circuits.

Chapter 4. EPWM-RoF Transmission against Echo Effect

In chapter 3 we have discussed RoF nonlinearity effect on the normal and EPWM-formatted OFDM signals. On the other hand, multiple light reflections in RoF channel, which is called echo, exist in most of the optical communication systems. Light echoes are caused by discontinuities of refractive-index that exist between fiber ends, E/O and O/E converters. The delay of optical echoes exceeds the guard time of current OFDM symbols when the length of optical fiber is long. Such light echoes can degrade the performance of optical transmission systems, even if relatively small amount of light are reflected back [13]. A common method to solve this issue is inserting an optical isolator between the transmitter and the fiber. However, even if an isolator is inserted, other reflections between connectors and splices still generate intensity noise and degrade the transmission performance. In RoF channel, interferometric conversion occurs when multiple reflections happen [70]. Theoretical analysis of the spectrum of the interferometric noise has been studied [70, 71]. Since the nonlinearity and echo exist simultaneously in RoF channels, their composite effect should be discussed. However, no studies have been covered this issue.

In this chapter, a model for the echo effect in RoF channel is proposed. An MZ modulator is employed as the E/O converter with nonlinearity. Then, EPWM-RoF transmission scheme is proposed for dealing with the nonlinearity and echo issues in RoF channel. Theoretical analysis of the composite effects on the normal and EPWM-formatted OFDM signals is performed by employing the proposed RoF-

echo model. The proposed model and theoretical analysis are confirmed by experiments. The performance of the EPWM-OFDM transmission against MZ modulator nonlinearity and echo in the RoF channel is evaluated by simulations. To eliminate the echo effect on the EPWM signal, we propose to employ a class-C PA at the output of the RoF channel. The performance of the echo effect cancellation by the PA is presented by simulation results.

The rest of this chapter is arranged as follows. Section 4.1 describes the echo effect and the RoF-echo model. Theoretical analysis is given in Sec. 4.2. The design of the class-C operated PA for the cancellation of echo effect is presented in Sec. 4.3. Section 4.4 and Sec. 4.5 show the simulation and experiment results. Finally, the chapter is summarized in Sec. 4.6.

4.1 Echo Effect and RoF-Echo Model

The RoF-echo process is shown in Fig. 4.1. B1 and B2 denote the boundaries where light reflections happen. The input light signal $v_{in}(t)$ passes through B1 and travels τ seconds though the optical fiber of several kilometers or less. Then the light arrives at B2. A part of the arriving light $v_{r1}(t)$ is reflected at B2 and the rest of the light $v_{p1}(t)$ passes through B2. After τ seconds traveling over the fiber, the

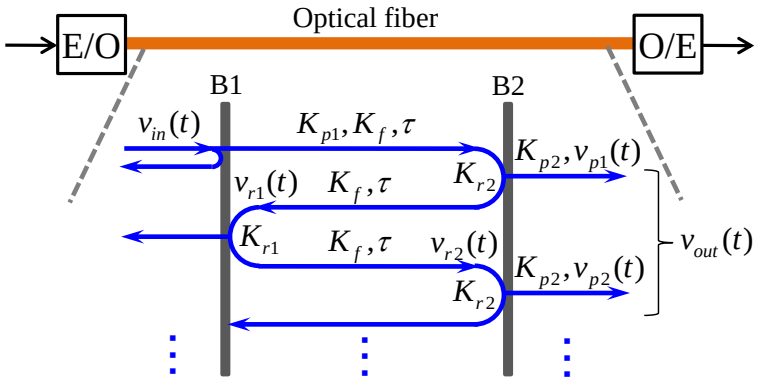

Fig. 4.1 RoF-echo process

reflected light $v_{r1}(t)$ arrives at B1 and it is again partly reflected. After τ seconds transmission through the fiber, the twice reflected light signal $v_{r2}(t)$ arrives at B2 again. The echo process goes on and the following processes are the repeats of the previous. Since the intensity of the light that is reflected more than twice is quite small, it can be neglected. Thus, we only consider two times reflections in this dissertation. Since the reflected light towards the E/O converter can be terminated by an optical isolator, it is not considered. On the other hand, the echo towards the O/E converter is difficult to remove. To investigate the RoF-echo effect, we propose a model as follows.

Assume that the length and the refractive index of the optical fiber in the RoF channel is L and n_f, respectively. Then the traveling time of light τ in the optical fiber is calculated by

$$\tau = \frac{Ln_f}{c}, \tag{4.1}$$

where c is the speed of light in vacuum. Based on Fig. 4.1, the light signal passing though B2 for the first time can be expressed as

$$\begin{aligned} v_{p1}(t) &= K_f K_{p1} K_{p2} v_{in}(t-\tau) \\ &= K_f K_p^2 v_{in}(t-\tau) \end{aligned}, \tag{4.2}$$

where $K_f = 10^{(-G_{fiber}/20)}$, G_{fiber} (dB) is the optical fiber attenuation. $K_{p1}=10^{(G_{p1}/20)}$ and $K_{p2} = 10^{(G_{p2}/20)}$, where G_{p1} (dB) and G_{p2} (dB) are the power gain of the signals that pass though B2 for the first time and the second time, respectively. Define a pair of composite factors as follows,

$$K_p = \sqrt{K_{p1} K_{p2}} \tag{4.3}$$

and

$$G_p = 20 \log K_p . \tag{4.4}$$

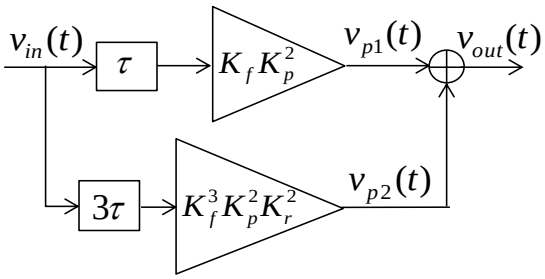

Fig. 4.2 RoF-echo model

G_p is called pass signal gain. The light signal passing though B2 for the second time is expressed as

$$\begin{aligned} v_{p2}(t) &= K_f^3 K_{p1} K_{p2} K_{r1} K_{r2} v_{in}(t-3\tau) \\ &= K_f^3 K_p^2 K_r^2 v_{in}(t-3\tau) \end{aligned}, \tag{4.5}$$

where $K_{r1} = 10^{(Gr1/20)}$ and $K_{r2} = 10^{(Gr2/20)}$. G_{r1} (dB) and G_{r2} (dB) are the power gain of the reflected signal at B1 and B2, respectively. Define another pair of composite factors as

$$K_r = \sqrt{K_{r1} K_{r2}} \tag{4.6}$$

and

$$G_r = 20 \log K_r . \tag{4.7}$$

G_r is called reflected signal gain. The relationship between K_{pi} and K_{ri} is

$$K_{pi}^2 + K_{ri}^2 = 1, \quad (i = 1, 2). \tag{4.8}$$

The output signal from B2 is given by

$$v_{out}(t) = v_{p1}(t) + v_{p2}(t). \tag{4.9}$$

Equation 4.2, 4.5 and 4.9 define the RoF-echo function. From these equations, the proposed RoF-echo model results in Fig. 4.2. The output echo signal is the sum of

$v_{p1}(t)$ and $v_{p2}(t)$. The signal $v_{p1}(t)$ is the input signal with τ delay and attenuation. The signal $v_{p2}(t)$ is the input signal with 3τ delay and attenuation.

4.2 Theoretical Analysis

In this section, we will give some mathematical analysis on the RF signal spectrum distortion due to the echo effect and the echo effect on the EPWM signal.

4.2.1 Composite Distortion caused by Nonlinearity and Echo Effect

Equation 3.19 in chapter 3 has shown that the output of the RoF channel employing MZ modulator without echo effect is composed of DC component, RF signal and odd order harmonic waves. Assume the Power Spectral Density (PSD) of input RF signal $v_{RF}(t)$ is

$$S(\omega)=\int_{-\infty}^{+\infty}R(\eta)e^{-j\omega\eta}d\eta\,, \tag{4.10}$$

where

$$R(\eta)=E\left[v_{RF}(t)v_{RF}(t-\eta)\right] \tag{4.11}$$

is the autocorrelation function of $v_{RF}(t)$. Then from Eq. 3.19, the PSD of output signal from the RoF channel $v_{RoF}(t)=R_L i_{PD}$ can be derived to

$$S_{RoF}(\omega)=\frac{R_L^2R_{PD}^2K_f^4A_{opt}^4}{4}\left[2\pi\delta(\omega)+\left(\frac{\pi^2}{V_\pi^2}-\frac{\pi^6\sigma^4}{12V_\pi^6}\right)S(\omega)-\frac{\pi^6}{18V_\pi^6}S(\omega)*S(\omega)*S(\omega)+\cdots\right], \tag{4.12}$$

where i_{PD} is given by Eq. 3.19 , R_L is the PD output load resister and σ^2 is the

average power of $v_{RF}(t)$. Derivation of $S_{RoF}(\omega)$ is shown in the appendix.

For the RoF channel with echo effect, the optical output of MZ modulator undergoes echo which is simulated by the RoF-echo model. Then it is reconverted to an electrical signal by the PD. Substitute the optical output of MZ modulator Eq. 3.14 to the RoF-echo functions of Eq. 4.2, Eq. 4.5 as v_{in}, output of the RoF-echo model is derived to

$$\begin{aligned} v_{out}(t) &= K_f K_p^2 v_{MZ}(t-\tau) + K_f^3 K_p^2 K_r^2 v_{MZ}(t-3\tau) \\ &= A_{opt} K_f K_p^2 \left\{ \cos\left[s(t) + \frac{3\pi}{4} \right] + K_r^2 K_f^2 \cos\left[s(t-2\tau) + \frac{3\pi}{4} \right] \right\}, \end{aligned} \tag{4.13}$$

$$s(t) = \pi v_{RF}(t-\tau)/2v_{\pi} . \tag{4.14}$$

Then the PD output signal is given by

$$\begin{aligned} v_{RoF-echo}(t) &= R_L R \left| v_{out}(t) \right|^2 \\ &= G\left\{ \frac{1}{2} + \frac{1}{2}\sin\left[2s(t) \right] \right. \\ &\quad + \frac{K_r^4 K_f^4}{2} + \frac{K_r^4 K_f^4}{2}\sin\left[2s(t-2\tau) \right], \\ &\quad + K_r^2 K_f^2 \sin\left[s(t) + s(t-2\tau) \right] \\ &\quad \left. + K_r^2 K_f^2 \cos\left[s(t) - s(t-2\tau) \right] \right\} \end{aligned} \tag{4.15}$$

where $G = R_L R A_{opt}^2 K_f^2 K_p^4$. Perform Taylor expansion for Eq. 4.15, then

$$\begin{aligned} v_{RoF-Echo}(t) = G\left\{ \right. & \frac{1}{2} + \frac{K_r^4 K_f^4}{2} + \frac{1}{2}\left[2s(t) - \frac{8}{3!}s^3(t) + \cdots \right] \\ & + \frac{K_r^4 K_f^4}{2}\left[2s(t-2\tau) - \frac{8}{3!}s^3(t-2\tau) + \cdots \right] \\ & + K_r^2 K_f^2 \left[s(t) + s(t-2\tau) - \frac{1}{3!}\left(s(t) + s(t-2\tau) \right)^3 + \cdots \right] \\ & \left. + K_r^2 K_f^2 \left[1 - \frac{1}{2!}\left(s(t) - s(t-2\tau) \right)^2 + \cdots \right] \right\} \end{aligned} . \tag{4.16}$$

The nonlinear components larger than 3rd order can be neglected because their

effects are very small. Therefore, Eq. 4.16 can be approximate by

$$\begin{aligned} v_{RoF-Echo}(t) = G\Bigg\{ & \frac{1}{2} + \frac{K_r^4 K_f^4}{2} + K_r^2 K_f^2 \\ & + (1 + K_r^2 K_f^2) s(t) + (K_r^2 K_f^2 + K_r^4 K_f^4) s(t - 2\tau) \\ & - \frac{K_r^2 K_f^2}{2} s^2(t) - \frac{K_r^2 K_f^2}{2} s^2(t - 2\tau) + K_r^2 K_f^2 s(t) s(t - 2\tau) . \\ & - \left(\frac{2}{3} + \frac{K_r^2 K_f^2}{6} \right) s^3(t) - \left(\frac{2K_r^4 K_f^4}{3} + \frac{K_r^2 K_f^2}{6} \right) s^3(t - 2\tau) \\ & - \frac{K_r^2 K_f^2}{2} s^2(t) s\ (t - 2\tau) - \frac{K_r^2 K_f^2}{2} s(t) s^2(t - 2\tau) \Bigg\} \end{aligned} \quad (4.17)$$

To distinguish the signal components in Eq. 4.17, let $v_{s1}(t)$, $v_{s2}(t)$ and $v_{s3}(t)$ denote the output RF signal component, 2nd and 3rd order harmonic waves, respectively. And they are expressed by

$$v_{s1}(t) = (1 + K_r^2 K_f^2) s(t) + (K_r^2 K_f^2 + K_r^4 K_f^4) s(t - 2\tau) , \quad (4.18)$$

$$v_{s2}(t) = \frac{K_r^2 K_f^2}{2} s^2(t) - \frac{K_r^2 K_f^2}{2} s^2(t - 2\tau) + K_r^2 K_f^2 s(t) s(t - 2\tau) , \quad (4.19)$$

and

$$\begin{aligned} v_{s3}(t) = & - \left(\frac{2}{3} + \frac{K_r^2 K_f^2}{6} \right) s^3(t) - \left(\frac{2K_r^4 K_f^4}{3} + \frac{K_r^2 K_f^2}{6} \right) s^3(t - 2\tau) \\ & - \frac{K_r^2 K_f^2}{2} s^2(t) s\ (t - 2\tau) - \frac{K_r^2 K_f^2}{2} s(t) s^2(t - 2\tau) \end{aligned} . \quad (4.20)$$

Thus, the PSD of the signal $v_{RoF\text{-}echo}(t)$ output from PD can be derived to

$$\begin{aligned} S_{RoF-echo}(\omega) = G^2 \Bigg\{ & 2\pi \left(\frac{1}{2} + \frac{K_r^4 K_f^4}{2} + K_r^2 K_f^2 \right)^2 \delta(\omega) \\ & + S_{S1}(\omega) + S_{S2}(\omega) + S_{S3}(\omega) \Bigg\} \end{aligned} , \quad (4.21)$$

where $S_{S1}(\omega)$, $S_{S2}(\omega)$ and $S_{S3}(\omega)$ are the PSD of the signal $v_{s1}(t)$, $v_{s2}(t)$ and $v_{s3}(t)$, respectively. Derivation of $S_{S1}(\omega)$, $S_{S2}(\omega)$ and $S_{S3}(\omega)$ are shown in the appendix.

From Eq. 4.18, Eq. 4.19 and Eq. 4.20 we can see that besides some attenuation, even order harmonic waves are generated by the RoF-echo effect. While, the output RoF signal without echo effect shown in Eq. 4.12 only consists odd order harmonic waves.

4.2.2 Echo Effect on EPWM Signal

In Sec. 4.2.1 we analyzed the echo effect commonly. In this section, analysis of the echo effect on the EPWM signal is presented. Since the amplitude $e_a(t)$ of the input EPWM-RF signal is a PWM signal and it is either zero or constant as below

$$e_a(t) = \begin{cases} 0 \\ \Delta \end{cases}, \tag{4.22}$$

where Δ is the constant amplitude. Then the EPWM-RF signal can be described by a piecewise function as below

$$v_{EPWM-RF}(t) = \begin{cases} 0, & (a_{EPWM-RF}(t) = 0) \\ e(t), & (a_{EPWM-RF}(t) = \Delta) \end{cases}, \tag{4.23}$$

$$e(t) = \Delta \cdot \mathrm{Re}\left[e^{j(2\pi f_c t + \phi(t))} \right]. \tag{4.24}$$

$e(t)$ is called burst on EPWM-RF signal. Substitute Eq. 4.24 to Eq. 3.14 yields the output optical signal from the MZ modulator as

$$v_{EPWM-MZ}(t) = \begin{cases} C_{mz}, & (a_{EPWM-RF}(t) = 0) \\ v_{mz}(t), & (a_{EPWM-RF}(t) = \Delta) \end{cases}, \tag{4.25}$$

where

$$C_{mz} = A_{opt}\cos\left[\frac{\pi}{2V_\pi}\left(0+V_{bias}\right)\right] = A_{opt}\cos\left(\frac{\pi V_{bias}}{2V_\pi}\right) \quad (4.26)$$

is a constant DC component and

$$v_{mz}(t) = A_{opt}\cos\left[\frac{\pi}{2V_\pi}\left(e(t)+V_{bias}\right)\right], \quad (4.27)$$

is the RF component. Let $v_{EPWM\text{-}Echo}(t)$ denotes the output optical EPWM-Echo signal from the RoF-echo model. By substituting Eq. 4.25 to the RoF-echo functions Eq. 4.2, Eq. 4.5 and Eq. 4.9, $v_{EPWM\text{-}Echo}(t)$ is given by

$$\begin{aligned} v_{EPWM-Echo}(t) &= v_{p1}(t) + v_{p2}(t) \\ &= K_f K_p^2 v_{EPWM-MZ}(t-\tau) + K_f^3 K_p^2 K_r^2 v_{EPWM-MZ}(t-3\tau) \end{aligned}, \quad (4.28)$$

and the output signal from PD of the RoF channel with echo effect is given by

$$\begin{aligned} v_{EPWM-RoF-Echo}(t) &= i_{PD}(t)R_L \\ &= R_L R\left|v_{EPWM-Echo}(t)\right|^2 \end{aligned}. \quad (4.29)$$

Express Eq. 4.29 by a piecewise function, then

$$v_{EPWM-RoF-Echo}(t) = \begin{cases} 0, & (0 \le t < \tau) \\ Gv_{mz}^2(t-\tau), & (\tau \le t < 3\tau, a_{EPWM-RF}(t-\tau) = \Delta) \\ GC_{mz}^2, & (\tau \le t < 3\tau, a_{EPWM-RF}(t-\tau) = 0) \\ GC_{mz}^2(1+K_r^2)^2, & (t \ge 3\tau, a_{EPWM-RF}(t-\tau) = 0 \\ & \quad \text{and } a_{EPWM-RF}(t-3\tau) = 0) \\ G\left[C_{mz} + K_r^2 v_{mz}(t-3\tau)\right]^2, & (t \ge 3\tau, a_{EPWM-RF}(t-\tau) = 0 \\ & \quad \text{and } a_{EPWM-RF}(t-3\tau) = \Delta) \\ G\left[v_{mz}(t-\tau) + K_r^2 C_{mz}\right]^2, & (t \ge 3\tau, a_{EPWM-RF}(t-\tau) = \Delta \\ & \quad \text{and } a_{EPWM-RF}(t-3\tau) = 0) \\ G\left[v_{mz}(t-\tau) + K_r^2 v_{mz}(t-3\tau)\right]^2, & (t \ge 3\tau, a_{EPWM-RF}(t-\tau) = \Delta \\ & \quad \text{and } a_{EPWM-RF}(t-3\tau) = \Delta) \end{cases}, \quad (4.30)$$

Comparing Eq. 4.23 and Eq. 4.30 we can find out that amplitude fluctuations are caused by RoF-echo effect and the constant envelop property of EPWM signal is destroyed.

4.3 Confirmation of Echo Model by Experiment

To confirm the validity of the RoF-echo model and the mathematical analysis on the echo effect, some experiments were executed. The experiment setup is shown in Fig. 4.3. The experiment conditions are listed in Table 1. The EPWM signal is generated by MATLAB and M8190A 12GSa/s arbitrary waveform generator. To see the spectrum of output signal with enough bandwidth and due to the sampling frequency limitation of the oscilloscope, the RF frequency is set to 640MHz in the experiment. Then the RF signal is amplified by an RF amplifier and input to a RoF

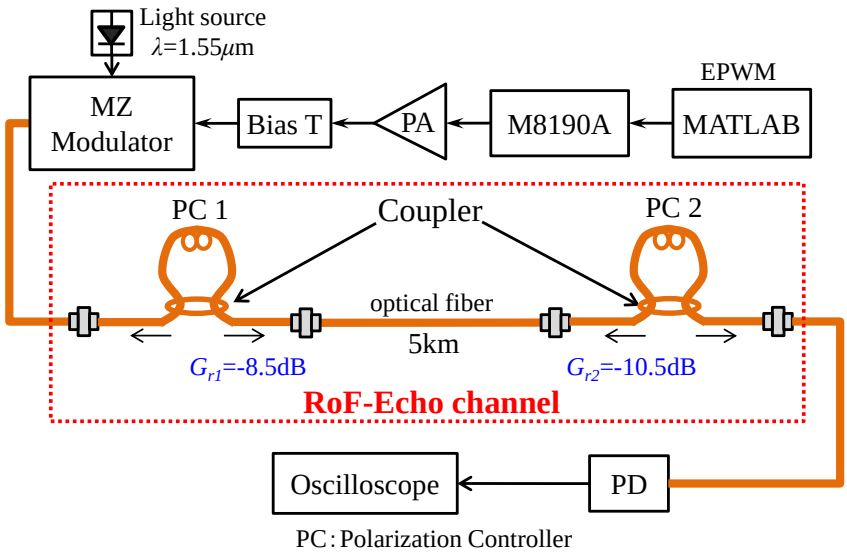

Fig. 4.3 Experiment setup

Table 4-1 Experiment conditions

Baseband OFDM Signal	modulation	64QAM
	subcarriers	52
	symbol duration	4μs
	guard interval	0.8μs
	bandwidth	16.6MHz
	PAPR (CCDF of 10^{-4})	11.5dB
EPWM Transmitter	1st-order Δ-Σ modulator, OSR=32, clipping probability is 0.1%	
RF Frequency	f_c=640 MHz	
MZ Modulator	V_π=1.75 V, V_{bias}=2.625 V, λ_0=1.55μm	
Optical Fiber	Single mode, 5*k*m	
Reflected Signal Gain (dB)	G_r=-9.5dB	
PD	*R*=0.6 A/W, 3dB bandwidth is 12GHz	

channel, which is composed of a T·MZH1.5-10PD-ADC-S-Y-Z MZ modulator, RoF-Echo generation part, and a DSC50S type PD. The Bias T is used to set a DC bias for the MZ modulator, and the light source provides a light with operation wavelength of 1550nm for the modulator. The RoF-Echo generation part consists of two Polarization Controllers (PC) that are used to adjust the reflected signal gain G_{r1} and G_{r2}, a five kilometers single mode optical fiber and two couplers where the light reflections are generated [72]. G_{r1} and G_{r2} in the experiment are -8.5dB and -10.5dB, respectively. According to Eq. 4.6 and Eq. 4.7, the composite reflected signal gain G_r is -9.5dB. To make the echo effect more obvious to be observed by the experiment, larger reflected signal gain was employed than the practical values. Parameters for the EPWM signal are same as in the simulation. The output signal from the PD is observed by a broadband oscilloscope.

Figure 4.4 (a) and (b) show the measured time domain input and output signals of the RoF channel with echo effect. The amplitude fluctuations caused by the echo

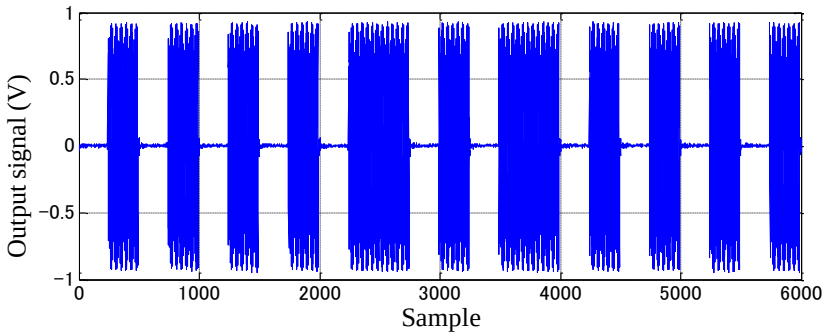

(a) EPWM RoF input signal

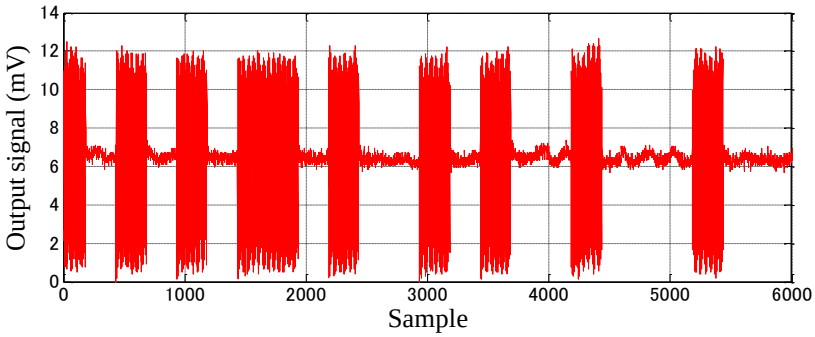

(b) EPWM RoF output signal with echo effect

Fig. 4.4 Experimental time domain input and output signals of the RoF channel with echo effect

effect can be observed clearly in Fig. 4.4 (b). The experiment results agree with the mathematical analysis of echo effect on the EPWM signal. Therefore, the proposed model is effective for modeling the echo effect in RoF channel.

Figure 4.5 shows the experimental power spectra of the signals output from the RoF channel with and without echo effect. OFDM signal was employed as an example of the input RF signal. Through comparison between Fig. 4.5 (a) and (b), we can see 2nd order harmonic wave is generated by the echo effect, which is same as we have analyzed in sec. 4.2.1. Figure 4.5 confirms that the mathematical analysis on the spectrum of signal with echo effect is effective, which also indicates the validity of the RoF-echo model.

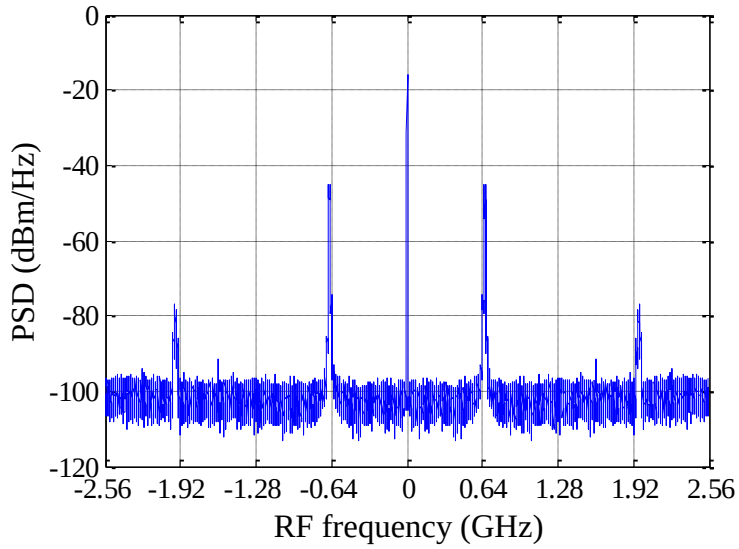

(a) Spectrum of RoF output signal without echo effect

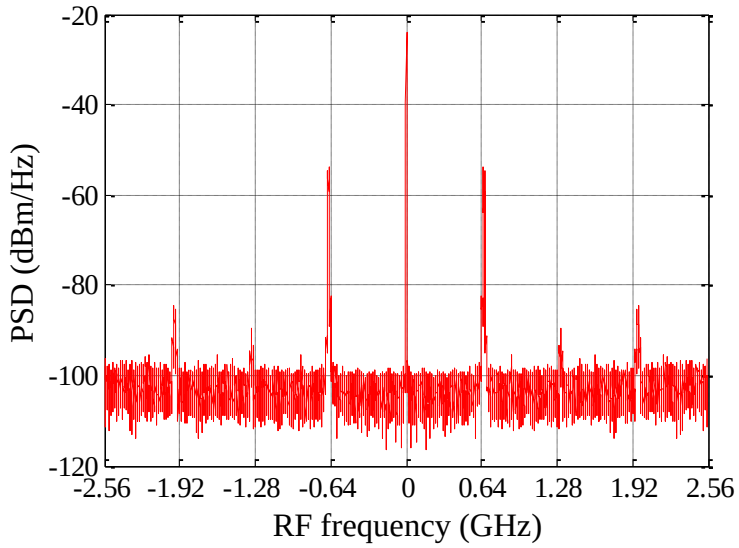

(b) Spectrum of RoF output signal with echo effect

Fig. 4.5 Measured PSD of output signals from the RoF channel with and without echo effect

4.4 Performance Evaluations by Simulation

To evaluate the composite effect of E/O nonlinearity and optical echo on EPWM-formatted OFDM transmission, some simulations are implemented by MATLAB. Simulation conditions are basically same as the experiment conditions except that the RF frequency is set 1.28GHz. The baseband OFDM signal was generated according to IEEE802.11a standard. For the EPWM transmitter, a 1st order delta-sigma modulator with over-sampling ratio of 32 is employed. The clipping probability of the delta-sigma modulator is 0.1%. The optical operation wavelength is 1550nm, and a 5*k*m single mode fiber is used in the RoF channel. An MZ modulator same as employed in chapter 3 is used as the E/O converter. The PD has linear input/output characteristic as shown in Fig. 3.24, and its bandwidth is wide enough for the input RF signals. The echo effect is modeled by the RoF-echo model. The reflected signal gain G_r in the echo model is set to -9.5dB, same as the measured value in the experiment.

4.4.1 EPWM-RoF Performance against Echo Effect

Simulation diagram for echo effect on the normal and EPWM-formatted OFDM signals is shown in Fig. 4.6. OFDM-RF and EPWM-RF signals are generated from the same baseband OFDM signal. Then they are transmitted through the RoF channel that is composed of the MZ modulator, optical fiber, PD and the RoF-echo model.

Figure 4.7 (a) and (b) show the simulated time domain input and output signals of the RoF channel with echo effect. The input EPWM-RF signal is a burst RF signal with constant envelope. However, the envelope of the output EPWM signal is no longer constant due to the echo effect. Amplitude fluctuations in the output EPWM signal can be observed in Fig. 4.7 (b).

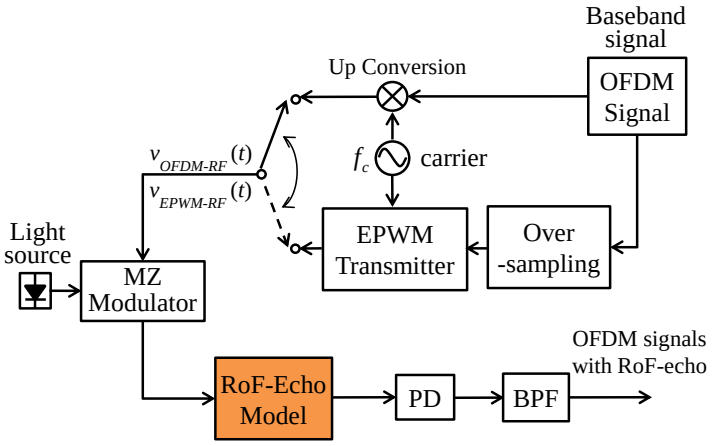

Fig. 4.6 Simulation diagram I

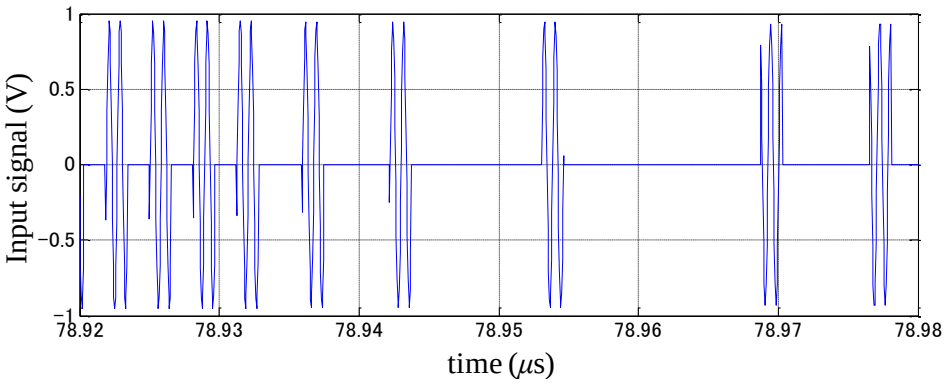

(a) EPWM RoF input signal

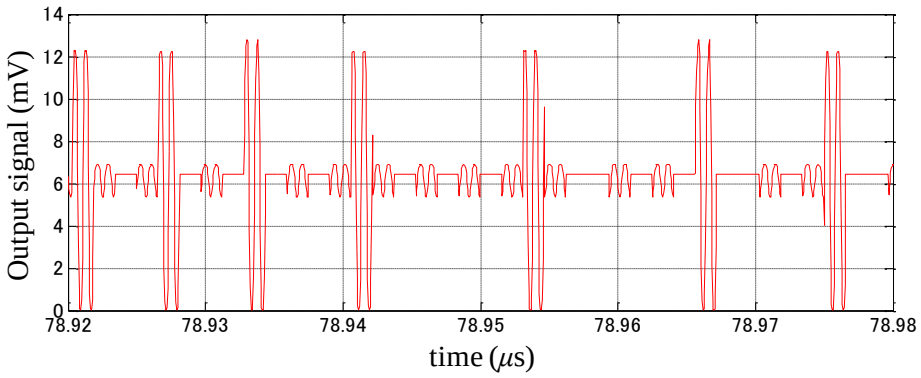

(b) EPWM RoF output signal with echo effect

Fig. 4.7 Simulated time domain input and output EPWM signals of the RoF channel with echo effect

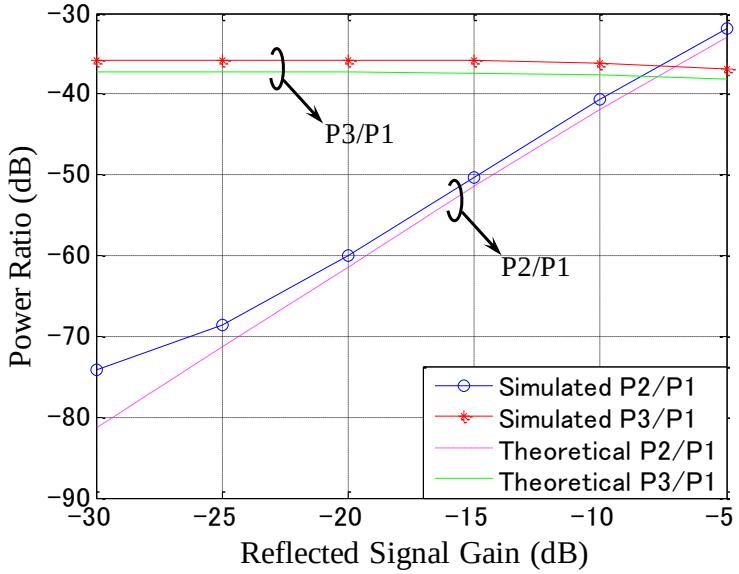

P1: mean power of RF signal at f_c.
P2: mean power of 2nd order harmonic wave at $2f_c$.
P3: mean power of 3rd order harmonic wave at $3f_c$.

Fig. 4.8 Simulated and theoretical power ratio of harmonic waves to RF signal

Figure 4.8 depicts the output power ratio of each harmonic wave to the RF signal. P3/P1 and P2/P1 are the power ratio of the 3rd and the 2nd order harmonic waves to the RF signal, respectively. Since the 2nd order harmonic wave is generated by the RoF-echo effect, P2/P1 increases as the reflected signal gain increases. When the reflected signal gain is larger than -20dB, difference between the theoretical and simulated results is about 1~1.5dB. When the reflected signal gain is smaller than -20dB, the difference between the theoretical and simulated results enlarges, which is because noise level is not considered in the theoretical analysis. When the reflected signal gain is very small, the power of generated 2nd order harmonic wave is also small.

The EVM of RoF output signals versus amplitude of input RF signal is shown in Fig. 4.9. Since EPWM-formatted OFDM signal is a burst RF signal with constant envelope, it is not affected by nonlinearities. Therefore, its EVM without echo does

not change and keep small. On the other hand, the EVM of the OFDM signal

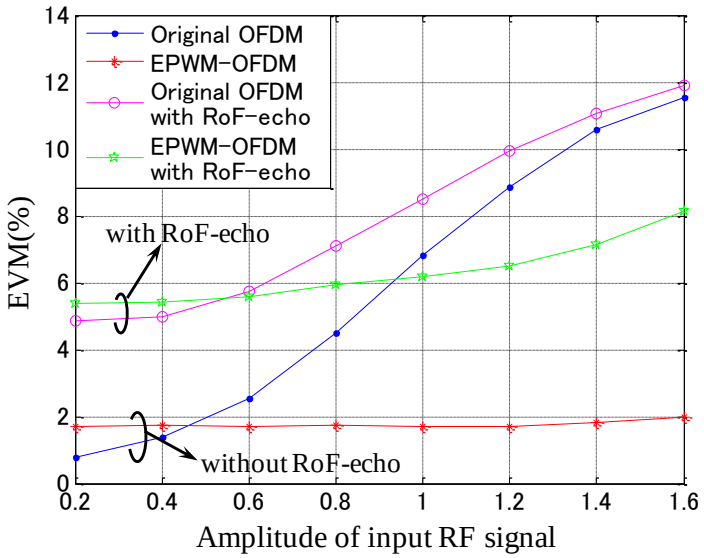

Fig. 4.9 EVM performance versus amplitude of input RF signal

without echo effect increases with the input amplitude due to the E/O nonlinearity. Under the influence of echo, the EVM of both the normal and the EPWM-formatted OFDM signals are degraded. Nevertheless, the EVM of the EPWM formatted signal is still much better than that of the normal OFDM signal.

Figure 4.10 depicts the EVMs versus the reflected signal gain. The amplitude of input RF signal is 0.95V. When the reflected signal gain is smaller than 20dB, the echo effect is small and does not affect the EVM of both the signals. As the reflected signal gain increases, the EVMs performance of both the normal and the EPWM formatted signals deteriorate. Nevertheless, the EVM of EPWM formatted signal is 0.5-4.4% lower than that of the normal OFDM signal.

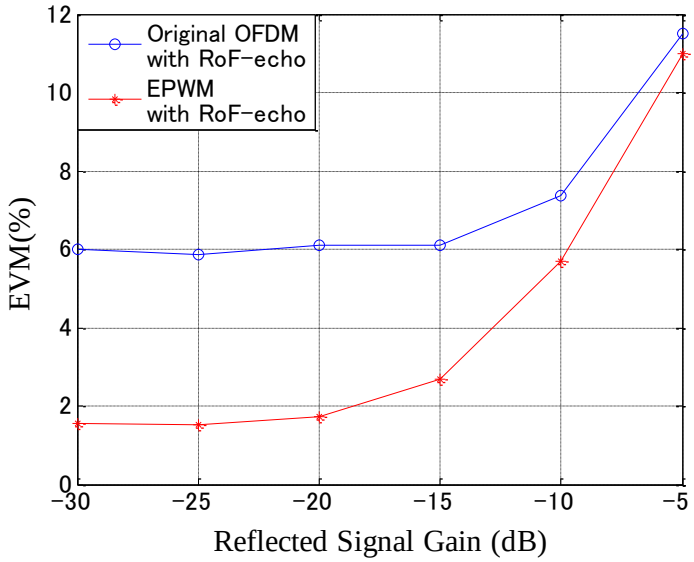

Fig. 4.10 EVM performance versus reflected signal gain

4.4.2 Elimination of Echo Effect by Class-C Operated PA

Since the EPWM signal quality can be degraded by the amplitude fluctuations caused by the echo, we propose an echo effect elimination scheme for the EPWM signal. The PA in the EPWM-RoF transmission system shown in Fig. 3.6 is designed as a class-C PA, as shown in Fig. 4.11. The output/input characteristic of the PA is shown in Fig. 4.12. It is designed by the Rapp model as follow

$$y=\begin{cases}\dfrac{K(x+V_b)}{\left[1+\left(\dfrac{K(x+V_b)}{E_{\max}}\right)^{2p}\right]^{\frac{1}{2p}}}, & (x+V_b)>0\\ 0, & (x+V_b)<0\end{cases}. \tag{4.32}$$

The parameters in Eq. 4.32 are set to K=5.6, E_{max}=11.3 and p=3. As shown in Fig. 4.12, by setting the bias voltage V_b to a proper value for the input signal of the PA, which is also the output EPWM-RoF-echo signal from the RoF channel, and let the

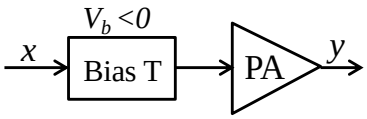

Fig. 4.11 Design of class-C PA

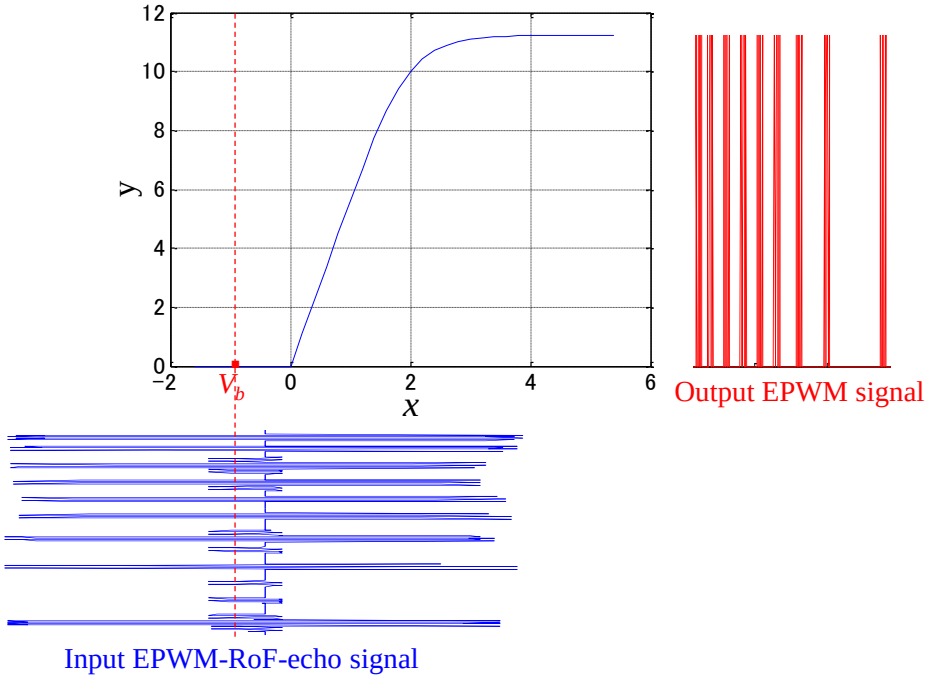

Fig. 4.12 Input/output characteristic of the PA

input signal stretch into the saturation region of the PA, the amplitude fluctuations in the EPWM signal can be removed and the constant envelope of EPWM signal can be recovered.

Simulation diagram for the echo effect cancellation by the class-C PA is shown in Fig. 4.13. As shown in the figure, after removing the DC component in the output EPWM-RoF-echo signal from the RoF channel, the class-C PA is employed. At the output of the PA, a BPF is used to remove quantization noise and recover the original OFDM signal. The simulation conditions are same as those employed in Sec. 4.4.1.

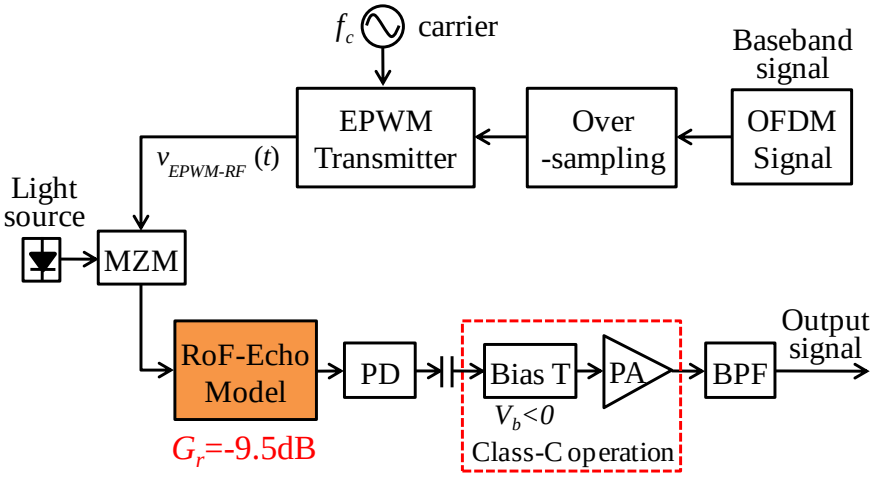

Fig. 4.13 Simulation diagram II

The relationship between EVM and the bias voltage V_b is shown in Fig. 4.14. When the bias voltage V_b for the PA is set to -1.4V, EVM performance of the output EPWM signal achieves the best. When V_b is smaller than -1.4V, the amplitude fluctuations on the top of the EPWM-RoF-echo signal cannot be removed completely. On the contrary, when V_b is larger than -1.4V the amplitude fluctuations in the middle of the EPWM-RoF-echo signal cannot be removed completely. Therefore, V_b of -1.4V is the optimal point, where the EVM achieves minimum.

By setting the bias voltage V_b to -1.4V, the EVM versus the input RF signal amplitude is simulated and shown in Fig. 4.15. As shown in the figure, the EVM is extremely large when the input signal is very small (0.2~0.4V). That is because the output signal is too small to be detected. As the input signal amplitude increases, the EVM decreases. When the input amplitude is around 1.2V, the EVM achieves minimum. That is because the amplitude fluctuations on the top of the EPWM-RoF-echo signal cannot be removed completely when the input amplitude is smaller than 1.2V. As the input amplitude increases further, the EVM performance degrades, which is because the amplitude fluctuations in the middle of the EPWM-

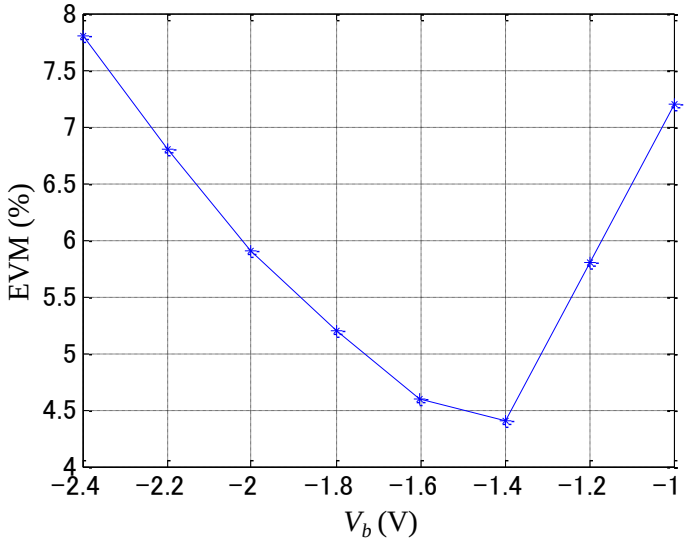

Fig. 4.14 EVM performance versus bias voltage V_b for the class-C PA

RoF-echo signal cannot be removed completely. Therefore, the input amplitude equals 1.2V is the optimal point, where the EVM achieves minimum. From Fig. 4.14 and Fig. 4.15 we can find out that the best EVM performance can be obtained by setting the bias voltage V_b to -1.4V and the input RF signal amplitude to 1.2V. Figure 4.16 shows the PSD of the output EPWM signal with echo effect elimination scheme when the EVM performance achieves the best. For reference, the WLAN spectrum mask is added in the figure.

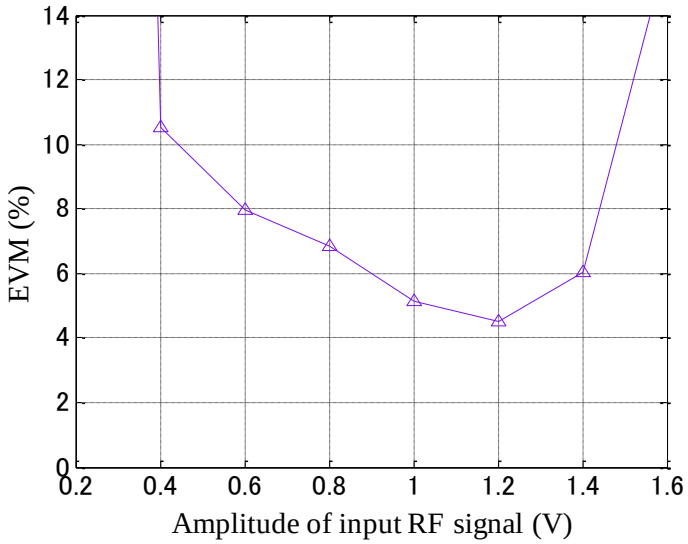

Fig. 4.15 EVM performance versus input RF signal amplitude

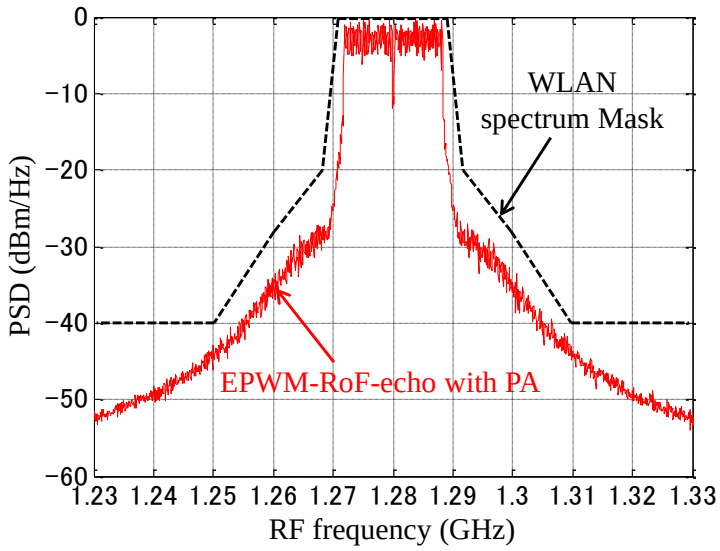

Fig. 4.16 PSD of output EPWM signal with cancellation of echo effect (V_b=-1.4V, input RF signal amplitude is 1.2V)

4.5 Chapter Summary

In this chapter, a RoF-echo model is proposed for the echo effect in RoF channel. Based on the RoF-echo model, the combined effect of nonlinearity and echo in RoF channel is mathematically analyzed. To confirm the validity of the proposed RoF-echo model and the theoretical analysis for the echo effect, some experiments were executed. The consistency of the mathematical analysis and the experiment results indicates that the proposed model is effective for modelling the echo in RoF channel. The transmission performance of the normal and the EPWM-formatted OFDM in the RoF channel with echo effect are evaluated through simulations. Although the EPWM-OFDM transmission can be affected by the echo effect, comparing with the original OFDM signal transmission it still has good performance in dealing with the nonlinearity and echo in the RoF channel. To eliminate the echo effect on EPWM signal, a class-C PA is introduced. Its performance is evaluated by the simulation results. By adjusting input signal level and the bias voltage V_b for the PA to a proper value, EVM performance of the EPWM-RoF transmission can be improved.

 错误!使用“开始”选项卡将 見出し 1,Chapter 应用于要在此处显示的文字。

Chapter 5. Conclusion

Since broadband wireless communications require high input signal power, dead spots exit in indoor and outdoor environments. RoF technology can penetrate RF signals to remote antenna units that close to users with low cost by delivering the RF signals though optical fibers. Therefore, RoF is a promising technology for extending coverage area of broadband wireless communications. The principle of RoF is introduced and its merits and disadvantages are illustrated in this dissertation.

Aiming at solving the E/O nonlinearity and echo effect issues in RoF channel, we proposed EPWM-RoF scheme for OFDM signal transmission. Since OFDM signal has high PAPR, it is easy to be contaminated by the E/O nonlinearity. EPWM transmitter can remove the OFDM signal amplitude variation by converting the amplitude to PWM format that has constant envelope. Therefore, EPWM-formatted OFDM signal does not suffer from nonlinearity. Echo effect commonly exists in RoF channel and degrades the RoF transmission performance. The echo effect is analyzed and modelled by the proposed RoF-echo model. The EPWM-RoF transmission against E/O nonlinearity and echo effect are summarized as follows.

1. **EPWM-RoF transmission against E/O nonlinearity**
   - Nonlinearity of MZ modulator and DFB LD is measured, modelled and mathematically analyzed.

- A modified Rapp model is proposed for representing the nonlinearity of the DFB LD. The modified Rapp model can enlarge the applicability of the original Rapp model. Its feasibility is confirmed by modelling different output/input characteristics of DFB LD with different bias currents.
- The performance of EPWM-RoF transmission in dealing with the nonlinearity of the MZ modulator and the DFB LD are presented by simulation and experiment results. The EVM performance of the proposal against MZ modulator and DFB LD nonlinearity are improved up to 10% and 15% comparing with the original OFDM signal transmission, respectively. The nonlinear distortions in OFDM signal caused by the E/O converters are removed by the proposed scheme.

2. EPWM-RoF transmission against echo effect

- RoF-echo model is proposed for analyzing echo effect on the RF signals.
- Composite effect of MZ modulator nonlinearity and RoF channel echo is mathematically analyzed. The analysis on the scenario without echo effect only shows odd order harmonic waves generated by the MZ modulator nonlinearity. However, even order harmonic waves are shown in the analysis on the scenario with echo effect. For EPWM signal, the binary property of its amplitude signal is destroyed and amplitude fluctuations are generated by the echo effect. The RoF-echo model and the theoretical analysis are confirmed by experiment results.
- A class-C PA is proposed to mitigate echo effect on EPWM signal. The PA is designed by the Rapp model. By choosing a proper input signal level and DC bias voltage, amplitude fluctuations in the EPWM-RoF-echo signal can be removed.
- Simulations of the echo effect on the normal and EPWM-formatted OFDM signals are implemented. The simulation results identify with the

theoretical analysis. The EVM of both normal and the EPWM-formatted OFDM signal transmission in RoF channel with echo effect deteriorate with the reflected signal gain increasing. However, the EVM of EPWM formatted signal is 0.5-4.4% lower than that of the normal OFDM signal.

Since the RoF channel studied in this dissertation is the simplest, studies on EPWM-RoF transmission for the other type RoF channels, such as SCM, Wavelength Division Multiplex (WDM) should be included in the future works. Moreover, the cancellation of echo effect on the EPWM signal by the Class-C operated PA can only improve the transmission performance by optimizing the DC bias. The flexibility of the scheme is low. New methods for the cancellation of echo effect should also be considered in our future works.

Appendix. PSD Derivation of the Output Signal from RoF Channel with and without Echo Effect

- ***PSD of the output signal from RoF channel without echo effect***

The output signal from the RoF channel employing MZ modulator without echo effect is

$$\begin{aligned} v_{RoF}(t) &= R_L i_{PD} \\ &= \frac{R_L R K_f^2 A_{opt}^2}{2}\left[1+\frac{\pi}{V_\pi}v_{RF}(t)-\frac{\pi^3}{6V_\pi^3}v_{RF}^3(t)+\cdots\right], \end{aligned} \tag{A.1}$$

where i_{PD} is given by Eq.3.19 and R_L is the PD output load resister. Express the second term which is the output RF signal component in Eq. A.1 by $s_1(t)$ and the third term which is third order harmonic wave by $s_3(t)$, then the autocorrelation functions of $s_1(t)$ and $s_3(t)$ are

$$R_1(\eta) = E\left[s_1(t)s_1(t-\eta)\right] = \frac{\pi^2}{V_\pi^2}R(\eta) \tag{A.2}$$

and

$$\begin{aligned} R_3(\eta) &= E\left[s_3(t)s_3(t-\eta)\right] \\ &= \frac{\pi^6}{12V_\pi^6}\sigma^2 R(\eta)+\frac{\pi^6}{18V_\pi^6}R^3(\eta) \end{aligned}. \tag{A.3}$$

Thus the PSD of $s_1(t)$ and $s_3(t)$ are

$$S_1(\omega)=\int_{-\infty}^{+\infty}R_1(\eta)e^{-j\omega\eta}d\eta=\frac{\pi^2}{V_\pi^2}S(\omega) \tag{A.4}$$

and

$$\begin{aligned}S_3(\omega)&=\int_{-\infty}^{+\infty}R_3(\eta)e^{-j\omega\eta}d\eta\\&=\frac{\pi^6}{12V_\pi^6}\sigma^2S(\omega)+\frac{\pi^6}{18V_\pi^6}S(\omega)*S(\omega)*S(\omega)\end{aligned}. \tag{A.5}$$

Then the PSD of $v_{RoF}(t)$ is

$$\begin{aligned}S_{RoF}(\omega)&=\frac{R_L^2R_{PD}^2K_f^4A_{opt}^4}{4}\left[2\pi\delta(\omega)+S_1(\omega)+S_3(\omega)\right]\\&=\frac{R_L^2R_{PD}^2K_f^4A_{opt}^4}{4}\left[2\pi\delta(\omega)+\left(\frac{\pi^2}{V_\pi^2}-\frac{\pi^6\sigma^4}{12V_\pi^6}\right)S(\omega)\right.\\&\left.-\frac{\pi^6}{18V_\pi^6}S(\omega)*S(\omega)*S(\omega)+\cdots\right]\end{aligned}. \tag{A.6}$$

- ***PSD of the output signal from RoF channel with echo effect***

The autocorrelation function for the signal $v_{s1}(t)$ shown in Eq. 4.18 is

$$\begin{aligned}R_{s1}(\eta)&=E\left[v_{s1}(t)v_{s1}(t-\eta)\right]\\&=\frac{\pi^2(1+K_r^2K_f^2)^2}{4V_\pi^2}\left[(1+K_r^4K_f^4)R(\eta)\right.\\&\left.+K_r^2K_f^2R(\eta+2\tau)+K_r^2K_f^2R(\eta-2\tau)\right]\end{aligned}. \tag{A.7}$$

According to Wiener-Khinchin theorem, the PSD of $v_{s1}(t)$ is calculated by

$$\begin{aligned}S_{s1}(\omega)&=\int_{-\infty}^{+\infty}R_{s1}(\eta)e^{-j\omega\eta}d\eta\\&=\frac{\pi^2(1+K_r^2K_f^2)^2}{4V_\pi^2}\left[(1+K_r^4K_f^4)S(\omega)\right.\\&\left.+2K_r^2K_f^2S(\omega)\cos(2\omega\tau)\right]\end{aligned}. \tag{A.8}$$

The autocorrelation function for the signal $v_{s2}(t)$ shown in Eq. 4.19 is

$$\begin{aligned} R_{s2}(\eta) &= E\left[v_{s2}(t)v_{s2}(t-\eta)\right] \\ &= \frac{\pi^4 K_r^4 K_f^4}{16V_\pi^4}\left[\sigma^4 + 2R^2(\eta) + R^2(2\tau)\right. \\ &+ \frac{1}{2}R^2(\eta+2\tau) + \frac{1}{2}R^2(\eta-2\tau) \\ &- 2R(\eta)R(\eta+2\tau) - 2R(\eta)R(\eta-2\tau) \\ &\left. + R(\eta+2\tau)R(\eta-2\tau) - 2\sigma^2 R(2\tau)\right] \end{aligned} \quad . \tag{A.9}$$

Then the PSD of $v_{s2}(t)$ is

$$\begin{aligned} S_{s2}(\omega) &= \int_{-\infty}^{+\infty} R_{s2}(\eta)e^{-j\omega\eta}d\eta \\ &= \frac{\pi^4 K_r^4 K_f^4}{16V_\pi^4}\left\{2\pi\left[\sigma^4 + R^2(2\tau) - 2\sigma^2 R(2\tau)\right]\delta(\omega)\right. \\ &+ \left[2+\cos(2\omega\tau)\right]\left(s(\omega) * s(\omega)\right) \\ &- 4s(\omega) * \left[s(\omega)\cos(2\omega\tau)\right] \\ &\left. + \left[s(\omega)e^{j2\omega\tau}\right] * \left[s(\omega)e^{-j2\omega\tau}\right]\right\} \end{aligned} \quad . \tag{A.10}$$

The autocorrelation function for the signal $v_{s2}(t)$ shown in Eq. 4.20 is

$$\begin{aligned} R_{s3}(\eta) &= E\left[v_{s3}(t)v_{s3}(t-\eta)\right] \\ &= (m_1^2 + m_2^2)\left[2R^3(\eta) + 3\sigma^4 R(\eta)\right] + m_1 m_2\left[2R^3(\eta+2\tau) + 3\sigma^4 R(\eta+2\tau)\right] \\ &+ m_1 m_2\left[2R^3(\eta-2\tau) + 3\sigma^4 R(\eta-2\tau)\right] \\ &+ (m_1 m_3 + m_2 m_3)\left[2\sigma^2 R(\eta)R(2\tau) + 2R^2(\eta)R(\eta+2\tau) + \sigma^4 R(\eta+2\tau)\right] \\ &+ (m_1 m_3 + m_2 m_3)\left[2\sigma^2 R(2\tau)R(\eta+2\tau) + 2R(\eta)R^2(\eta+2\tau) + \sigma^4 R(\eta)\right] \\ &+ (m_1 m_3 + m_2 m_3)\left[2\sigma^2 R(\eta)R(2\tau) + 2R^2(\eta)R(\eta-2\tau) + \sigma^4 R(\eta-2\tau)\right] \\ &+ (m_1 m_3 + m_2 m_3)\left[2\sigma^2 R(2\tau)R(\eta-2\tau) + 2R(\eta)R^2(\eta-2\tau) + \sigma^4 R(\eta)\right] \\ &+ m_3^2\left[\sigma^4 R(\eta-2\tau) + 2R(\eta+2\tau)R^2(2\tau) + 2R^2(\eta)R(\eta+2\tau)\right] \\ &+ m_3^2\left[\sigma^4 R(\eta+2\tau) + 2R(\eta-2\tau)R^2(2\tau) + 2R^2(\eta)R(\eta-2\tau)\right] \\ &+ 2m_3^2\left[\sigma^2 R(\eta-2\tau)R(2\tau) + \sigma^2 R(\eta+2\tau)R(2\tau)\right. \\ &\left. + R(\eta-2\tau)R(\eta+2\tau)R(\eta) + R(\eta)R^2(2\tau) + R^3(\eta)\right] \end{aligned} \tag{A.11}$$

where

$$m_1 = -(\frac{2}{3} + \frac{K_r^2 K_f^2}{6}), \tag{A.12}$$

$$m_2 = -(\frac{2K_r^4 K_f^4}{3} + \frac{K_r^2 K_f^2}{6}), \tag{A.13}$$

and

$$m_3 = -\frac{K_r^2 K_f^2}{2}. \tag{A.14}$$

Then the PSD of $v_{s3}(t)$ is derived to

$$\begin{aligned}
S_{s3}(\omega) &= \int_{-\infty}^{+\infty} R_{s3}(\eta) e^{-j\omega\eta} d\eta \\
&= \frac{\pi^2}{4V_\pi^2} S(\omega)\left[3\sigma^4(m_1^2 + m_2^2)\right. \\
&\quad \left. + \left(4\sigma^2 R(2\tau) + 2\sigma^4\right)(m_1 m_3 + m_2 m_3) + 2m_3^2 R^2(2\tau)\right] \\
&\quad + \frac{\pi^2}{4V_\pi^2} S(\omega)\cos(2\omega\tau)\left[6\sigma^4 m_1 m_2\right. \\
&\quad + (m_1 m_3 + m_2 m_3)\left(4\sigma^2 R(2\tau) + 2\sigma^4\right) \\
&\quad \left. + 2m_3^2(\sigma^4 + 2\sigma^2 R(2\tau) + 2R^2(2\tau))\right] \\
&\quad + \frac{\pi^8}{32V_\pi^8}\left(m_1^2 + m_2^2 + m_3^2\right) S(\omega) * S(\omega) * S(\omega) \\
&\quad + \frac{\pi^8}{16V_\pi^8} m_1 m_2 \left[S(\omega) * S(\omega) * S(\omega)\right]\cos(2\omega\tau) \\
&\quad + \frac{\pi^8}{16V_\pi^8}\left[m_1 m_3 + m_2 m_3 + m_3^2\right] S(\omega) * S(\omega) * \left(S(\omega)\cos(2\omega\tau)\right) \\
&\quad + \frac{\pi^8}{16V_\pi^8}(m_1 m_3 + m_2 m_3) S(\omega) * \left[\left(S(\omega) * S(\omega)\right)\cos(2\omega\tau)\right] \\
&\quad + \frac{\pi^8}{32V_\pi^8} m_3^2 \left(S(\omega) e^{j2\omega\tau}\right) * \left(S(\omega) e^{-j2\omega\tau}\right) * S(\omega)
\end{aligned}, \tag{A.15}$$

References

[1] D. Raychaudhuri and N. B. Mandayam, "Frontiers of wireless and mobile communications," Proceedings of the IEEE, vol. 100, no. 4, pp. 824-840, April, 2012.

[2] A. F. Molisch, Wireless Communications, 2nd Edition, John Wiley & Sons Ltd., 2011.

[3] N. B. A. Shah, R. Ramle, N. Awang, and M. F. Yusuf, "Fixed and Mobile WiMAX: a comparison towards the distance and height effects on performance degradation," Lecture Notes on Software Engineering, vol.1 no.1, pp. 80-83, Feb. 2013.

[4] A. Ghosh, D. R. Wolter, J. G. Andrews and R. Chen, "Broadband wireless access with WiMax/802.16: current performance benchmarks and future potential," IEEE Communications Magazine, vol. 43, issue 2, pp. 129-136, Feb. 2005.

[5] E. Dahlman, S. Parkvall, and J. Skold, 4G: LTE/LTE-advanced for mobile broadband, Academic Press, 2013.

[6] M. Sauer, A. Kobyakov and J. George, "Radio over fiber for picocelllar network architectures," Journal of Lightwave Technology, vol. 25, issue 11, pp. 3301-3320, 2007.

[7] A. Hamed, and S. Komaki, Radio over Fiber Technologies for Mobile Communications Networks, Artech House Publishers, 2002.

[8] D. Novak, "Fiber optics in wireless applications," OFC 2004 Short Course 217, 2004.

[9] D. Wake, and K. Beachman, "A novel switched fibre distributed antenna system," in Proceedings of European Conference on Optical Communications(ECOC'04), Vol. 5, pp. 132 – 135, 2004.

[10] D. K. Mynbaev, L. L. Scheiner, Fiber-Optic Communications Technology, Prentice Hall, New Jersey, 2001.

[11] Y. Ding, J. Zhu, W. D. Fang, X. G. Ge and X. Chen, "Study of millimetre-wave generation based on optical frequency multiplication," InWireless Mobile and Computing (CCWMC 2011), Conference on IET International Communication , pp. 1-5, Nov. 2011.

[12] J.E Mitchell and J.C. Attard, "Optical network architectures for dynamic reconfiguration of full duplex, multiwavelength, radio over fiber," Journal of Optical Networking, vol. 5, no. 6, pp. 435-444, 2006.

[13] G. P. Agrawal, Fiber-Optic Communications Systems, 3nd ed., John Wiley & Sons, Inc., 2002.

[14] K. Kikushima and Y. Suematsu, "Nonlinear distortion properties of laser diode influenced by coherent reflected waves," IEICE Trans. on Optical and Quantum Electronics, vol.E67, no.1, pp.19-25, Jan. 1984.

[15] P. K. Pepeljugoski and K. Y. Lau, "Interferometric noise reduction in fiber-optic links by superposition of high frequency modulation," Journal of Lightwave Technology, vol. 10, o. 7, July 1992.

[16]I. Frigyes, Z. V´arallyay, O. Schwelb, L. Jakab and P. Richter "Investigations in the joint effect of fiber dispersion and nonlinear refraction in microwave optical links," International Topical Meeting on Microwave Photonics, MWP 2003 Proceedings. Pp. 299-302, Sept. 2003.

[17]B. Zhang, Y. Lu, J. Zhang and B.Yang, "Nonlinear effect of OFDM in Radio-over-Fiber transmission," International Conference on Microwave and Millimeter Wave Technology, 2007. ICMMT '07, pp. 1-3, April 2007.

[18]C. T. Lin, J. Chen, S. P. Dai, P. C. Peng, and S. Chi, "Impact of nonlinear transfer function and imperfect splitting ratio of MZM on optical up-conversion employing double sideband with carrier suppression modulation," Journal of Lightwave Technology,vol.26, Aug.1, 2008.

[19]P. Assimakopoulos, A. Nkansah, N. J. Gomes and D. Wake, "Statistical distribution of EVM measurements for direct-modulation Radio-Over-Fiber links transporting OFDM signals," IEEE Transactions on Microwave Theory and Techniques, vol.61 , issue. 4, April 2013.

[20]G Zhang, X Zheng, S Li, H Zhang and B. Zhou, "Postcompensation for nonlinearity of Mach–Zehnder modulator in radio-over-fiber system based on second-order optical sideband processing," Optics Letters vol. 37, issue 5, pp. 806-808, 2012.

[21]F. P. Guiomar, J. D. Reis, A. L. Teixeira and A. N. Pinto, "Digital postcompensation using Volterra series transfer function," IEEE Photonics Technology Letters, vol. 23, issue. 19, Oct. 2011.

[22]R. Shi, P. Li, M. Chen, S. Yang, H. Chen and S. Xie, "RF-IF downconversion and linearization of an analog photonic link based on digital signal post-compensation," Asia Communications and Photonics Conference, Optical Society of America, Nov. 2013.

[23]Y. Shen, B. Hraimel, X. Zhang, G. E. Cowan, K. Wu, and T. Liu, "A novel analog broadband RF predistortion circuit to linearize electro-absorption modulators in multiband OFDM radio-over-fiber systems," IEEE Transactions on Microwave Theory and Techniques, vol. 58, issue. 11, Nov. 2010.

[24]A. Hekkala, M. Hiivala, M. Lasanen, J. Perttu, , L. C. Vieira, N. J. Gomes and A.Nkansah, "Predistortion of radio over fiber links: algorithms, implementation, and measurements," IEEE Transactions on Circuits and Systems I: Regular Papers, vol. 59, issue. 3, March 2012.

[25]J. Li, L. Mao, S. Xie and S. Zhang, "A laser driver with analog pre-distortion technique for Radio-over-Fiber system," 8th International Conference on Wireless Communications, Networking and Mobile Computing (WiCOM), 2012, pp. 1-4, Sept. 2012.

[26]A. Awoye, M. S. Leeson and R. J. Green, "Neural network based adaptive predistortion for Radio over Fiber links," 2012 14th International Conference on Transparent Optical Networks (ICTON), pp. 1-4, July 2012.

[27]A. Hekkala and M. Lasanen, "Performance of adaptive algorithms for compensation of radio over fiber links," Wireless Telecommunications Symposium (WTS 2009), pp. 1-5, April 2009.

[28]G. Cao, T. Xu, T. Liu, Y. Ye, H. Lin, X. Luo and L. Li, "Memory polynomial based adaptive predistortion for Radio over Fiber systems," International Conference on Microwave and Millimeter Wave Technology (ICMMT) 2012, pp. 1-4, May 2012.

[29]Y. Yamao, Y. Toyama and E. Umali, "Power Efficiency of OFDM Signal Amplification with Doherty Extended Doherty and EPWM Transmitters," Proc. TriSAI2007, Sept. 2007.

[30]E. M. Umali, K. Kawazoe, and Y. Yamao, "Quantization Noise and Distortion Analysis of Envelope Pulse-Width Modulation (EPWM) Transmitters for OFDM Signal Amplification," IEICE Trans. Fundamentals, vol. E93-A, no. 10, pp. 1724-1734, Oct. 2010.

[31]E. M. Umali, S. Yokozawa and Y. Yamao, "Quantization Noise Suppression for Envelope Pulse-Width Modulation (EPWM) Transmitters," Proc. of IEEE VTC2010-Fall, Sep. 2010.

[32]S. Yokozawa and Y. Yamao, "Suppression of Quantization Noise for EPWM Transmitter by Controlling Phase Modulator Output with 2ndorder Δ-ΣModulator," Proc. of IEEE VTC2011-Spring, May. 2011.

[33]U. Gliese, T. N. Nielsen, S. Norskov, and K. E. Stubkjaer, "Multifunction fibre-optic microwave links based on remote heterodyne detection," IEEE Trans. On Microwave Theory and Techniques, vol. 46, no. 5, pp. 458 - 468, 1998.

[34]S. Nadarajah, X. N. Fernando and R. Sedaghat, "Adaptive digital predistortion of laser diode nonlinearity for wireless applications," Canadian Conference on Electrical and Computer Engineering, 2003, IEEE CCECE 2003, vol. 1, pp. 159-162, 2003.

[35]X.N. Fernando and A.B. Sesay, "Adaptive asymmetric linearization of Radio Over Fiber links for wireless access," IEEE Transactions on Vehicular Technology, vol. 51, issue 6, pp. 1576-1586, Nov. 2002.

[36]R. C. Alferness, "Waveguide Electrooptic Modulators," IEEE Trans. On Microwave Theory Tech., vol. MTT-30, no. 8, Aug. 1982.

[37]F. Koyama and K. Iga, "Frequency chirping in external modulators," Journal of Lightwave Technology, vol. 6, no. 1, pp. 87-93, Jan. 1988.

[38]K. Kawano, T. Kitoh, H. Jumoni, T. Nozawa and M. Yanagibashi, "New traveling-wave electrode Mach-Zehnder optical modulator with 20GHz bandwidth and 4.7V driving voltage at 1.52μm Wavelength," Electron. Letter, vol. 25, no. 20, pp. 1382-1383. Sept. 1989.

[39]A. F. Elrefaie, R. E. Wagner, and D. G. Daut, "Chromatic Dispersion Limitation in Coherent Lightwave Transmission Systems," Journal of Lightwave Technology, vol. 6, pp. 704-709, 1988.

[40]W. P. Ng, W. Loedhammacakra, Z. Ghassemlooy, and R. A. Cryan, "Characterisation of a parallel optical all pass filter for chromatic dispersion equalisation in 10 Gb/s system," Circuits, Devices & Systems, IET, vol. 2, pp. 112-118, 2008.

[41]R. Nee and R. Prasad, OFDM for Wireless Multimedia Communications, Artech House, Inc., 2000.

[42]L. Hanzo, M. Münster, B. J. Choi and T. Keller, OFDM and MC-CDMA for Broadband Multi-user Communications, WLANs and broadcasting. John Wiley & Sons, 2003.

[43]L. Hanzo, W. Webb and T. Keller, Single- and Multi-Carrier Quadrature Amplitude Modulation: Principles and Applications for Personal Communications, WLANs and Broadcasting, New York: John Wiley & Sons, 2000.

[44]A. Gangwar and M. Bhardwaj, "An overview: Peak to Average Power Ratio in OFDM system & its effect," International Journal of Communication and Computer Technologies, vol. 1, no.2, issue. 2, Sept. 2012.

[45]H.Ochiai, H. Imai, "Performance of the deliberate clipping with adaptive symbol selection for strictly band-limited OFDM systems," IEEE Journal on Selected Areas in Communications, vol. 18, issue. 11, pp. 2270 –2277, Nov. 2000.

[46]D. Wulich, N. Dinur and A. Glinowiecki, “Level clipped high-order OFDM,” IEEE Transactions on Communications, vol. 48, issue 6, pp. 928 –930, June 2000.

[47]S. Müller and J. Huber, “A comparison of peak power reduction schemes for OFDM,” In IEEE Global Telecommunications Conference (GLOBECOM '97), Phoenix, Arizona, USA, pp. 1-5, Nov.1997.

[48]Hyo-Joo Ahn, Yoan Shin and Sungbin Im, “A block coding scheme for peak-to- average power ratio reduction in an orthogonal frequency division multiplexing system,” 2000 IEEE 51st Vehicular Technology Conference Proceedings, (VTC 2000-Spring), Tokyo, vol. 1, pp. 56 –60, 2000.

[49]P. Fan and X. Xia, “Block coded modulation for the reduction of the peak to average power ratio in OFDM systems,” IEEE Transactions on, Consumer Electronics, vol. 45, issue. 4, pp. 1025-1029, Nov. 1999.

[50]W. A. C. Fernando and R. M. A. P. Rajatheva, “Performance of turbo and trellis coded OFDM for LEO satellite channels in global mobile communications,” 1998 IEEE International Conference on Communications, 1998. ICC 98. Conference Record, vol. 1, pp. 412 –416, 1998.

[51]S. Müller and J. Huber, “A novel peak power reduction scheme for OFDM,” In IEEE Int. Symposium on Personal, Indoor and Mobile Radio Communications(PIMRC '97), Helsinki, Finland, pp. 1090-1094, Sep. 1997.

[52]M. Breiling, S. Müller-Weinfurtner, and J. Huber, “SLM peak-power reduction without explicit side information,” In IEEE Communications Letters, vol. 5, no. 6, pp. 239-241, Jun. 2001.

[53]S. Müller and J. Huber, “OFDM with reduced Peak-to-Average Power Ratio by optimum combination of partial transmit sequences,” Electronics Letters, vol. 33, no. 5, pp. 368-369, Feb. 1997.

[54]H. Rohling, R. Grunheid, “Performance of an OFDM-TDMA mobile communication system”, IEEE 46th Vehicular Technology Conference, 1996. Mobile Technology for the Human Race, vol. 3, pp. 1589 -1593. 1996.

[55]H. Schmidt, and K. D. Kammeyer, “Reducing the peak to average power ratio of multicarrier signals by adaptive subcarrier selection”, IEEE 1998 International Conference on Universal Personal Communications, 1998. ICUPC '98. vol. 2, pp. 933-937, 1998.

[56]Y. London and D. Sadot, “Nonlinear effects mitigation in coherent optical OFDM system in presence of high peak power,” IEEE Journal of Lightwave Technology, vol.29, no.21, pp.3275-3281, Nov. 2011.

[57]D. Roerich, X. Wang, M. Bernhard and J. Speidel. “Optimal modulation index of the Mach-Zehnder modulator in a coherent optical OFDM system employing digital predistortion,” in Proc. ITG Symposium on Photonic Networks, pp. 1-6, May, 2013.

[58]A. R. Islam, R. A. Shafik, M. S. Rahman and J. B. Song “On the nonlinear distortion effects in an OFDM-RoF link,” Proc. IEEE-ICET2006, pp.20-26.Nov.2006.

[59]H. Yang, J. Zeng, Y. Zheng, H. D. Jung, B. Huiszoon, J. H. C. van Zantvoort, E. Tangdiongga and A. M. J. Koonen, “Evaluation of effects of MZM nonlinearity on QAM and OFDM signals in RoF transmitter,” in Proc. IEEE International Topical Meeting on Microwave Photonics, Canada, pp. 90–93, Sep. 2008.

[60]D. Kolev, K. Wakamori, and M. Matsumoto, “Transmission analysis of OFDM-based services over Line-of-Sight indoor infrared laser wireless links,” IEEE Journal of Lightwave Technology, vol.30, no. 23, pp. 3727 - 3735, Dec. 2012.

[61]S. Zhang, Y. Liu, H. Li and Y. Liu, "Characterization of nonlinearity using polynomial transfer function of all-optical sampling," Microwave and Optical Technology Letters, vol. 53, no.1, pp. 216-219, Nov. 2010.

[62]A. M. Marhros, M. M. Tharwat, "Implementation of a radio over fiber OFDM communication system in the Simulink environment", International Journal of Advanced Computing, Engineering and Application, vol.1, pp. 123-128, Dec. 2012.

[63]L. C. Vieira and N. J. Gomes. "Baseband behavioral modeling of OFDM-Radio over fiber link distortion," in Proc. IEEE International Topical Meeting on Microwave Photonics 2012, pp. 188 – 191, Sept. 2012.

[64]R. Schreier and G. Temes, Understanding Delta-Sigma Data Converters, IEEE Press, 2005.

[65]M. Daoud, U. Maheeka, T. Alam and X. Fernando, "Modulator bias optimization of radio over fiber links considering noise figure and RF gain," in Proc. IEEE 25th Biennial Symposium on Communications, pp. 234-237, May 2010.

[66]W. I. Way, "Subcarrier multiplexed lightwave system design considerations for subscriber loop applications", IEEE Journal of Lightwave Technology, vol.7, pp. 1806-1818, Nov. 1989.

[67]C. H. Lee, V. Postoyalko, and T. O'Farrell, "Analysis and simulation of AM-AM/PM nonlinear distortion due to direct laser modulation in radio over fiber systems," in Proc. IEEE International Topical Meeting on Microwave Photonics, pp. 137-140, Awaji, Japan, Nov. 2002.

[68]C. Rapp, "Effects of HPA-nonlinearity on a 4-DPSK/OFDM-signal for a digital sound broadcasting signal," In ESA, Second European Conference on Satellite Communications (ECSC-2), vol. 1, pp. 179-184, 1991.

[69]W. P. Ng, W. Loedhammacakra, Z. Ghassemlooy, and R. A. Cryan, "Characterisation of a parallel optical all pass filter for chromatic dispersion equalisation in 10 Gb/s system," IET Circuits, Devices & Systems, vol. 2, pp. 112-118, 2008.

[70]P. K. Pepeljugoski and K. Y. Lau, "Interferometric noise reduction in fiber-optic links by superposition of high frequency modulation," Journal of Lightwave Technology, vol.10, no.7, pp. 957-963, July 1992.

[71]B. Moslehi, "Noise power spectra of two-beam interferometers induced by the laser phase noise," Journal of Lightwave Technology, vol. LT-4, no.11, pp. 1704-1709, Nov. 1986.

[72]D. B. Mortimore, "Fiber Loop Reflectors," Journal of Lightwave Technology, vol.6, no.7, pp.1217-1224, July, 1988.

Publications

Journal Papers:

1. X. Yu, Y. Yamao and M. Matsuura, "EPWM-OFDM Signal Transmission against Nonlinearities of E/O Converters in Radio over Fiber Channel," *IEICE Trans. Commun.*, vol. E97-B, no.2, pp. 484-494, Feb. 2014. (Related to Chapter 3)

International Conference Papers:

1. X. Yu, M. Matsuura, S. Yokozawa and Y. Yamao, "OFDM Signal Transmission by EPWM Transmitter in Nonlinear RoF Channel," *Proc. IEEE 75th Vehicular Technology Conference (VTC2012-Spring)*, Yokohama, Japan, May 2012. Presentation number: 10G: OFDM2, no.2. (Related to Chapter 3)
2. X. Yu, M. Matsuura and Y. Yamao, "Nonlinearity Effect of DFB Laser Diode RoF channel on EPWM-OFDM Signal Transmission," *Triangle Symposium on Advanced ICT 2012 (TriSAI 2012)*, Tokyo, Japan, Sep. 2012. Presentation number: Student Session 8 (S-OP/EDU) Optical/Education, S-8-2.
3. X. Yu, M. Matsuura and Y. Yamao, "Analysis of RoF-Echo Effect on OFDM Signal Transmission with EPWM Format", *Proc.16th International Symposium on Wireless Personal Multimedia Communications (WPMC) 2013*, Atlantic City, USA, June 2013. Presentation number: PLCCM3: Physical layer, channel coding and modulation 3, no.3. (Related to Chapter 4, WPMC2013 Best Student Paper Award)

Domestic Workshop Papers:

1. X. Yu, M. Matsuura, S. Yokozawa and Y. Yamao, "Nonlinear RoF Transmission of EPWM-OFDM Signal," *IEICE Society Conference*, BS-3-5, pp. 41-42, Sept. 2011.
2. X. Yu, M. Matsuura, S. Yokozawa and Y. Yamao, "ANC-EPWM Transmission of OFDM Signal in RoF Channel," *IEICE Technical Report*, RCS 2012-11, pp. 7-12, Apr. 2012.
3. X. Yu, M. Matsuura, and Y. Yamao, "EPWM-OFDM Transmission against Nonlinearity and Echo in Radio over Fiber Channel," *IEICE Society Conference*, BS-7-28, pp. 87-88, Sept. 2013.